MINISTRY OF SCIENCE AND HIGHER EDUCATION OF THE RUSSIAN FEDERATION
Federal State Autonomous Educational Institution of Higher Education
«Far Eastern Federal University»
(FEFU)

SCHOOL OF ENGINEERING

Department of Offshore and Structural Mechanics

Makarov Oleg Arturovich

NUMERICAL MODELING OF ICE LOAD FORMATION PROCESSES ON THE VERTICAL SUPPORTS OF OFFSHORE STRUCTURES
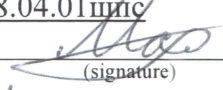
GRADUAL QUALIFICATION WORK
(MASTER'S THESIS)

08.04.01 – Construction
master program
«Offshore and coastal engineering»

Vladivostok – 2020

Student M3118-08.04.01ппс
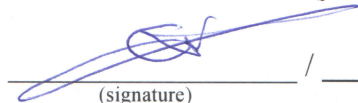
Makarov O. A. _____
   (Full name)   (signature)

« 03 » July _____ 2020 г.

«Допустить к защите»

Leader of master's program

        Dr. of Eng. Sc., Professor
        (position, scientific degree)

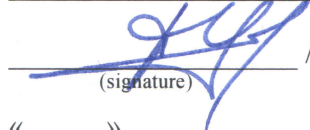_____ / ___ Bekker A. T. ___ /
   (signature)   (Full name)

« _____ » _____ 2020 г.

Head of department ___ Cand. of Eng. Sc., ___
               (position, scientific degree)

Associate Professor _____

_____ / Tsimbelman N. Ya. /
   (signature)   (Full name)

« _____ » _____ 2020 г.

GQW materials do not contain / contain
          (underline whatever applicable)

State commercial secret information subject to export control

Commissioner for Export Control

_____ / _____ /
   (signature)   (Full name)

« _____ » _____ 2020 г

Scientific adviser

        Dr. of Eng. Sc., Professor
        (position, scientific degree)

_____ / ___ Bekker A. T. ___ /
   (signature)   (Full name)

« _____ » _____ 2020 г.

Consultant for _____

_____

_____ / _____ /
   (signature)   (Full name)

« _____ » _____ 2020 г.

Consultant for _____

_____

_____ / _____ /
   (signature)   (Full name)

« _____ » _____ 2020 г.

Consultant for _____

_____

_____ / _____ /
   (signature)   (Full name)

« _____ » _____ 2020 г.

Reviewer

        Cand. of Eng. Sc., Head of
        (position, scientific degree)

the Department of Computational Research,

Research Center "StaDiO",

_____ / ___ Dmitriev D. S. ___ /
   (signature)   (Full name)

« _____ » _____ 2020 г.

Valuated with State Certification Commission

with mark _____

Secretary of State Certification Commission

Cand. of Eng. Sc., Associate Professor, L. I. Sheveleva

_____
   (signature)

« _____ » _____ 2020 г.

Contents

Introduction

Timeliness of the topic. The fuel and energy complex is an important element of the Russian and world economy. One of the main trends of its development at present is the development of hydrocarbon deposits on the continental shelf. Based on various data, we can say that in the world today, up to 35% of oil and gas is produced on the shelf and coastal waters.

The main hydrocarbon reserves of the Russian Federation are concentrated in the regions of the Far North, which are characterized by difficult climatic conditions. At the same time, most of these reserves belong to deposits located on the shelf of the Arctic Ocean. The development of these fields requires the creation of special technical means, due to the difficult ice regime, which is common for the northern seas.

Hydrocarbon production on the Arctic shelf currently involves the construction of unique marine structures – offshore ice-resistant platforms, which are characterized by increased responsibility. These platforms are exposed to various environmental factors. An important role in the complex of external forces acting on the structure is played by loads from drifting ice fields. This requires a detailed evaluation of the ice load in the design of such unique structures as offshore platforms. Currently, models of projected platforms on a smaller scale, as well as special experimental devices are being created to analyze the impact of ice formations, which affects the timing and cost of construction.

At the moment, the use of digital technologies is widespread in the world, including in the field of construction. With the help of mathematical and computer modeling many problems are being solved, such as creating of numerical models of structures, modeling of physical processes (heat transfer, deformation, corrosion, cracking, crushing), describing of various material properties (plasticity, viscoelasticity, fatigue, creep) and many others. One of the important questions is the modeling of loads and impacts on buildings and structures.

Methods for evaluation of ice loads acting on hydraulic structures are described in modern domestic and foreign standards. However, these methods have a several disadvantages, such as the lack of a qualitative description of the anisotropic properties of ice, nature of the ice destruction in the contact zone, influence of cracking in ice formation and so on. The influence of the geometric dimensions of the structure on the process of its interaction with the ice cover is also little studied.

In this study will be considered the numerical simulation of the ice formations destruction process during the impact on the vertical offshore structures. The use of modern methods of numerical modeling can contribute to a more accurate evaluation of the impact of ice on offshore structures, which will positively affect the analysis of the stress-strain state of structures and their design.

Nowadays state of problem. The question of the influence of the ice regime of freezing water areas on structures has been actively discussed and considered since the second half of the 20th century.

Various conferences are regularly held and many articles on ice issues are being published. Increased attention to this topic is largely associated with the development of fuel and energy complex in the world and with the increasing rate of industrial development of oil and gas deposits on the Arctic shelf.

However, the question of exactly numerical simulation of processes of ice interaction and structures on the shelf is appeared relatively recently, due to the development of digital technologies in the world. Nowadays there are a number of studies on the impacts of ice formations on structures using numerical simulation. But these studies do not sufficiently describe the properties of ice and ice formations, the processes occurring at the contact of interaction, the influence of the geometric dimensions of structures on the nature of the destruction of the ice and other important aspects that should be considered in the simulation.

Goals and objectives of the study. The main goal of research – to develop a methodology for numerical modeling of ice load formation processes on the vertical supports of offshore structures and to evaluate its applicability to solving real engineering tasks.

In this paper, the objectives are as follows:

- to study the properties of ice as a material, to determine the degree of knowledge of the issue of ice-structure interaction modeling;

- to study the mechanism of interaction between ice and offshore structures;

- select and apply constitutive material models, taking into account the various physical properties of ice and fracture mechanism;

- to develop an algorithm for modeling the interaction of ice formation and vertical structures;

- to conduct numerical experiments using developed model in order to study and improve it;

- to verify the developed model, compare the results of numerical simulation with experimental data.

The object of the research is the process of interaction process between ice formations and offshore structures. The subject of research is numerical modeling of ice load formation processes.

Academic novelty. The academic novelty of the study is provided by the new formulation of the problem of numerical simulation of the ice loads formation processes. Methodology of modeling of ice impacts is developed in detail in order to take into account the many factors and features of ice-structure interaction process that were not previously considered. The modeling of fracture of ice formations is conducted considering various physical and mechanical properties of ice.

Theoretic and practical relevance. Theoretical significance is to consider the features of numerical modeling of ice impacts, describing the approaches, advantages and disadvantages of the methods used.

The practical significance is that numerical model being developed here as well as methods for the numerical simulation of ice-structure interaction can contribute to an accurate assessment of the

influence of the ice regime in the analysis of the stress-strain state and the design of offshore ice-resistant platforms and other structures, that will positively affect the cost and speed of design. The methods presented in this thesis, will contribute to improvement of methods for calculating ice loads given in modern codes.

Global problem of this study is the production of hydrocarbons in the Arctic region and its development. The local problem of the research is the assessment of the impact of ice formations on the shelf structures.

Methodology and research methods. In this study, numerical experiments are performed in the SIMULIA Abaqus finite element software package. Final methodology and numerical model are verified using by comparing the results with experimental data.

The following research methods were used in this work: review and analysis of existing researches on the topic, deductive decomposition of the problem of numerical simulation of interaction, synthesis of the general methodology for performing numerical experiments. axiomatic method for creating initial numerical models, qualitative and mathematical comparison of the results.

The main states for defense:

- statistical relation of ice properties;

- constitutive models used for modeling of ice material;

- methodology for creating of numerical model;

- numerical model parameters and features.

Approbation. The main results of the master thesis were published in two papers in School of Engineering Bulletin of Far Eastern Federal University and presented at the seminars and meetings of the Offshore and Coastal Engineering department.

Also, the thesis was presented at seminars and scientific meeting at Kindai University and Toyo Construction Company (Osaka, Japan).

The thesis structure is 109 pages, 4 chapters, 92 pictures and 20 tables.

1 Ice mechanics research review

1.1 Molecular structure

There are several ice types with different microstructures. But almost all of ice in the world is ice Ih. Ice Ih has a hexagonal structure. When water freezes hydrogen bonds are formed between its oxygen atoms. In solid Ih ice crystal the oxygen atoms of the nearest molecules line up in a repeating unit cell of a tetrahedral shape – four nearby molecules are located at the vertices of a three-sided pyramid, in the center of which is the fifth water molecule, as shown in the Figure 1.1
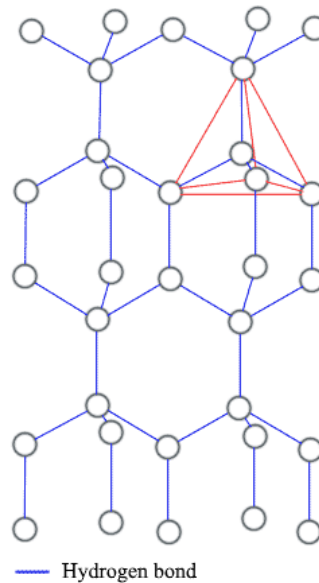

—— Hydrogen bond

Figure 1.1 – Ice lattice structure

Another feature of the molecular structure of ice is the fact that the molecules are arranged in the order of hexagonal symmetry, in consequence of which the structure of ice is called hexagonal. At the same time, the hexagonal structure of ice consists of layers parallel to each other, called basal planes. All basal planes are oriented perpendicular to the main crystallographic axis, called the c-axis [77]. Figure 1.2 shows the projections of the three-dimensional crystal lattice of ice along two main directions.
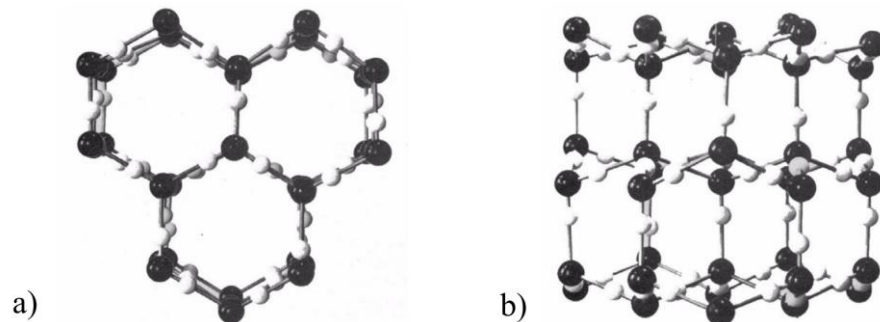

a)   b)

Figure 1.2 – Idealized arrangement of atoms in ice, where oxygen atoms are shown black, and hydrogen atoms white: a) view of the crystal lattice along the C-axis; b) view of the crystal lattice along the basal plane [64]

To analyze the effects of ice formations on structures, it is important to take into account the microstructure of ice formations. The formation of natural ice features is closely related to the physical processes occurring during freezing. During ice solidification in nature, various natural factors influence it, such as snow, wind, currents, temperature changes, etc. In addition, air bubbles, salts in sea water, alternate freezing and melting affect the microstructure of ice formations. As a result, the ice body has a non-uniform microstructure.

The process of solidification of floating ice sheets initiates on or near the surface, and then continues unidirectionally through the downward movement of the ice–water interface as heat is transferred from the relatively warm water below to the colder atmosphere above [66]. The thicker the ice, the slower it grows, since ice prevents the penetration of cold temperatures from the air. The top layer of ice usually consists of crystals of a variety of shapes. The most common are needle-shaped crystals with c-axes inclined in many directions, but granular ice can be observed. This layer is a small part of the total thickness of thick ice sheets. As the ice–water interface advances, favorably oriented crystals expand at the expense of less favorably oriented ones which are wedged out as presented in Figure 1.3. The plate-like structure of the crystals denotes the orientation of the basal planes. This process is termed geometric selection and accounts for the development of growth texture.
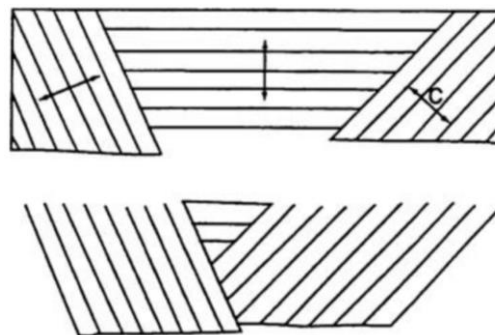

Figure 1.3 – A schematic sketch showing the process of geometrical selection during the unidirectional solidification of water [66]

Thus, when sheets grow from thin layers in which crystals of all orientations are present, they are expected to possess predominantly the *c*-axis horizontal texture. Sheets of first-year sea ice, for instance, are generally composed of columnar-shaped grains, elongated in the growth direction [66] as presented in Figure 1.4 and Figure 1.5. In all sea ice formed by unidirectional freezing, c-axis-horizontal orientations develop rapidly after an initial ice skim forms, and they dominate the rest of the ice growth [80]. Thus, the c-axes of crystals that make up sea ice, for instance, are more or less horizontally oriented (i.e., perpendicular to the growth direction), and are occasionally aligned within this plane [66].

Also, during freezing process, the brine movement can be observed. As ice grows and the ice–water interface advances downwards into the melt, salt ions are rejected from the ice. The salt builds up ahead of the advancing interface, increasing the salinity of a thin layer of a few millimeters to a few

centimeters in thickness. The resulting gradient in salt concentration leads to diffusion of salt away from the interface towards the less saline ocean [72]. Within sea ice, a downward flow increases the local bulk salinity and porosity and ultimately leads to the formation of brine channels: Locally, brine is replaced by more saline brine from above. Since the more saline brine is superheated (i.e. above the freezing point) with respect to the temperature of the surrounding ice, it will dissolve surrounding ice partially to attain thermodynamic equilibrium. These channels can be thought of as tubular river systems in which the tributaries are arranged with cylindrical symmetry around the main drainage channels [67].
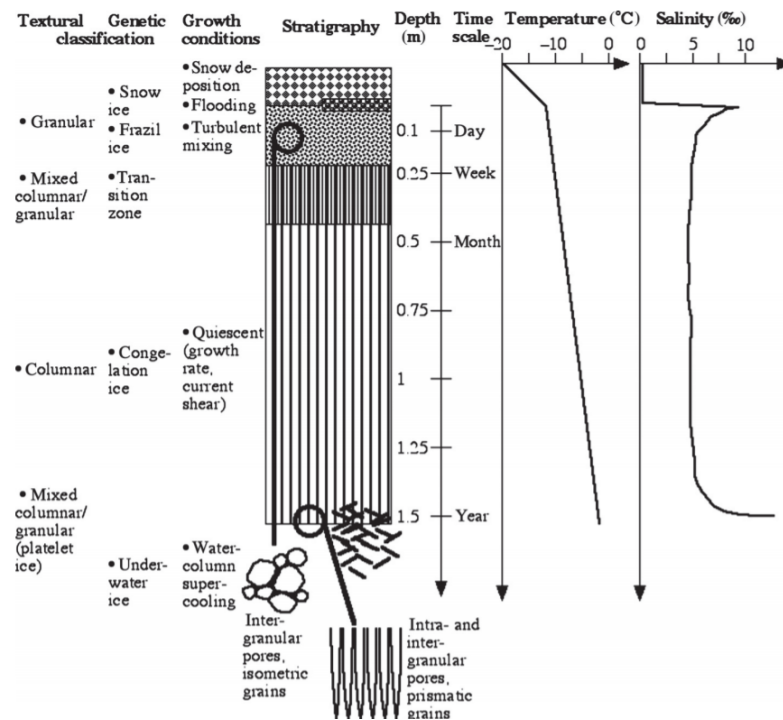

Figure 1.4 – Schematic summarizing the main ice textures, growth conditions and timescales, and typical winter temperature and salinity profiles for first-year sea ice [72]
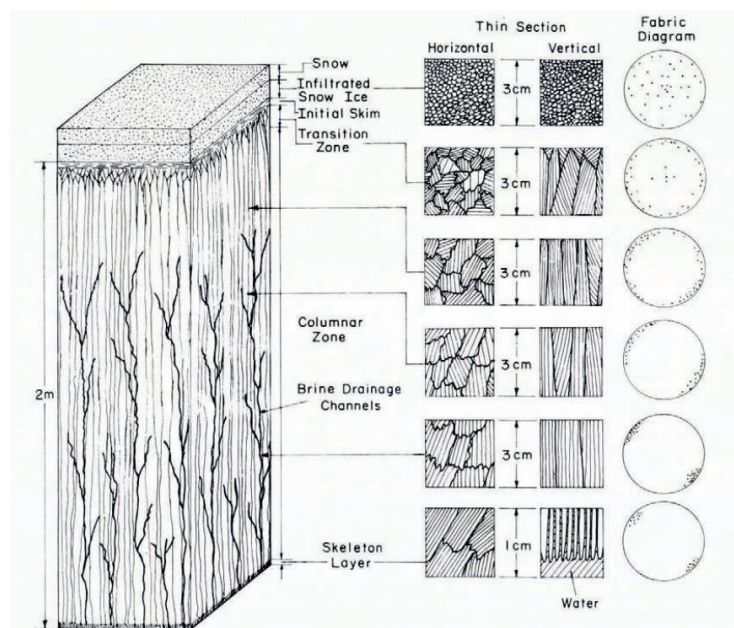

Figure 1.5 – Schematic drawing showing the heterogeneity of the structure of FY sea ice [67]

9

1.2 Physical properties of ice

After the appearance of the task of developing offshore oil and gas fields in the Arctic zone, where the ice-free period could be only a few months, active research began in the areas of offshore construction and ice engineering. Today, there are a lot of research on various characteristics of the ice. However, due to the fact that ice, especially sea ice, is a rather heterogeneous and anisotropic material, the research results vary widely. The anisotropy of ice is primarily due to its molecular structure.

The determination of the characteristics of ice has been carried out by many researchers since the second half of the 20th century. The main characteristics of ice, which have been studied most widely, are the elastic modulus, Poisson's ratio, density, compressive strength, tensile strength and bending strength. Friction coefficients of ice on various materials, its salinity, porosity, and various dependencies between the listed characteristics are also studied.

The following authors made a great contribution to the study of ice properties: Weeks W. F., Assur A., Frankenstein G., Garner R., Cox G. F. N., Kovacs A., Timco G. W., Frederking R. M. W., Sodhi D. S., Saeki H. A review of the data and many other significant studies of sea ice properties has been performed by **Timco and Weeks (2010)** [74].

Also, quite extensive investigations of the properties of both fresh and sea ice have been carried out by many Russian authors. In this thesis, will be used the studies of Ryvlin, Nazintsev Yu. L., Panov V. V. Dmitrash J. A., Moiseev V. I. and Doronin Yu. P.

1.2.1 Ice thickness

Ice thickness is one of the most important parameters of ice fields. Proper assessment of ice thickness directly affects the accuracy of the ice load. Often, the assessment of the maximum thickness of ice is made from the condition of the energy balance at the ice-water interface [74]:

$$\varphi_i dt = \rho_i L dh_i, \tag{1.1}$$

where φ_i – heat flow from ice to air, W/m^2;

ρ_i – ice density, kg/m^3;

L – latent heat of fusion of ice, J/kg

Thus, if we make the assumption that the temperature of the upper surface of the ice is equal to the air temperature, and the temperature gradient along the vertical is equal to the temperature difference between the lower and upper surfaces, the ice thickness h_i, m, can be determined by the equation [19, 20, 74]

$$h_i = \frac{\lambda_i (T_b - T_a)}{\varphi_i}, \tag{1.2}$$

where λ_i – thermal conductivity of ice, W/(m·°C)

T_b and T_a – temperature on the lower surface of the ice and air temperature, respectively, °C.

Integrating equation (1.1) with expressing φ_i from equation (1.2), gives the following equation for ice thickness h_i [19, 20]:

$$h_i(t) = h_0 \left(1 + \frac{2}{h_0^2} \int_0^t \lambda_i \frac{(T_b - T_a)}{L\rho_i} dt \right)^{\frac{1}{2}},$$ (1.3)

where h_0 – ice thickness at $t = 0$.

Assuming that $h_0 = 0$ and ice properties (λ_i, L, ρ_i) are unchanged, we can get the Stefan equation to determine the thickness of the ice:

$$h_i = \left(\frac{2\lambda_i}{L\rho_i} (T_b - T_a)t \right)^{\frac{1}{2}}$$ (1.4)

In this case, the integral of the temperature difference in the equation (1.3) is often called the sum of the number of freezing degree days, the approximate value of which is used in practice in equation (1.4) and is determined by the following expression

$$\int_0^t (T_b - T_a)dt \approx \sum (T_b - T_a)\, t$$ (1.5)

The strong influence on the growth of ice thickness has snow. Assuming that the temperature of the upper surface of the snow cover is equal to the air temperature T_a, the formula (1.3), when accounting for snow, takes the following form [19, 20]:

$$h_i(t) = h_0 \left(1 + \frac{2}{h_0^2} \int_0^t \frac{\lambda_i(T_b - T_a)}{L\rho_i \left(1 + \frac{\lambda_i h_s}{\lambda_i h} \right)} dt \right)^{\frac{1}{2}},$$ (1.6)

The above equations usually show an overestimated value of ice thickness, since they do not take into account the effect of wind on heat transfer between the ice surface and air, as well as the effect of heat flow at the ice-water interface.

1.2.2 Phase composition

The phase composition of sea ice has a very large impact on almost all its properties. In sea ice, in addition to crystals, there are a liquid phase, air and salts in a dissolved and solid state. The mass m, g, of a certain volume of ice is determined by the following equation [19, 20, 51]

$$m = m_i + m_w + m_s,$$ (1.7)

where m_i – mass of freshwater ice, g;

m_w – the mass of water in the liquid state, g;

m_s – mass of salts, g:

$$m_s = m_{bs} + m_{cs},$$ (1.8)

m_{bs} – the mass of salts in the dissolved state (in brine), g;

m_{cs} – mass of salts in the crystalline state, g;

Salinity of ice is the ratio of the mass of salts to the total mass of ice. Thus, the salinity of ice s_i, fraction by weight, is determined by the equation

$$s_i = \frac{m_s}{m},$$ (1.9)

Brine salinity s_b, fraction by weight, is the mass of dissolved salts per unit mass of brine

$$s_b = \frac{m_{bs}}{m_b}$$ (1.10)

where m_b – brine weight, g:

$$m_b = m_{bs} + m_w$$ (1.11)

Doronin Yu. P. on the basis of research Schwerdtfeger (1965) received the following dependence of brine salinity on temperature:

$$\frac{ds_b}{dT} = \frac{\beta}{1 + \frac{m_{bs}}{m_w}},$$ (1.12)

where β – empirical coefficient of proportionality between brine concentration and temperature, °C⁻¹.

Mass of brine m_b, g, Doronin Yu. P. defines by the following expression

$$m_b = m_{bs} + m_w = \frac{m \cdot s_i - m_{cs}}{s_b},$$ (1.13)

Nazintsev and Panov in their book [51] on the basis of the experiments of Nelson and Thompson (1954) and Gitterman (1937) determined the values of β and m_{bs}/m_w, used in the equation (1.12):

$$\beta = \begin{cases} -1.848 \cdot 10^{-2}, & \text{at } 0 \geq T \geq -7.5\,°C \\ -1.077 \cdot 10^{-2}, & \text{at} -7.5 \geq T \geq -22.4\,°C \\ -0.532 \cdot 10^{-2}, & \text{at} -22.4 \geq T \geq -30.0\,°C \end{cases}$$ (1.14)

$$\frac{m_{bs}}{m_w} = \begin{cases} \beta T \cdot 10^{-2}, & \text{at } 0 \geq T \geq -7.5\,°C \\ (5.670 - 1.077 \cdot T) \cdot 10^{-2}, & \text{at} -7.5 \geq T \geq -22.4\,°C \\ (16.770 - 1.532 \cdot T) \cdot 10^{-2}, & \text{at} -22.4 \geq T \geq -30.0\,°C \end{cases}$$ (1.15)

Thus, the dependence of the ratio of the mass of salts to the mass of water in brine is represented by a piecewise linear function of temperature as shown in Figure 1.6. In general, Nazintsev Yu. L. identified the following equations [51]:

$$m_b = s_i \frac{1 + (\beta T + l)}{\alpha T + k},$$ (1.16)

$$m_{st} = s_i(1 + \gamma)\left(1 - \frac{\beta T + l}{\alpha T + k}\right),$$ (1.17)

$$s_b = \frac{\beta T + l}{1 + \beta T + l},$$ (1.18)

where m_{st} – mass of salts in brine (taking into account salts, including crystallized water), g;

α, β, k и l – empirical coefficients presented in the Table 1.1.
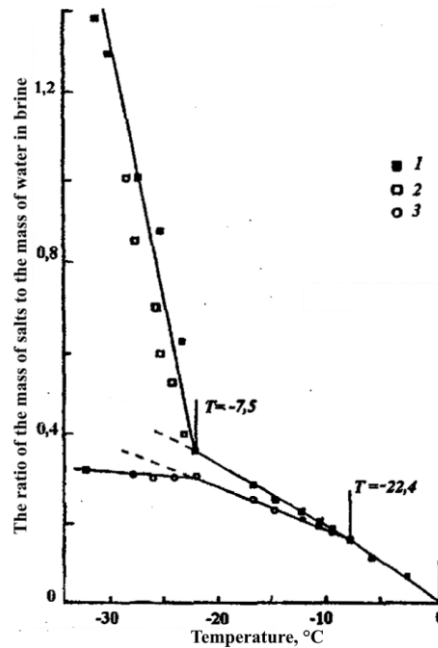

Figure 1.6 – Chart of equilibrium salt concentrations in sea ice [51]

Table 1.1 – The values of empirical coefficients according to [51]

Ice temperature T_i, °C	Coefficient			
	α, °K^{-1}	β, °K^{-1}	k	l
$0 \geq T \geq -7.5$	-0.01848	-0.01848	0	0
$-7.5 \geq T \geq -22.4$	-0.01367	-0.01077	0.0332	0.0567
$-22.4 \geq T \geq -30.0$	-0.10567	-0.00532	-1.9920	0.1677
Notation: the boundaries of temperature ranges are determined by the points of deposition of salts $Na_2SO_4 \cdot 10H_2O$ (at -7,5 °C) and $NaCl \cdot 2H_2O$ (at -22,4 °C) [51].				

Brine volume v_b, ‰, is also used in practice. Nazintsev Yu. L. suggests the following formula for determining the brine volume

$$v_b = \frac{m_b \rho_{si}}{\rho_b},$$ (1.19)

where ρ_{si} – sea ice density g/cm^3;

ρ_b – brine density g/cm^3.

USA researchers Frankenstein and Garner (1967) [21] propose to determine v_b by the equation

$$v_b = s_i \left(\frac{a}{|T_i|} + b \right), \tag{1.20}$$

where a and b – empirical coefficients presented in the Table 1.2.

Table 1.2 – Empirical coefficients a and b according to Frankenstein and Garner [21]

Ice temperature T_i, °C	Coefficient	
	a	b
$-0.5 \geq T \geq -2.06$	52.56	-2.28
$-2.06 > T \geq -8.2$	45.917	0.93
$-8.2 > T \geq -22.9$	43.795	1.189

The equation (1.20) is widely used by many authors, as well as regulatory documents. For cases where a simple but less accurate equation is required Frankenstein and Garner determine the brine volume at temperatures from 0.5 to 20 °C, taking $a = 49.185$ and $b = 0.532$.

Equations for determining the total phase composition of ice have been also described by Cox and Weeks (1983) [14]. Based on previous studies by different authors, Cox and Weeks suggested using some approximating functions to determine the volume fractions of brine, air, and solid salts in sea ice. The volume fractions of brine v_b, air v_a and solid salts v_{ss} according to Cox and Weeks (1983) are respectively defined as follows:

$$v_b = \frac{\rho_{si} s_i}{F_1(T)}, \tag{1.21}$$

$$v_a = 1 - \frac{\rho_{si}}{\rho_i} + \rho_{si} s_i \frac{F_2(T)}{F_1(T)}, \tag{1.22}$$

$$v_{ss} = C \frac{\rho_b}{\rho_{ss}} + v_b, \tag{1.23}$$

where $F_1(T)$, $F_2(T)$, C – empirical functions of temperature:

$$F_{1,2}(T) = \alpha_0 + \alpha_1 T + \alpha_2 T^2 + \alpha_3 T^3, \tag{1.24}$$

$$C = \frac{F_2(T) - \frac{\rho_b}{\rho_i} + 1}{\frac{\rho_b}{\rho_i} - \frac{\rho_b}{\rho_{ss}}}, \tag{1.25}$$

where $\alpha_0, \alpha_1, \alpha_2, \alpha_3$ – empirical coefficients presented in Table 1.3;

ρ_i – density of pure freshwater ice, t/m³;

ρ_{ss} – the average solid salt density assumed to be constant at 1.5 t/m³ [14].

Nazintsev Yu. L and Panov V. V determine the density of brine ρ_b, t/m³, using the expression obtained by Cox and Weeks (1975) [51]:

$$\rho_b = 1 + 0.0008 s_b \tag{1.26}$$

In equation (1.26) the brine salinity s_b is taken in ‰.

Table 1.3 – Empirical coefficients α_i

Ice temperature T_i, °C		Coefficient			
		α_0	α_1	α_2	α_3
$-2 \geq T \geq -22.9$	F_1	-4.732	-22.45	-0.6397	-0.01074
	F_2	8.903 10⁻²	-1.763 10⁻²	-5.33 10⁻⁴	-8.801 10⁻⁶
$-22.9 > T \geq -30$	F_1	9899	1309	55.27	0.716
	F_2	8.547	1.089	4.518 10⁻²	5.819 10⁻⁴

Kovacs (1997) [39] derived following equation based on ice core measurements made at 10- cm increments through 44 Beaufort Sea winter ice floes shown in the Figure 1.7:

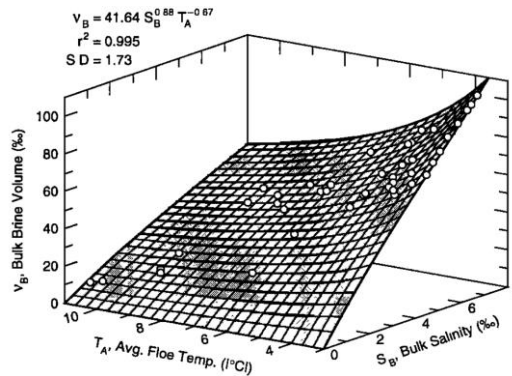$$v_b = 41{,}64 s_i^{0,88}|T|^{-0,67}, \tag{1.27}$$

Figure 1.7 – Sea ice bulk brine volume versus average ice floe temperature and bulk salinity according to Kovacs (1997) [39]

Since in the sea ice there are not only inclusions of brine but also air inclusions, the total porosity of sea ice v_b, volume fraction, is determined by the equation [74]

$$v_t = v_b + v_a, \tag{1.28}$$

where v_b – relative brine volume;

v_a – the relative air volume;

The volume of air in sea ice as well as the methods for determining it are less studied than the volume of brine. In practice, usually the volume fractions of air and solid salts are neglected due to their small value. The equation for determining the total porosity of sea ice v_t, ‰, was obtained by Kovacs (1997) [39]:

$$v_t = 19.37 + 36.18 s_i^{0.91}|T|^{-0.69}, \tag{1.29}$$

1.2.3 Salinity

Sea ice salinity has also been studied for quite a long time. Typically for measuring salinity of sea ice cores are taken. Then the cores are cut into separate plates, placed in separate sealed containers and left until complete melting. After special device (salimeter) is used to measure the electrical conductivity of melt water. On the basis of electrical conductivity and temperature values the salinity is determined [74].

Ryvlin (1974) [61] was one of the first who empirically expressed the salinity of ice s_i, ‰, vs. ice floe thickness. His equation takes into account the seawater salinity and the ice growth rate:

$$s_i = s_w(1 - s_r)e^{-a \cdot h_i^{0.5}} + s_w s_r, \tag{1.30}$$

where s_w – salinity of water, ‰;

h_i – ice thickness, m;

a – growth rate coefficient;

s_r – salinity ratio:

$$s_r = \frac{s_{if}}{s_w}, \tag{1.31}$$

here s_{if} – final bulk salinity at end of growth season, ‰.

Ryvlin A. Ya proposed to use the following values of the parameter a:

$$a = \begin{cases} 0.35 & \text{at } G_R \geq 4 \text{ cm/day} \\ 0.5 & \text{at } G_R \leq 0.5 \text{ cm/day} \end{cases} \tag{1.32}$$

where G_R – ice sheet growth rate, cm/day.

Ryvlin also suggests that where G_R is not known, one may assume the value of 0.5 and $a \approx 0.13$.

At the same time, the salinity of the ice was investigated by American researchers Cox and Weeks (1974) [15]. The authors analyzed the results of measuring the salinity of ice accumulated over several years by many authors as it shown at Figure 1.8 and obtained the following dependences of the salinity s_i, ‰, of ice on its thickness:

$$s_i = \begin{cases} 14.237 - 19.39h_i & \text{at } h_i < 0.4 \text{ m} \\ 7.88 - 1.59h_i & \text{at } h_i \geq 0.4 \text{ m} \end{cases} \tag{1.33}$$

Large and significant ice studies were performed by Timco and Frederking (1990) [75]. In this paper, the authors analyzed more than 400 tests of small samples and obtained empirical equations for some physical and mechanical properties of ice. As for the salinity of the ice, they used additional data together with the data shown in Figure 1.8 and obtained modified equations:

$$s_i = \begin{cases} 13.4 - 17.4h_i & \text{at } h_i \leq 0.34 \text{ m} \\ 8 - 1.62h_i & \text{at } h_i > 0.34 \text{ m} \end{cases} \tag{1.34}$$
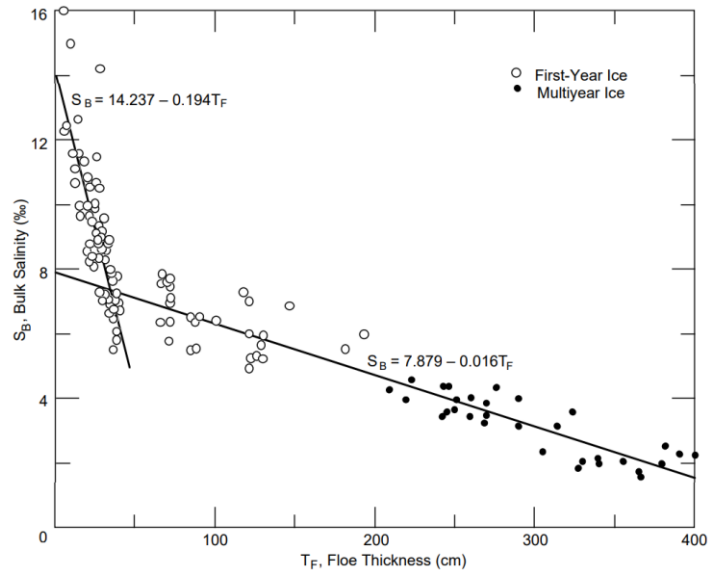
Figure 1.8 – Sea-ice bulk salinity vs. floe thickness according to Cox and Weeks (1974) [15]

Some empirical dependences of ice salinity were obtained by Kovacs (1996) [40] based on the experiments of Fedotov (1973), Cox and Weeks (1974), Ryvlin (1974) and others. He combined all Arctic and Antarctic first-year sea-ice bulk salinity vs. floe thickness data compiled from numerous sources as it shown on Figure 1.9.
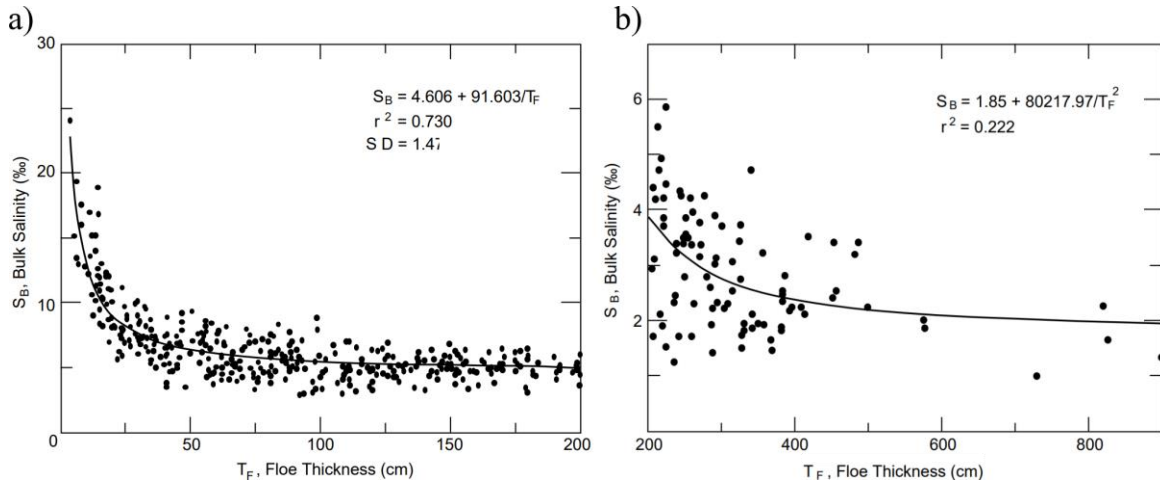
Figure 1.9 – All Arctic and Antarctic sea-ice bulk salinity vs. floe thickness data compiled from numerous sources according to Kovacs (1996) [40]: a) for first-year ice; b) for multi-year ice

For one-year ice, when ice thickness is less than 2 m, the salinity s_i, ‰, according to Kovacs (1996) [40] is determined by equation

$$s_i = 4.606 + \left(\frac{91.603}{h_i}\right),$$ (1.35)

where h_i – ice thickness, sm.

For multi-year ice the salinity s_i, ‰, when ice thickness is from 2 to 9 m, is determined by equation

$$s_i = 1.85 + \left(\frac{80217.9}{h_i^2}\right)$$ (1.36)

17

It should be noted that the square value of the correlation coefficient r^2 obtained by Kovacs for the regression equation (1.35) is 0.730, and for regression equation (1.36) it is equal to 0.222.

1.2.4 Ice density

Ice density is an important property of ice. The density of ice directly affects the buoyancy of ice formations, as well as the load from its own ice weight. The density of ice was studied widely by many authors. Reported values vary over a wide range from 0.72 t/m^3 to 0,94 t/m^3 [74].

Nazintsev Yu. L and Panov V. V [51] determine the density of pure freshwater ice $\rho_i(T)$, t/m^3, by the equation

$$\rho_i = \frac{\rho_0}{1 + \gamma T},$$ (1.37)

where ρ_0 – pure freshwater ice density at 0 °C equal to 916.8 kg/m^3;

γ – bulk ice thermal expansion coefficient equal to 1.58·10^{-4} K^{-1}.

Nazintsev Yu. L [51] also performed calculations of the phase composition of sea ice using equations (1.16)-(1.19). The density of sea ice ρ_{si}, t/m^3, he determined by the equation

$$\rho_{si} = \frac{\rho_0}{1 + 1.65 \cdot 10^{-4} \cdot T}$$ (1.38)

Cox and Weeks (1983) [14] used the following equation, that was calculated by Pounder (1965), to determine the density of pure freshwater ice ρ_i, t/m^3, which is directly or indirectly used in equations (1.21)-(1.25):

$$\rho_i = 0.917 - 1.403 \cdot 10^{-4}T$$ (1.39)

Authors also suggests the expression for determining the density of sea ice ρ_{si}, t/m^3, taking into account its gas and brine volumes [14]:

$$\rho_{si} = (1 - v_a)\frac{\rho_i \cdot F_1(T)}{F_1(T) - \rho_i \cdot s_i \cdot F_2(T)},$$ (1.40)

where v_a – relative air volume, volume fraction;

$F_1(T)$, $F_2(T)$ – empirical functions of temperature determined by equation (1.24).

If we accept that there are no air inclusions in the ice, i.e. $v_a = 0$, the density of sea ice can be easily determined.

Some empirical equation for determining the density of ice monocrystals was used by Gammon et al. (1983) [25] in series of experiments for obtaining elastic properties of ice:

$$\rho_i = \frac{\rho_0}{1 + 1.576 \cdot 10^{-4}T - 2.778 \cdot 10^{-7}T^2 + 8.850 \cdot 10^{-9}T^3 - 1.778 \cdot 10^{-10}T^4}$$ (1.41)

According to authors the equation (1.41) gives the maximum standard deviation ±1.5%.

1.3 Mechanical properties of ice

1.3.1 Elastic properties

As in the case of most materials, under small loads, deformations are recoverable and proportional to stresses according to Hooke's law [66]:

$$\sigma_{ij} = C_{ijkl}\varepsilon_{kl}, \tag{1.42}$$

C_{ijkl} – elastic stiffness constants, Pa;

σ_{ij} and ε_{kl} – the components of stress and strain tensors T_σ and T_ε respectively:

$$T_\sigma = \begin{bmatrix} \sigma_{11} & \sigma_{12} & \sigma_{13} \\ \sigma_{12} & \sigma_{22} & \sigma_{23} \\ \sigma_{13} & \sigma_{23} & \sigma_{33} \end{bmatrix} = \begin{bmatrix} \sigma_1 & \sigma_6 & \sigma_5 \\ \sigma_6 & \sigma_2 & \sigma_4 \\ \sigma_5 & \sigma_4 & \sigma_3 \end{bmatrix},$$

$$T_\varepsilon = \begin{bmatrix} \varepsilon_{11} & \varepsilon_{12} & \varepsilon_{13} \\ \varepsilon_{12} & \varepsilon_{22} & \varepsilon_{23} \\ \varepsilon_{13} & \varepsilon_{23} & \varepsilon_{33} \end{bmatrix} = \begin{bmatrix} \varepsilon_1 & \varepsilon_6 & \varepsilon_5 \\ \varepsilon_6 & \varepsilon_2 & \varepsilon_4 \\ \varepsilon_5 & \varepsilon_4 & \varepsilon_3 \end{bmatrix}$$

Ih ice possesses only five independent stiffness constants: $C_{11}, C_{12}, C_{13}, C_{33}, C_{44}$ which are parameters of the material that characterize the ability of a material to deform elastically. The stiffness matrix for monocrystals of ice Ih become [66]:

$$C_{ij} = \begin{pmatrix} C_{11} & C_{12} & C_{13} & 0 & 0 & 0 \\ C_{12} & C_{11} & C_{13} & 0 & 0 & 0 \\ C_{13} & C_{13} & C_{33} & 0 & 0 & 0 \\ 0 & 0 & 0 & C_{44} & 0 & 0 \\ 0 & 0 & 0 & 0 & C_{44} & 0 \\ 0 & 0 & 0 & 0 & 0 & 1/2(C_{11} - C_{12}) \end{pmatrix}$$

These constants are expressed with respect to a rectangular coordinate system whose axes are specified in terms of the unit cell of the monocrystal. For ice Ih, axis X_3 is parallel to the c-axis and X_1 and X_2 may be taken as any pair of axes within the basal plane.

The values have been obtained by Gammon et al. (1983) [25]. They applied the method of Brillouin spectroscopy in which incident laser light was scattered from thermally induced acoustic waves and Doppler shifted. Table1.4 lists the weighted mean elastic constants calculated from the four sets of Brillouin measurements, along with several quantities derived from these elastic constants.

The values in Table 1.4 were established using the value of the ice density calculated by the equation (1.41). The authors also derived an equation for determining the values of stiffness coefficients at other temperatures. According to value Gammon et al. (1983) the value $C(T)$ of any of the fundamental stuffiness constants at temperature T may be given by the relationship:

$$C(T) = C(T_r) \cdot \left(1 - a(T - T_r)\right), \tag{1.43}$$

where T_r – reference temperature at which the constant was measured;

a – empirical factor equal to $1.42 \cdot 10^{-3} \text{ K}^{-1}$.

Table 1.4 – Elastic parameters for ice monocrystals at -16 °C [25, 66]

Property	Units	Symbol	Value
Dynamic elastic moduli	GPa	C_{11}	13.929 ± 0.041
		C_{12}	7.082 ± 0.039
		C_{13}	5.765 ± 0.023
		C_{33}	15.010 ± 0.046
		C_{44}	3.014 ± 0.011
Bulk modulus	GPa	K	8.899 ± 0.017
Poisson's ratio	-	μ_{12}	0.415
		μ_{13}	0.224
		μ_{31}	0.274

Thus, the authors determined the elastic properties of the ice monocrystals. In addition, the desired values are the so-called "true" values. Since the elastic modulus has a strong dependence on the strain rate and the time of their action, there is a true elastic modulus and effective elastic modulus.

The true elastic modulus of ice characterizes the deformation of a purely elastic, time-independent character [33]. Its value is determined using dynamic measurements and therefore it is often called the dynamic modulus of elasticity. An effective modulus characterizes time-dependent recoverable and inelastic non-recoverable deformations. The effective modulus is determined by static methods, and therefore it is sometimes called the static modulus of elasticity. The effective modulus is lower than the true modulus of elasticity.

Since the problems solved in this work have a scale much larger than the scale of the microstructure of one ice crystal, the best solution would be to consider the properties of polycrystals of ice Ih. In principle the elastic properties of polycrystals free from porosity, inclusions and other defects can be calculated from the fundamental elastic constants and from the orientations, sizes and shapes of the grains [66]. In this case, two approaches can be considered to determining the elastic characteristics of ice formation:

- consider that the ice feature has isotropic properties if we accept the fact that ice crystals or grains are randomly oriented in space throughout the ice body;

- consider the ice growth process described earlier. Since the ice texture develops during growth and in most cases has more or less established orientation of crystals and *c*-axes, in this case we can say that ice formations will have orthotropic properties.

Isotropic elasticity. First, let's consider the elastic properties of ice features, in the case of isotropy. Elastic properties in that case are completely described by only two independent constants, chosen from

Young's modulus E, the shear modulus G, Poisson's ratio ν and the bulk modulus K [66]. Any combination of the two parameters described above can be represented, since they are interdependent and the equations for their determination are well known from the strength of materials, for example:

$$G = \frac{E}{2(1 + \mu)}, \tag{1.44}$$

$$K = \frac{E}{3(1 - 2\mu)}, \tag{1.45}$$

It is more common to talk about the most widely used elastic parameters: Poisson's ratio and Young's modulus. The modulus of ice is a strong function of the loading rate, temperature, grain size, and ice type. A large number of studies have been performed to determine the modulus of elasticity of ice.

The true values of the parameters of ice elasticity were also calculated by Gammon et al. (1983) [25] based on acoustic measurements. These values are presented In Table 1.5.

Table 1.5 – Polycrystalline (isotropic) averaged elastic parameters at temperature -16 °C [25]

Property	Units	Symbol	Value
Bulk modulus	GPa	K	8.899
Young's modulus		E	9.332
Shear modulus		G	3.521
Poisson's ratio	-	μ	0.325
Lame constants	GPa	λ	6.551
		μ	3.521

The dynamic modulus of elasticity $E_{i,d}$ and static modulus of elasticity $E_{i,s}$, GPa, of freshwater ice can be determined by the following equations [41]:

$$E_{i,d} = 9.21(1 - 0.00146T), \tag{1.46}$$

$$E_{i,s} = 5.69 - 0.0648T, \tag{1.47}$$

where T – ice temperature, °C.

For sea ice, the elastic modulus also depends on the brine volume. The dependence of the modulus of elasticity of sea ice E_{si}, GPa, on the volume of brine was proposed by Weeks and Assur (1967) [81]:

$$E_{si} = E_i(1 - \nu_b)^4, \tag{1.48}$$

where E_i – modulus of elasticity of freshwater ice, MPa;

ν_b – brine volume fraction.

An equation that directly defines the effective modulus of elasticity of sea ice proposed by

Vaundrey (1997) [78]. This equation is used in international ISO/FDIS 19906:2019(E) standard:

$$E_{si,s} = 5.316 - 0.436\nu_b^{0.5}, \tag{1.49}$$

Langleben and Pounder (1963) [42] processed the results of over 300 measurements of elastic modulus of sea ice from several locations in the Canadian Arctic and Greenland. They obtained a linear relation between elastic modulus and brine volume with a small scatter of data as presented in Figure 1.10. True elastic modulus of sea ice $E_{si,d}$, GPa, as function of brine volume according to Langleben and Pounder (1963) [42] is defined as follows
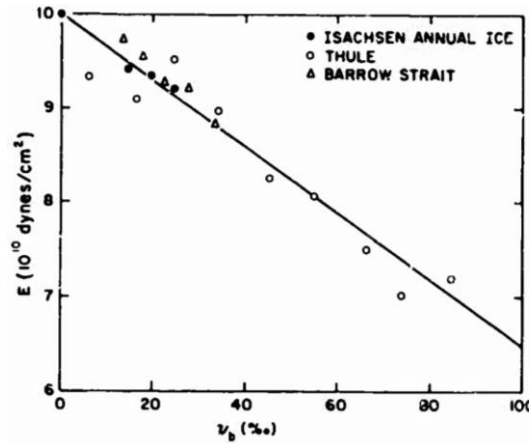
$$E_{si,d} = 10 - 35.1\nu_b, \tag{1.50}$$

Figure 1.10 – Elastic modulus as a function of brine volume for first-year sea ice according to [42]

The equations for determining the dynamic elastic modulus according to the Abele and Frankenstein (1966) and Tabata (1958), respectively, are presented in [8] as follows

$$E_{si,d} = 9.01 - 46.4\nu_b, \tag{1.51}$$

$$E_{si,d} = 9.27 - 28.2\nu, \tag{1.52}$$

In equations (1.46)-(1.52) ν_b is the brine volume fraction and ν is total porosity.

Poisson's ratio is one of the main mechanical properties that characterize the behavior of a material under load. Poisson's ratio μ is defined as the ratio of the lateral strain to the longitudinal strain in a homogeneous material for a uniaxial loading condition. The Poisson's ratio, just like the elastic modulus, can be dynamic and static (true and effective).

One of the earliest proceedings in which an equation was proposed for determining the Poisson's ratio is a monograph by Weeks and Assur (1967) [81]. Authors obtained the following formula of dynamic Poisson's ratio $\mu_{i,d}$ based on *in-situ* seismic observations of Lin'kov (1958) at Kap Shmit, Siberia:

$$\mu_{i,d} = 0.333 + 0.06105 \exp\left(\frac{T}{5.48}\right) \tag{1.53}$$
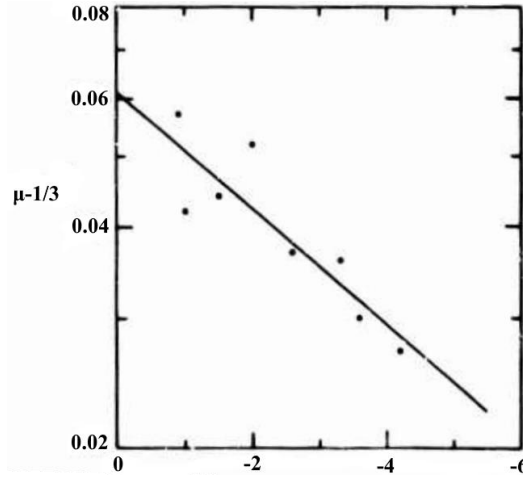
Figure 1.11 – ($\mu - 1/3$) vs ice temperature, based on in-situ seismic determinations [81]

Murat and Lainey (1982) [49] measured the longitudinal and transverse strains on simply supported beams loaded in flexure. The tests were performed at different temperatures and loading rates on columnar ice. As a result, authors proposed the following equations for the effective (static) Poisson's ratio $\mu_{i,s}$:

$$\mu_{i,s} = 0.24 \left(\frac{\dot{\sigma}}{\dot{\sigma}_1}\right)^{-0.29} + \mu_{i,d}, \tag{1.54}$$

$$\mu_{i,s} = 0.0024 \left(\frac{\dot{\varepsilon}}{\dot{\varepsilon}_1}\right)^{-0.29} + \mu_{i,d}, \tag{1.55}$$

where $\dot{\sigma}$ and $\dot{\sigma}_1$ – stress rate and unit stress rate respectively, kPa·s⁻¹; $\dot{\sigma}_1 = 1 \text{ kPa} \cdot \text{s}^{-1}$;

$\dot{\varepsilon}$ and $\dot{\varepsilon}_1$ – strain rate and unit strain rate respectively, s⁻¹; $\dot{\varepsilon}_1 = 1 \text{ s}^{-1}$.

Orthotropic elasticity. If to take into account the ice growth process of ice feature, it can be said that the structure of the sheet has three mutually perpendicular mirror planes (two in the vertical plane) and so possesses orthotropic symmetry [66]. In this case elastic properties of ice formations can be described by three Young's moduli E_1, E_2, E_3, by the three shear moduli G_{12}, G_{13}, G_{23}, and to six Poisson's ratios μ_{12}, μ_{21}, μ_{13}, μ_{31}, μ_{23}, μ_{32} (where $\mu_{ij} = -\varepsilon_j/\varepsilon_i$ and i – direction of uniaxial loading).

Schulson E. M., Duval P. (2009) calculated the values of these parameters for 3 texture types of ice sheets, denoted S1, S2 and S3 ice. These values are presented in Table 1.6 and related with rectangular coordinate system where X_1 and X_2 lie within the horizontal plane of the sheet and X_3 is parallel to the vertical direction. In ice S1 c-axes are parallel to X_3, in ice S2 c-axes are randomly oriented in X_1–X_2 plane and in ice S3 c-axes are parallel to X_1.

The most convenient approach for modeling ice properties is to consider both isotropic and orthotropic elasticity regarding to ice structure. As it was mentioned in subsection 1.2 ice in general there are two different types of ice structure in ice floe. Top part of ice field is granular ice with more or less randomly oriented c-axes. For this type of ice isotropic elastic properties can be considered. On the

other hand, bottom layers of ice floe are composed of columnar ice. This type of ice has different parameters of elasticity and strength in vertical and horizontal directions, so it should be considered as orthotropic ice.

Table 1.6 – Elastic properties of homogeneous orthotropic sheets of ice Ih at -16 °C [66]

Texture	Young's modulus E, GPa			Shear modulus G, GPa			Poisson's ratio					
	E_1	E_2	E_3	G_{12}	G_{13}	G_{23}	μ_{12}	μ_{21}	μ_{13}	μ_{31}	μ_{23}	μ_{32}
S1	9.71	9.71	11.8	3.42	3.01	3.01	0.415	0.415	0.224	0.274	0.224	0.274
S2	9.58	9.58	9.71	3.61	3.21	3.21	0.327	0.327	0.344	0.320	0.344	0.320
S3	11.8	9.71	9.71	3.01	3.01	3.42	0.274	0.224	0.274	0.224	0.415	0.415

1.3.2 Compressive strength

The compressive strength is another fundamental property of sea ice. The destruction of ice during its impact on vertical structures occurs mainly due to the stresses reaching the compressive strength. Thus, the compressive strength of ice plays the largest role in the magnitude of the load on the vertical offshore structures.

Uniaxial compressive strength. The typical apparatus of compressive strength measurements is shown in Figure 1.12 [74]. To conduct the compressive strength test, cores of sea ice usually are cut into cylinders. The samples are placed in a test apparatus that can generate high loads. A load cell is included in-line to measure the applied load. Among the important factors affecting the results of the experiment are the stiffness of the testing machine, the parallelism of the faces of the samples, as well as the aspect ratio and shape of the samples [66].
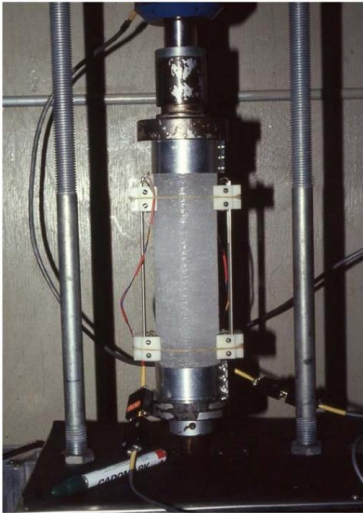

Figure 1.12 – Typical apparatus for a uniaxial compression test on ice [74]

Many investigators measured the compressive strength of sea ice. Based on their research, it can be said that the compressive strength of sea ice depends on many factors. Among such factors, one can especially distinguish the strain rate, the texture of ice, temperature and porosity.

If we talk about the strain rate, then it plays a very large role in the behavior of ice during compression. It is well known that ice in compression can exhibit both plastic and brittle behavior depending on the strain rate as presented in Figure 1.13. This property of ice has been observed and confirmed by many authors.
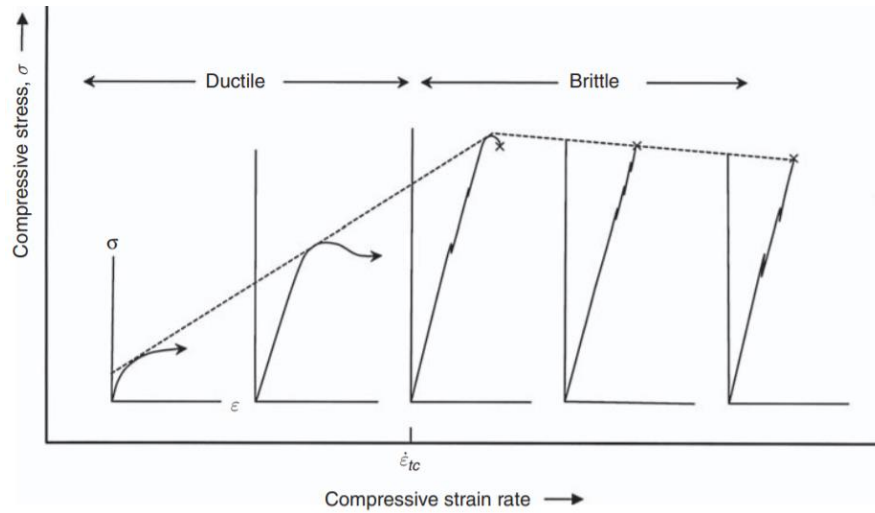

Figure 1.13 – Schematic compressive stress–strain curves [66]

At low strain rates, usually less than 10^{-4} s^{-1}, the ice exhibits plastic behavior, which is characterized by a smooth stress-strain curve and hardening. Also, at these speeds, the compressive strength of ice is little dependent on grain size, but slowly increases with decreasing grain size [13] as presented in Figure 1.14 (a).
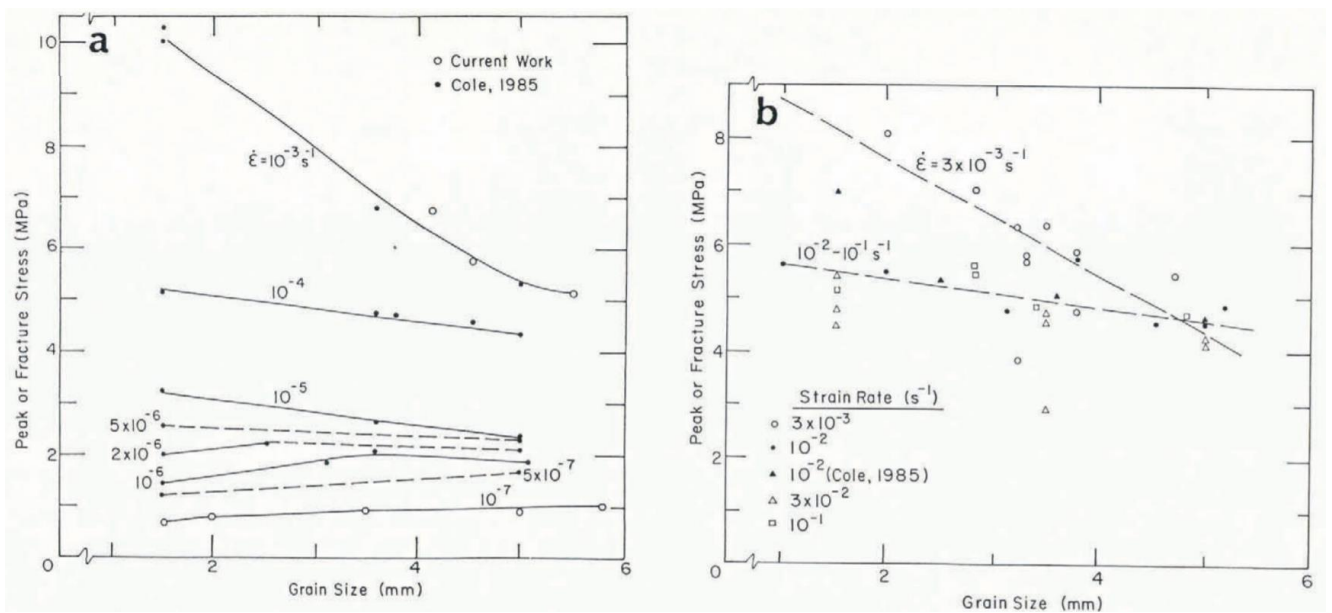

Figure 1.14 – Peak stress vs grain-size: a) strain-rates between 10^{-7} and 10^{-3} s^{-1}; b) strain-rates between $3 \cdot 10^{-3}$ and 10^{-1} s^{-1}

The brittle behavior of ice can be observed at strain rates of 10^{-3} and higher. Stress-strain curves in this case are close to linear in shape as shown in the Figure 1.13. Also, these curves are characterized by small "drops" associated with the appearance and development of microcracks. The effect of grain size in this case is stronger than with plastic behavior as presented in the Figure 1.14 (b).

A consequence of both strain-rate hardening (ductile regime) and strain-rate softening (brittle regime) is that the compressive strength reaches a maximum at the ductile-to-brittle transition and at strain rate from 10^{-4} to 10^{-3} s^{-1} [13, 28, 65, 66, 67]. Thus, the transition from plastic to brittle behavior does not occur instantly. The reason is that the overall inelastic deformation comprises a mixture of creep via dislocation slip and cracking, the proportion of which varies in the vicinity of the transition [66]. In Figure 1.13, the transition point is characterized by a strain rate equal to $\dot{\varepsilon}_{tc}$. The magnitude of these strain rates, i.e., the rates of ductile-brittle transition, has been studied many times and ranges from about 10^{-4} to 10^{-3} s^{-1}. Since the ice strength is maximum at these rates, today the ice load acting on the structures is calculated precisely at the strength corresponding to this transition zone. This behavior is exhibited by both single crystals and polycrystals. Typical results of ice compression experiments showing the dependence of strength on the strain rate are shown in Figure 1.15, Figure 1.16 and Figure 1.17.
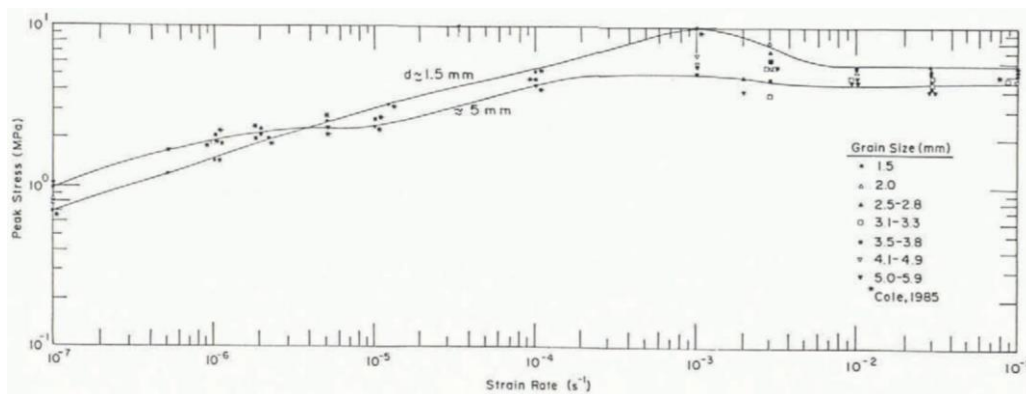

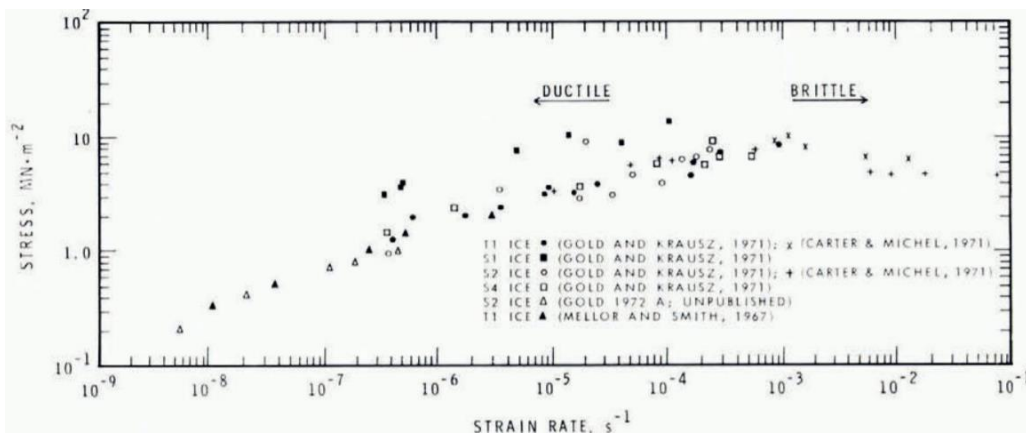Figure 1.15 – Peak stress vs strain-rate in experiments of Cole D. M. [13]

Figure 1.16 – Strain rate dependence of compressive strength of ice according to Gold L. W. [28]
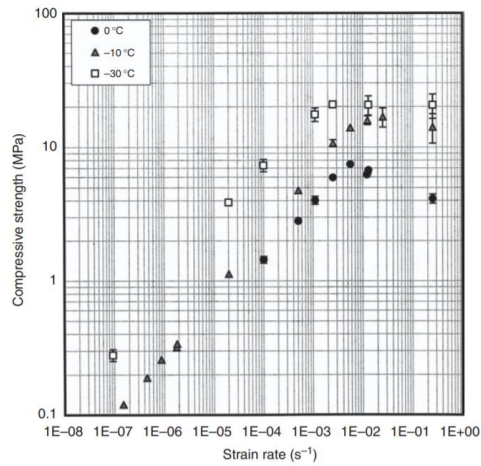
Figure 1.17 – Unconfined compressive strength of single crystals of ice vs. strain rate [66]

It is also worth considering the effect of load direction on ice strength. The direction of the load on the strength was investigated to a much lesser extent. Nevertheless, today the fact is known that the compressive strength of ice reaches its minimum when the load direction is oriented at an angle of 45 degrees to the c-axes [66]. This feature is confirmed by the studies of Payton (1966) [67] and Carter (1971) [66] as shown in figures below. In Figure 1.18 the loading-angle notation is as follows: the first number gives the angle between the axis of the test cylinder and the vertical, while the second number gives the angle between the sample and the c-axis of the single ice crystal being tested.
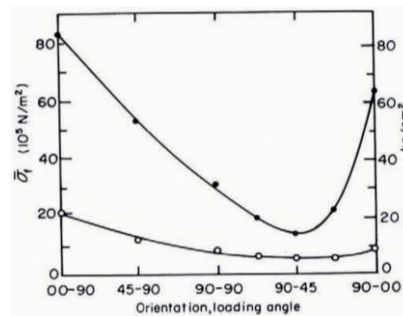

Figure 1.18 – Average failure strength in compression (solid circles) and in direct tension (open circles) versus sample orientation [67]
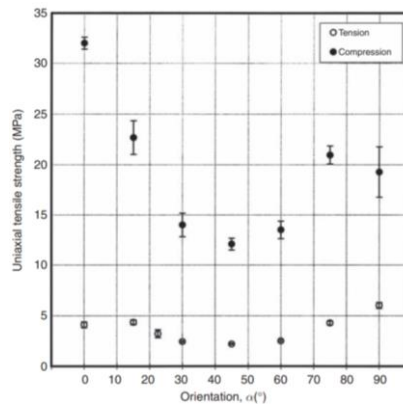

Figure 1.19 – Unconfined brittle compressive strength (and tensile strength) of single crystals of ice at −10 °C vs. orientation of the basal plane [66]

Schulson E. M. and Duval P (2009) collected a data from uniaxial compression experiments performed by many authors such as: Jones (1997), Schulson et al. (2005) and Shazly et al. (2006) as presented in the Figure 1.20. Taken collectively, the measurements indicate that dynamic strength σ_c, MPa, at -10 °C may be described by the following relationship with variance r^2 equal to 0.71 [66]:

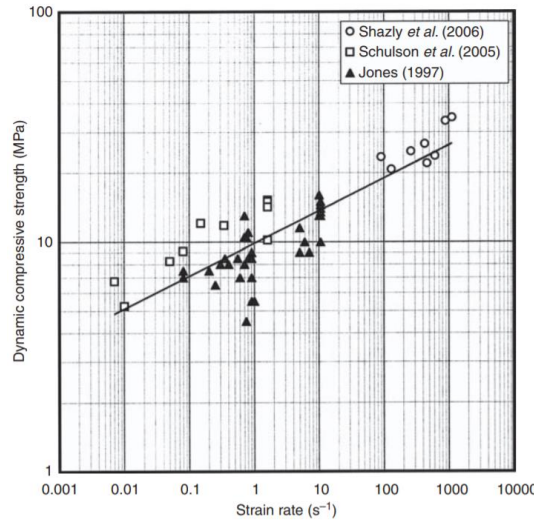$$\sigma_c = 9.8(\dot{\varepsilon})^{0.14}, \tag{1.56}$$

Figure 1.20 – The compressive strength of ice at -10 °C according to Schulson and Duval (2009)

Timco and Frederking (1990) [75] developed some equations for calculating the compressive strength of sea ice sheets. They compiled 283 compressive strength test results on first-year sea ice. They derived the equations for the uniaxial compressive strength of first-year sea ice for several different grain structures. For horizontally loaded columnar ice, the uniaxial compressive strength σ_c, MPa, is defined as follows

$$\sigma_c = 37(\dot{\varepsilon})^{0.22}\left(1 - \sqrt{\frac{v_t}{270}}\right), \tag{1.57}$$

where $\dot{\varepsilon}$ – strain rate, s^{-1};

v_t – total porosity, ‰.

For vertically loaded columnar ice, the uniaxial compressive strength σ_c, MPa is defined as follows

$$\sigma_c = 160(\dot{\varepsilon})^{0.22}\left(1 - \sqrt{\frac{v_t}{200}}\right) \tag{1.58}$$

For granular ice, the uniaxial compressive strength σ_c, MPa is defined as follows

$$\sigma_c = 49(\dot{\varepsilon})^{0.22}\left(1 - \sqrt{\frac{v_t}{280}}\right) \tag{1.59}$$

The applicable range of strain rates for these equations is from 10^{-7} s^{-1} to about $2 \cdot 10^{-4}$ s^{-1}.

Kovacs (1997) [39] obtained the following equation for the unconfined compressive strength of first-year sea ice floes

$$\sigma_c = B_2(\dot{\varepsilon})^{1/n}v_t^m, \tag{1.60}$$

where B_2, n and m – empirical parameters, values of which can be taken equal $B_2 = 2700$, $n = 3$, $m = -1$.

Compressive strength of confined ice. The above features and the presented equations are obtained on the basis of uniaxial compression strength tests of ice. However, when ice fields interact with structures, a complex stress-strain state arises in them. In this case, it would be incorrect to characterize this state by the ice strength characteristics obtained from uniaxial tests. Therefore, in recent years, studies on the strength of ice under "confined" conditions corresponding to biaxial and triaxial stress states of the ice sheet have begun to appear more often. The confinement induces biaxial and triaxial stress states, which have a large effect on the strength of the ice and on its mode of failure [66].

There are several ways to perform biaxial and triaxial compression experiments on ice samples, such as: triaxial loading using pressurized fluid, passive proportional loading, true triaxial loading and indentation. The most convenient is the true triaxial loading method, because the three principal stresses σ_1, σ_2 and σ_3 (σ_1 is taken as the most compressive stress) can be varied independently and all loading paths in principal stress space can be explored, including biaxial ones. The loading paths in this method of testing are defined by the ratio $(\sigma_1 : \sigma_2 : \sigma_3) = (1 : R_{21} : R_{31})$, where $R_{21} = \sigma_2 / \sigma_1 \leq 1$ and $R_{31} = \sigma_3 / \sigma_1 \leq 1$.

To consider the behavior of confined ice during compression, it is better to consider granular and columnar ice separately. As mentioned earlier, polycrystalline granular ice has a random orientation of single crystals and therefore can be considered as isotropic.

Some features of the behavior of granular ice during compression can be made based on the results of experiments performed by Weiss and Schulson (1994) [82]. Authors used cubes (l55 mm on edges) of fresh-water ice to investigate the failure of granular ice under multiaxial compressive loading using solids platens at temperatures -10 °C, -20°C and -40 °C at a strain-rate of 10^{-3} s^{-1}. Some particular triaxial tests with $\sigma_2 = \sigma_1$ (and $\sigma_3 = R\sigma_1$), as well as biaxial tests ($\sigma_3 = 0$, $\sigma_2 = R\sigma_1$) showed that the intermediate principal stress σ_2 bas no significant effect on the compressive strength in either the low-confinement or the high-confinement regime. Indeed within the scatter of the data, failure stress σ_{1f} biaxial tests is roughly equal to the uniaxial failure stress [82].

With triaxial compression of granular ice, an increase in compressive strength is observed. Under triaxial loading the confining stress acts upon all inclined primary cracks, regardless of orientation. Consequently, it raises the maximum principal stress to effect sliding and crack growth, thereby increasing strength [66]. As in case of biaxial tests the triaxial strength appears to be independent of the intermediate principal stress. In this regard, many authors determine the strength of ice by the stress difference $(\sigma_1 - \sigma_3)$ known as the differential stress at failure. Generally speaking, under lower confinement, the stress difference increases with increasing pressure and under higher confinement, the stress difference is independent of pressure as presented in Figure 1.21 and Figure 1.22. This feature was

investigated by many authors [34, 59, 66, 82]. In the case of columnar ice, a different picture is observed due to anisotropic properties.
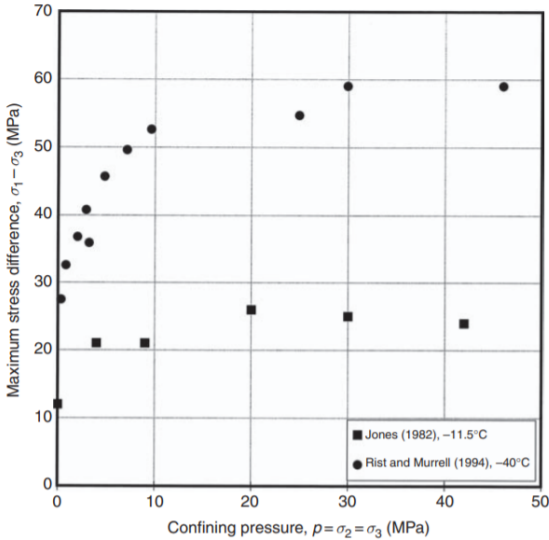

Figure 1.21 – Maximum differential stress vs. confining pressure for fresh-water granular ice of 1 mm grain size [66]
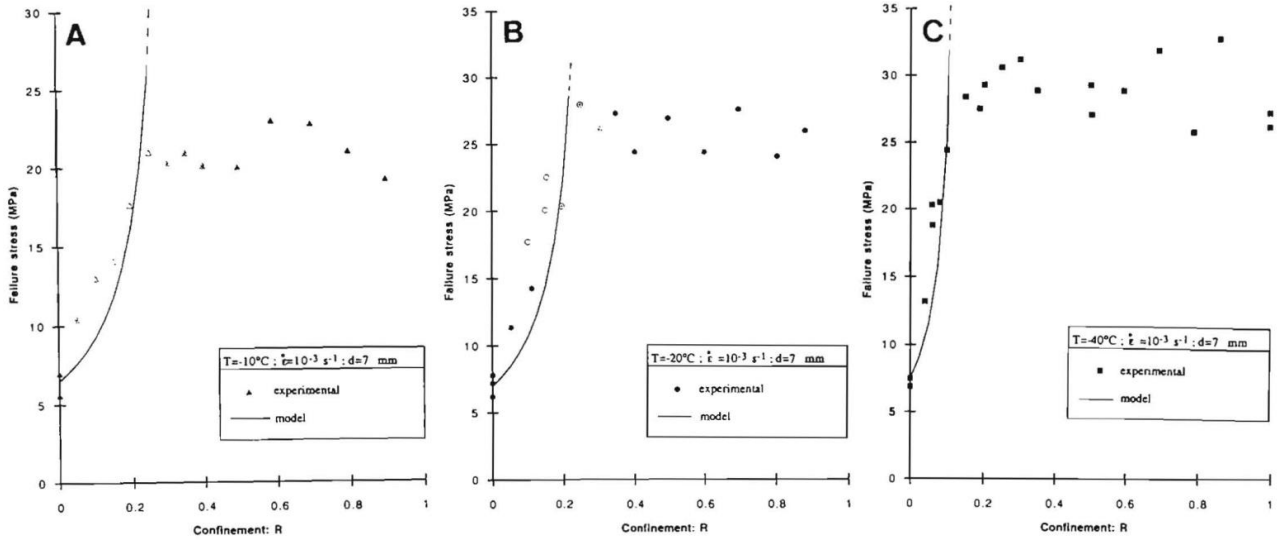

Figure 1.22 – Failure stress of ice vs. confining ratio according to Weiss and Schulson (1994) [82]

1.3.3 Tensile and shear strengths

The tensile and shear strengths of ice are less studied than compressive one, because of difficulties of conducting experiments. However, some authors presented results of their investigations described below.

The tensile strength of ice increases with decreasing temperature, but the values of ice tensile strength can be several times less than the compressive strength. There are several methods to investigate

the tensile strength of ice, but the most usable is direct tensile test. If talk about single crystals of ice, sufficient study of tensile behavior was performed by Carter (1971). His study was described by Schulson and Duval (2009) [66]. Carter performed over 600 tests on cylindrical-shaped Ø50x150 mm crystals of fresh-water ice loaded under either tension or compression at strain rates from $4 \cdot 10^{-7}$ s^{-1} to $2.5 \cdot 10^{-1}$ s^{-1} at temperatures from -30 °C to 0 °C. He also varied the orientation of the crystallographic *c*-axis, from angle equal from 0° to 90° with respect to the tensile axis. He examined the following facts which was described earlier:

- when deformed at strain rates below about 10^{-4} s^{-1} ice single crystals showed ductile behavior and while at rates above about 10^{-3} s^{-1} they showed brittle behavior. Between these limits they exhibit transitional behavior.

- the brittle tensile strength is essentially independent of strain rate and temperature but depends strongly upon the orientation of the *c*-axis as presented in Figure 1.23.

In the case of ice polycrystals, the situation is more complicated due to the influence of the structure and relative position of the crystals in the ice texture. Many factors influence tensile strength such as: temperature, grain size, growth texture and others. It should be mentioned that under "quasistatic" loading polycrystals fail under a tensile stress that is essentially independent of strain rate.
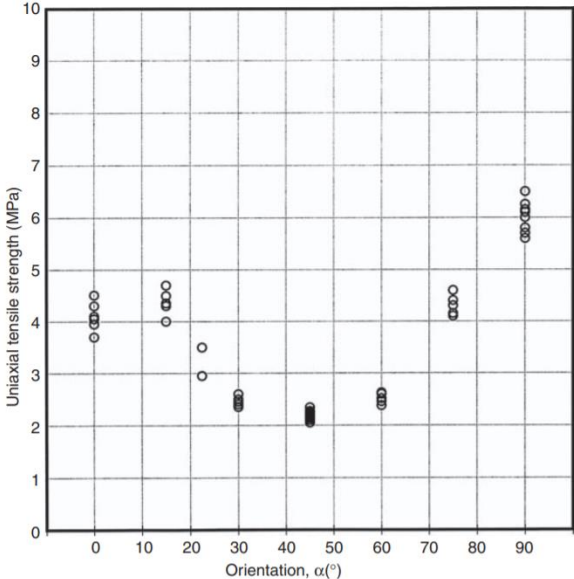

Figure 1.23 – Tensile strength of single crystals of ice at -10 °C vs. orientation α of the basal plane, where α denotes the angle between the *c*-axis and the tensile load [66]

The most famous equations for determining the tensile strength of ice were obtained by Dykins (1967) [21] and Weiss and Meyssonnier (2001) [83]. These equations are used in international standards such as ISO/FDIS 19906:2019(E) [33].

For the vertical direction of columnar ice tensile strength σ_t, MPa is defined as follows

$$\sigma_t = 2.2 \left(1 - \sqrt{\frac{v_b}{310}} \right) \tag{1.61}$$

For the horizontal direction of columnar ice tensile strength σ_t, MPa is defined as follows

$$\sigma_t = 1 \cdot \left(1 - \sqrt{\frac{v_b}{140}}\right) \qquad (1.62)$$

Significant measurements of tensile strength of columnar ice were performed by Richter-Menge and Jones (1993) [58]. Tensile load was applied along the *c*-axes of the test specimens, which were perpendicular to the growth direction of the ice. The data presented in this paper provide information on the tensile behavior of columnar, first-year sea ice at four different temperatures (-20°, -10°, -5° and -3°C) and two strain rates.

Shear strength of ice was measured by Timco and Frederking (1986) [76]:

$$\sigma_\tau = 1.5 \left(1 - \sqrt{\frac{v_b}{390}}\right) \qquad (1.63)$$

1.4 Ice-structure interaction mechanism in case of vertical structures

The interaction of ice with vertical structures can occur under different scenarios and limiting processes. There are 3 limiting processes that are associated with factors limiting the ice load on structures [33, 54]: limit stress process, limit energy (or momentum) process, limit force process which are presented in Figure 1.24.

In the case of limit stress process, the ice formation has enough driving force to begin its destruction during the interaction and its cutting through the support to its full width.

In the case of limit energy (or momentum) process, the ice load is limited by the kinetic energy of the ice formation, depending on its speed and mass. When an ice field collides with a structure, it stops with partial cutting and dissipation of energy.

In the case of limit force process, the load is limited by natural forces acting on the ice formation. After the ice formation stops, it can continue to act on the structure, transferring the load to it under the action of external forces (wind, current, wave or other ice formations).

When assessing the impact of ice on the designed structure, several of the above scenarios are considered, as well as their combinations. Moreover, as a rule, the smallest of the values obtained is taken as the resulting load. However, due to the fact that the choice of ice regime parameter values to the present is a difficult task, the calculated load values should be carefully justified.

Ice load during ice failure has the most important role in assessing the critical condition of a structure. The mode of ice failure against the structure has a significant effect on the magnitude of the ice action. The failure mode for sea ice (e.g. crushing, shear, flexure, creep) depends on parameters such as ice thickness, presence of ridges, ice velocity, ice temperature, structure profile and plan shape, etc.

Also, different modes can occur on the same structure type depending on ice conditions and

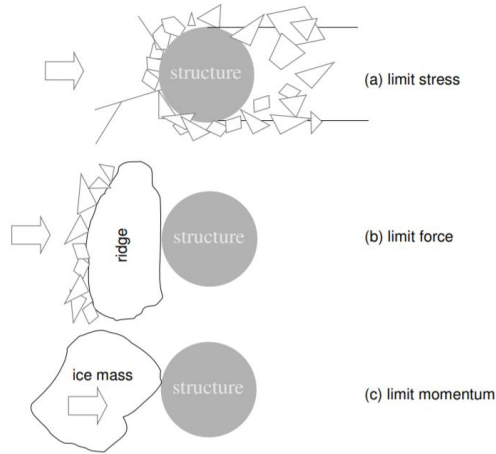interaction velocity, even during the same event as presented in Figure 1.25.

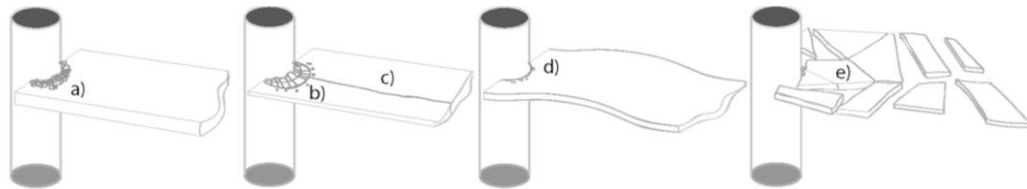Figure 1.24 – Limit factors of ice loads [54]

Figure 1.25 – Failure modes of ice during interaction: a) crushing failure; b) bending failure; c) splitting failure; d) buckling failure; e) pushing floes [42]

The process of ice impact in case of crushing failure mode is shown schematically in the Figure 1.26. One of the main features of this type of interaction is presence of "high pressure zones". These are small areas that quickly appear and disappear randomly at the ice-to-structure contact, on which the main interaction force is concentrated as presented in Figure 1.26. At any one time, there are several HPZs, and they occupy only a small fraction of the nominal contact area, generally but not always towards the middle and away from the edges [54]. The presence of high-pressure zones is justified by the heterogeneous structure and properties of ice and is confirmed by many authors. As a rule, currently used ice load calculation methods, including in normative documents, do not take into account the presence of HPZs. Instead, the so-called nominal contact area is use, which is the projection of the structure onto the ice formation.

a) Ice sheet interaction with the flat surface of a narrow vertical structure   b) Profile of ice sheet interaction with vertical structure
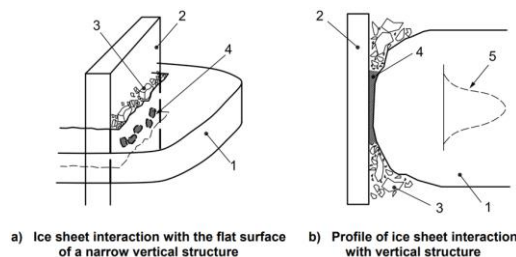
Figure 1.26 – Schematic picture of ice action during ice-structure interaction in case of ice sheet compression (1 – ice sheet; 2 – structure; 3 – spalls and extrusion; 4 – high pressure zones; 5 – pressure distribution over the contact surface) [35]

If circumferential crack is observed the bending type of flexural failure is occurred. Also, many radial cracks can be observed behind this crack. Splitting failures are usually observed when the interacting ice sheet has low lateral confinement or small size. The buckling type of flexural failure is governed by a buildup of curvature in the ice sheet or occurs under special wave conditions. In this regard, this process can be observed very rarely. The last type of interaction corresponds to the limit force process explained before. The floes split and pass around the structure, while wind and wave actions contribute significantly to the total force [53]. Conditions that induce ice failure by flexure generally result in smaller ice actions than for crushing [33]. In addition, the interaction of ice with the structure can cause dynamic loads, which is associated with the periodic destruction of ice during compression.

1.5 Researches in the field of numerical modeling of ice problems

The problem of assessing the impacts of ice fields regarding the destruction of ice is a highly specialized task. The issue of numerical modeling of the destruction of ice is little studied. Some studies with different objectives in the field of numerical modeling of ice have been performed by several researchers: Derradji-Aouat (2005) [18], Bjørnar Sand (2008) [63], J. Pernas-Sánchez et al (2012) [55], Rüdiger von Bock und Polach and Sören Ehlers (2013) [60], Aleksandrov A.A. et al (2014, 2017) [2, 3], Li Liang (2014) [44], Politko V.A. (2018) [56] and others.

J. Pernas-Sánchez et al (2012) performed numerical simulations of experiments conducted by Pereira et al. (2006) and described by Carney et al. (2006) [12]. In these experiments, cylindrical ice projectiles were launched onto a steel plate bounded to a strain gauge using a helium gas gun. The experiment equipment is presented in Figure 1.27. The size of the ice cylinders was 17.5 mm in diameter and 42.2 mm in length. The tests were carried out at different impact speeds.
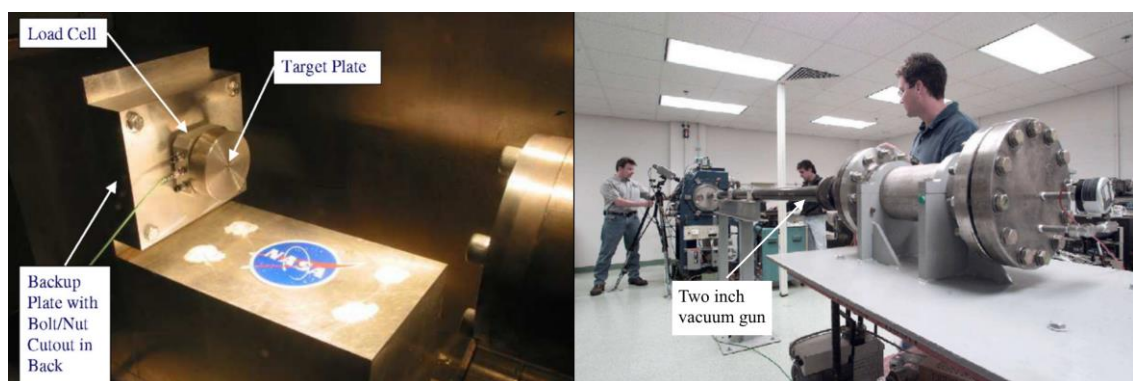

Figure 1.27 – Equipment in the experiments described by Carney et al. (2006)

To perform the numerical simulation, three different numerical methods were used: the finite element method in the Lagrange formulation (Lagrange), the arbitrary Lagrange-Eulerian method (ALE)

and smoothed particle hydrodynamics (SPH) method. Figure 1.28 shows three models of an ice cylinder made by J. Pernas-Sánchez et al.
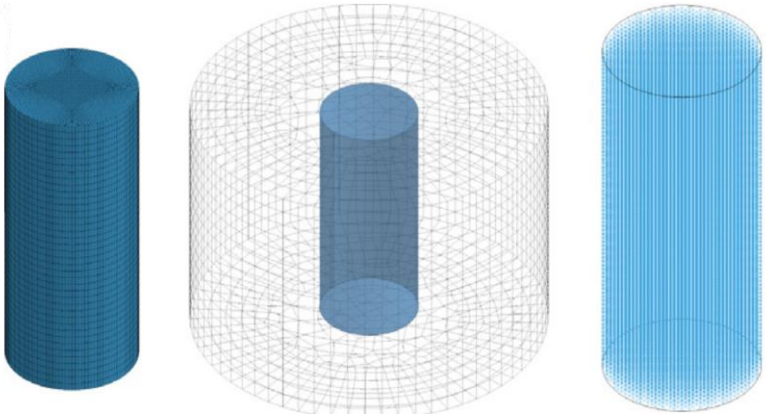

Figure 1.28 – Numerical models of the ice cylinder in the study of J. Pernas-Sánchez [55] (left – Lagrange, in the center – ALE, right – SPH)

To model the ice material at high strain rates, the Drucker-Prager model was chosen. The process of destruction of the ice cylinder when striking a steel plate at a speed of 152 m/s, as well as the dependence of the impact force on the time of the experiment are shown in Figure 1.29.

The Lagrangian finite element solver showed the greatest convergence with experimental data, despite the strong distortion of elements. Based on the results of this study, it can conclude that the Drucker-Prager model shows high convergence with experimental data at high strain rates. However, the real drift velocities of ice fields have values ten times less than in this experiment. In this connection, additional computational studies of the applicability of the Drucker-Prager model are required for modeling the impact of the ice formations on the offshore facilities.
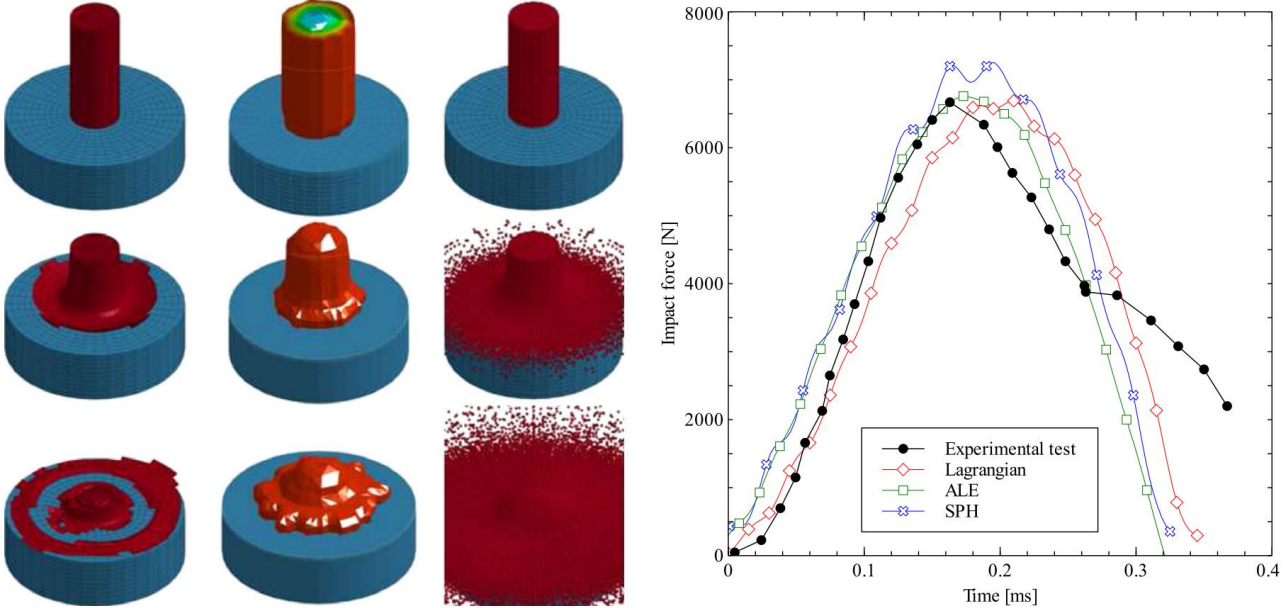

Figure 1.29 – The process of destruction of the ice cylinder on impact (left) and the dependence of the impact force on time (right) for the three numerical methods (from left to right: Lagrange, ALE, SPH)

Aleksandrov A.A. et al (2014, 2017) in their investigations used various approaches to modeling the ice material.

In [2], the authors carried out a computational study in which ice parameters were determined using the ANSYS software (the inverse problem was solved). Prior to the beginning of numerical simulation, the authors conducted experiments on three-point bending of ice beams (700x100x100 mm) and uniaxial compression of ice cubes (100x100x100 mm). Samples were obtained from the bottom layer of ice, which formed naturally on the surface of the freshwater pond. Loading was carried out using a hydraulic cylinder. The indenter had a cylindrical shape when testing beams and a plate shape when testing cubes. A grid of dots, shown in Figure 1.30, was applied to the central part of the samples before each test using a water-based paint. The load force, the geometric dimensions of the sample, and the deformations at the grid nodes on the ice surface were measured.
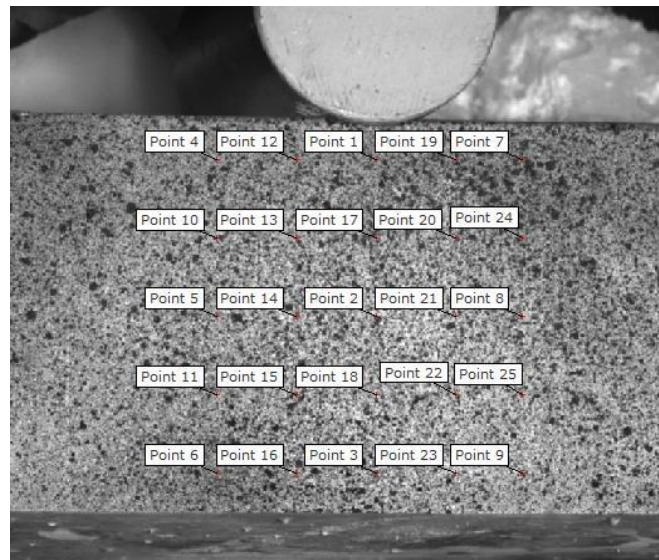

Figure 1.30 – Grid of dots in the center of the ice sample [2]

The mesh motion during the tests was recorded using a three-dimensional computer vision system and digital image correlation for contactless measurements of shape and deformation. The calculation of the elastic modulus of ice was made using the formulas of the standard beam theory. An example of the dependence of the strain values of the samples on the load is shown in Figure 1.31.

To determine the mechanical properties of ice, the authors used an optimization method using the strain values obtained from the experiment. Two models of the material were used to model the ice: the model of an ideally elastic body, which is deformed according to Hooke's law, and the viscoelastic Maxwell model. Shear modulus G, MPa, in these material models was in the following dependence on the modulus of elasticity E, MPa:

$$G = \frac{E}{2(1 + 3\nu)}, \tag{1.64}$$

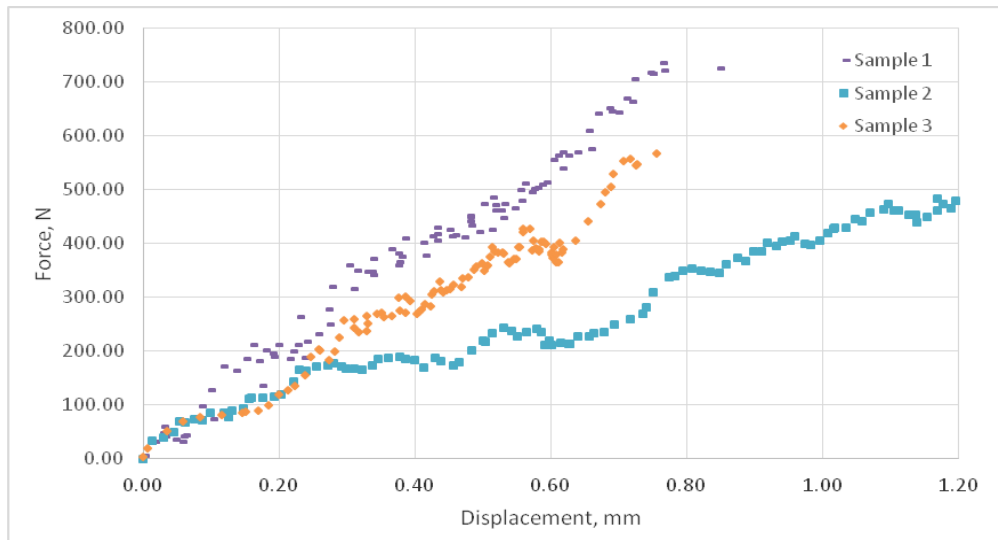where ν – Poisson's ratio, which was taken equal to 0.33.

Figure 1.31 – Dependence of strain on the load at the center of the samples [2]

When determining the parameters of ice by the optimization method for the case of the Maxwell model, the viscosity coefficient η was also determined. The results of optimization are presented in Tables 1.7-1.8.

Table 1.7 – Values of the properties of ice obtained using the standard beam theory and optimization by the finite element method [2]

Sample	Standard beam theory	Numerical simulation (elastic material model)	Numerical simulation (viscoelastic material model)
№ 1	$E = 390\,\text{MPa}$	$E = 490\,\text{MPa}$	$E = 500\,\text{MPa}; \eta = 250\,\text{GPa} \cdot \text{s}$
№ 2	$E = 200\,\text{MPa}$	$E = 220\,\text{MPa}$	$E = 230\,\text{MPa}; \eta = 100\,\text{GPa} \cdot \text{s}$
№ 3	$E = 310\,\text{MPa}$	$E = 390\,\text{MPa}$	$E = 400\,\text{MPa}; \eta = 420\,\text{GPa} \cdot \text{s}$

Table 1.8 – Differences in displacements calculated by various methods relative to the experiments, mm

Sample	The number of compared points	Standard beam theory	Numerical simulation (elastic material model)	Numerical simulation (viscoelastic material model)
№ 1	1	0.031	0.023	0.021
	25	-	0.029	0.026
№ 2	1	0.091	0.119	0.088
	25	-	0.121	0.107
№ 3	1	0.029	0.022	0.018
	25	-	0.029	0.025

Thus, there is little difference between the results of numerical modeling using elastic and viscoelastic material models, but these results are quite different from the results of the calculating the parameters according to the standard beam theory. According to the authors, the Maxwell viscoelastic model shows the greatest convergence with experimental data. In this regard, adding the additional parameters into the material model (in this case, the viscosity coefficient) allows to describe the behavior of ice during deformation more accurately and to obtain more acceptable values of its characteristics.

Also, during bending tests at three points, various types of specimen failure were recorded. The authors identified three main types of damage: fracture due to the formation of a straight crack, fracture in the form of a zigzag crack, and fracture in the form of a curve crack, presented in Figure 1.32.

When searching for the relationship between the type of crack and the parameters of the external load (loading rate, limit values of the load) or the physical and mechanical properties of ice, the authors did not find a correlation.

Figure 1.32 – Typical types of cracks: a) straight, b) zigzag, c) curve [2]

In [3] **Aleksandrov et al.** considered the applicability of numerical modeling for solving the problem of scaling ice loads in the study of ice impacts on vertical structures in the ice pool. According to the authors, numerical modeling can help solve the problem of determining the physical and mechanical properties of ice formations.

First, the authors conducted a series of tests in the ice pool. The block-conductor model was towed in an ice field with low speeds of 0.04÷0.15 m/s, the thickness of the ice field was 20 and 30 mm. During the tests, components of the ice load were recorded.

At the next research step, the authors performed a numerical simulation of the experiments. They proposed the use of the isomorphism principle of the limiting surface to obtain the necessary combination of material parameters. The principle of isomorphism of the limiting surface states that the characteristic form of the limiting surface of the material is preserved. In this case, the limit surface should be understood as the surface in the axes of the main stresses, upon reaching which the material stops to obey the Hook's law of elastic deformation (yield surface). The achievement of yield surface by stresses means the beginning of plastic flow or -is a criterion of brittle fracture.

Based on the proposed principle, the authors solved the numerical problem of introducing a block-conductor model into an ice field in an ice pool. For a finite element modeling, the ANSYS software

was chosen. The block conductor used in the experiments, as well as the finite element model are presented in Figure 1.33.
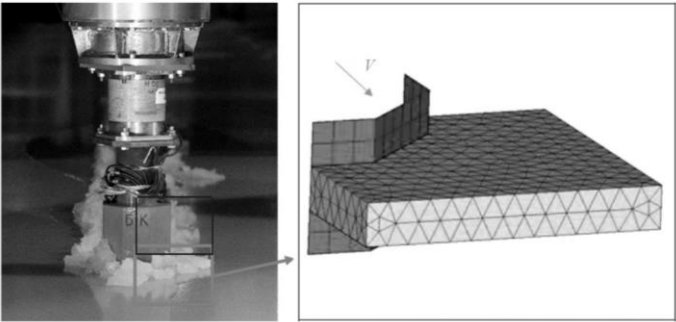

Figure 1.33 – Block-conductor during tests in the ice pool and FE model [3]

The surface of the block-conductor was modeled by membrane non-deformable finite elements. The ice field was modeled using 4-node finite elements and fixed at the boundaries in all degrees of freedom. The movement of the indenter is set using the pilot point and does not exceed 0.1 m.

The authors chose the Drucker-Prager Cap model as a model for the ice material. The shape of the yield surface is approximated according to the data obtained as a result of tests for biaxial compression of cubic samples of natural ice [65]. The data are presented in Figure 1.34. The approximation is performed by solving an optimization problem for the control parameters of the model.

To restore the yield surface in the field of tensile stresses, the authors accepted the fact that the compressive strength exceeds the tensile strength 5 times. When modeling the modulus of elasticity is taken from the tests performed on the bending of cantilever beams $E = 23.5\ MPa$, Poisson's ratio $\nu = 0.33$.
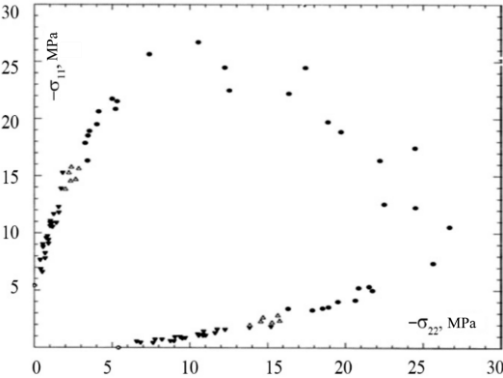

Figure 1.34 – Chart of destruction of ice cubic samples under biaxial compression in the axes of main stresses [65]

The results of the numerical simulation of experiments were compared with experimental data. Comparison of data is presented in Table 1.9. The difference between the results of numerical simulation and experimental research does not exceed 10%, which may indicate a close correspondence of the Drucker-Prager Cap model to the actual behavior of ice under loads. The authors argue that the

coordination of the results of numerical modeling perfectly illustrates the application of the isomorphism principle of the limiting surface to the solution of the problem of introducing a body into an ice field.

But looking at Figure 1.33, I can conclude. that the authors did not complete the qualitative creation of the mesh. The ice field in thickness has only 2 finite elements and thus cannot adequately describe the process of interaction with the block conductor.

Table 1.9 – Comparison of the results of experiments and numerical simulation [3]

Ice thickness, mm	Force of drag, N	
	Experiment	Numerical model
20	36	39
30	64	59

Politko (2018) analyzed the applicability of the Mohr-Coulomb model for modeling the impact of an ice field on vertical structures. He used the element erosion technique to model the ice fracture. Two experiments were considered to verify the applicability of material model: interaction of a rectangular horizontal stamp with the ice field [70] and laboratory model testing of the interaction of ice field with a four-support structure in the basin of the Krylov Research Center [36].

When modeling the experiments [70], the physical and mechanical properties of ice presented in Table 1.10 were determined. A numerical model of stamp-ice interaction process and boundary conditions are shown in Figure 1.35. A graph comparing the ice load between an experiment and numerical simulation is presented in Figure 1.36. Analyzing Figure 1.36, it can be said that the numerical model showed similar results regarding the nature of the ice load in the contact zone of ice and a rectangular stamp.

Table 1.10 – Physical and mechanical properties of ice in the numerical model created by Politko (2018)

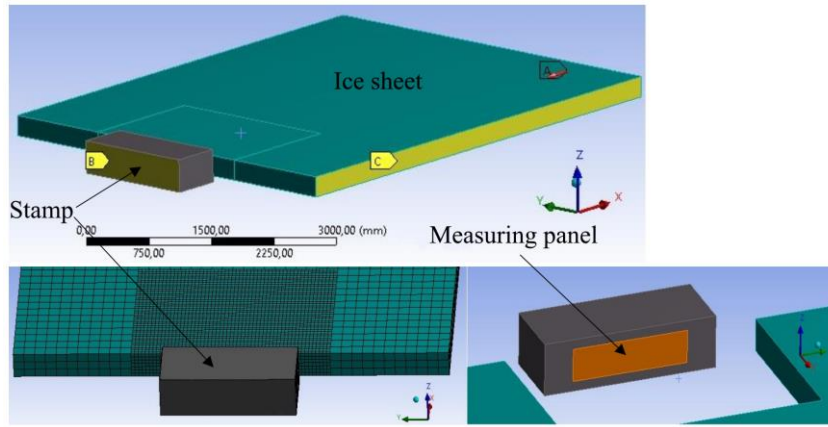| Property	Units	Value
Elastic modulus E	MPa	1000
Poisson's ratio ν	-	0.3
Angle of internal friction (to assign parameters of the Mohr-Coulomb model)	degrees	35
Cohesion (to assign parameters of the Mohr-Coulomb model)	MPa	0.6
Ice salinity	‰	6.2
Ice temperature	°C	-2.7

Figure 1.35 – Numerical model for introducing a rectangular stamp into an ice field [56]
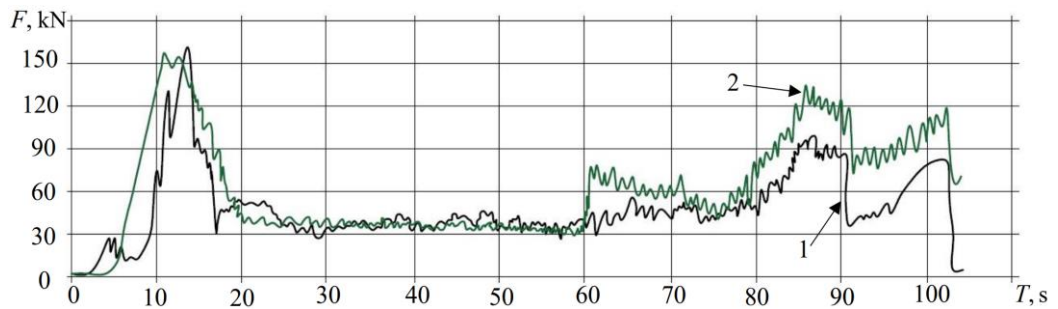

Figure 1.36 – Graph of ice load acting on stamp: 1 – field tests; 2 – numerical simulation [56]

When simulating laboratory tests of the interaction of an ice field with a four-support structure in the ice pool of the Krylov Research Center, the same characteristics of ice are used, presented in Table 1.10. The model that was used in the laboratory tests is shown in Figure 1.37. The numerical model presented by the author is shown in Figure 1.38.
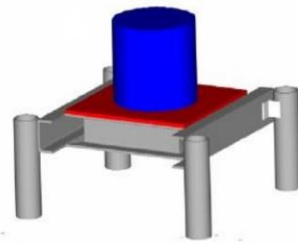

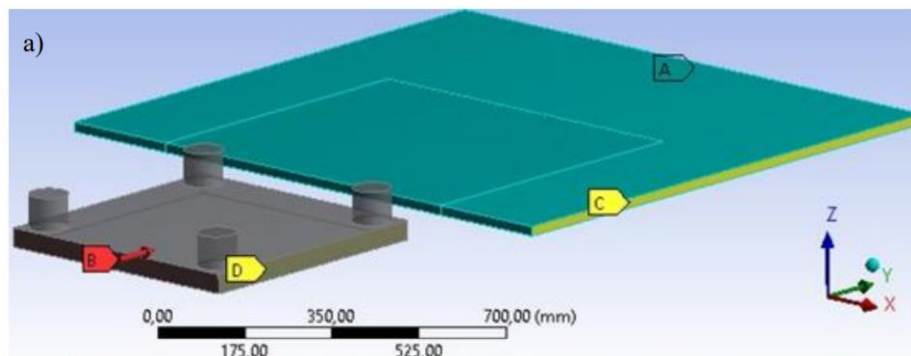Figure 1.37 – Model of a four-support hydraulic structure used in field tests [36]

Figure 1.38 – Numerical model of the impact of the ice field on a four-support structure according to [56]

Numerical experiments, as well as laboratory experiments, were carried out at three different angles of ice effect on the model: $\alpha = 0°$, $\alpha = 30°$, $\alpha = 45°$. The main purpose of the model tests in the Krylov Research Center basin was to study the mutual influence of the supports at various angles of action of the ice field. As a result of the studies, the influence coefficient of the supports was determined, which shows how many times the load on the four-support structure is more than on one-support. The picture of the destruction of ice during interaction in numerical simulation and during model tests, in general, coincides and is presented in Figure 1.39. The results of the experiment and numerical simulation are given in the Table 1.11.
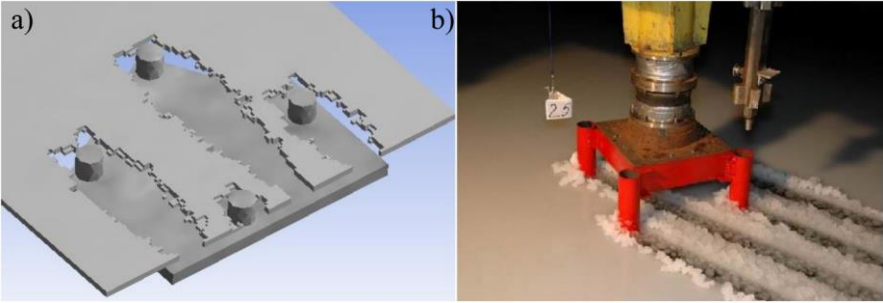

Figure 1.39 – The destruction of ice in the interaction with the four-support structure at angle $\alpha = 30°$:

a) in numerical simulation; b) during the model tests [56]

Table 1.11 – The coefficient of influence of the supports of the four-support structures [56]

The angle of impact of the ice field α	The results of the experiment, at a speed V, m/s		Numerical simulation results
	0.01	0.05	
0°	1.73	2.34	2.1
30°	2.9	3.62	3.4
45°	2.53	2.51	2.5

Although the results of numerical simulation of both experiments show a good correlation with field tests, the use of the Mohr-Coulomb model may be a wrong decision in case of assessing non-brittle behavior, since this model does not take into account the average principle stress σ_2 when estimating the complex stress-strain state of the ice field. Additional studies are needed to confirm the possibility of application of the Mohr-Coulomb model for determination of the onset of plastic behavior. There is also no discussion about the values of accepted parameters of the Mohr-Coulomb model.

As can be seen in Figure 1.35, the finite element mesh is incompatible in the region of transition to larger finite elements, which indicates the use of contact pairs for modeling the interaction of these two parts of the ice field. In my opinion, this approach is incorrect due to the relatively large errors that occur during the deformation process. For adequate transmission of stresses throughout the body of the simulated field, it is necessary to create a mesh with compatible nodes.

In addition, one of the main assumptions in these calculations is the fact that only brittle fracture of ice without any hardening is considered at relatively fast strain rates. In this case, it is assumed that for ice before fracture, only elastic deformations appear. Plastic properties of ice and strain-rate dependence are not taken into account.

Further, in his work, the author investigated the influence of the shape of the structure and the presence of zones of frozen ice on the ice load. Table 1.12 presents the results of numerical simulation, which shows the values of the maximum ice load on the supports of various shapes in the plan and the corresponding shape factors m.

Table 1.12 – The results of the study of the influence of the structure shape and the presence of frozen ice on the ice load

Ice impact case	Ice load, MN (support shape factor m)		
	Front edge in the form of		
	rectangle	semi-circular	polyhedron
Lack of ice freezing with support	5.2 (1)	4.7 (0.9)	4.8 (0.92)
The presence of ice freezing with support	6.4 (1.23)	6.7 (1.29)	6.6 (1.27)

The author compared these results with the support form factor specified in Russian code SP 38.13330.2018 [68] and got two main conclusions:

- in the case of the absence of freezing of ice for the front face of a semicircular outline and in the form of a polygon, the simulation results show the support shape factors higher than in [68], namely 0.90 and 0.92, instead of 0.83;

- in case of freezing of ice with a rectangular support, the support shape factor becomes equal to 1.23 instead of 1.

Thus, the values of support shape factors obtained by the author are consistent with SP 38.13330.2018 only for the case of a rectangular support in the absence of ice freezing and a semi-circular outline (polyhedron) in the presence of freezing. The value 0.9 of shape factor for the case of semicircular outline form in the absence of a freezing effect, obtained by the author, is consistent with another code – ND 2-020201-015 [52].

When analyzing studies in the field of numerical modeling of ice impacts on vertical structures, it is worth highlighting the following numerical experiments: **Gürtner et al. (2009) [30], Gürtner et al. (2010) [29], Hilding et al. (2011) [31], Hilding et al. (2012) [32].** These papers are united by the fact that the authors performed a numerical simulation of the actions of level ice fields on the Norströmsgrund

lighthouse. This lighthouse was chosen by the authors, because it was involved in the Low Level Ice Forces (LOLEIF) and Measurements on Structures in Ice (STRICE) projects in 1999-2003 years. In the LOLEIF project, this lighthouse located in the subarctic Gulf of Bothnia was equipped with load panels covered 162° of the lighthouse perimeter and special devices that monitor environmental conditions. Thus, comprehensive measurements of ice loads were conducted, and full-scale ice load data was obtained. The investigated interaction velocity in these papers is 0.15 m/s, which represents the relatively low interaction velocities for real ice-structure interaction situations.

In these works, the authors used the principles of cohesive zone model (CZM) to simulate the destruction of ice during interaction with the structure. Finite element models are presented in Figure 1.40, Figure 1.41 and Figure 1.42. The interpretation of this method in a finite element analysis is called the cohesive element model (CEM) and will be described later in this thesis. The main idea of the method is to model an ice body in the form of a set of volumetric finite elements having ice properties and connected with cohesive elements of zero thickness, which are possible crack paths.
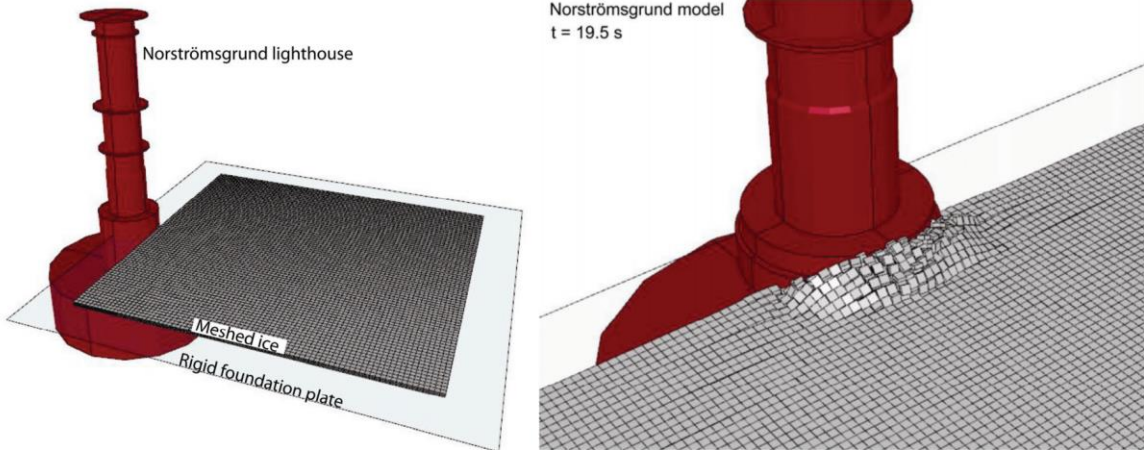

Figure 1.40 – Finite element model of ice interaction with Norströmsgrund lighthouse [30]
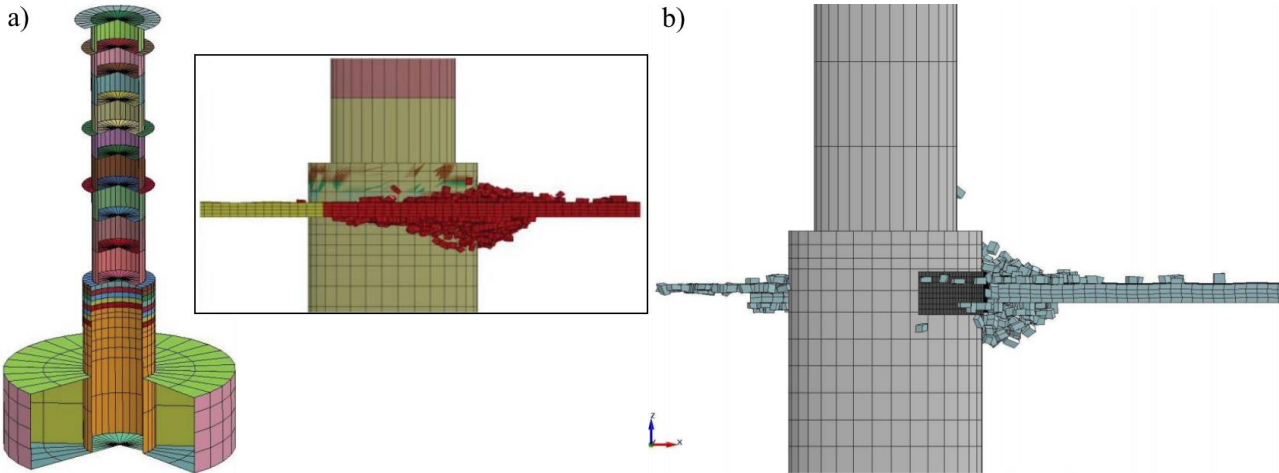

Figure 1.41 – Finite element analysis of ice interaction with Norströmsgrund lighthouse: a) Gürtner et al. (2010) [29]; b) Hilding et al. (2011) [31]
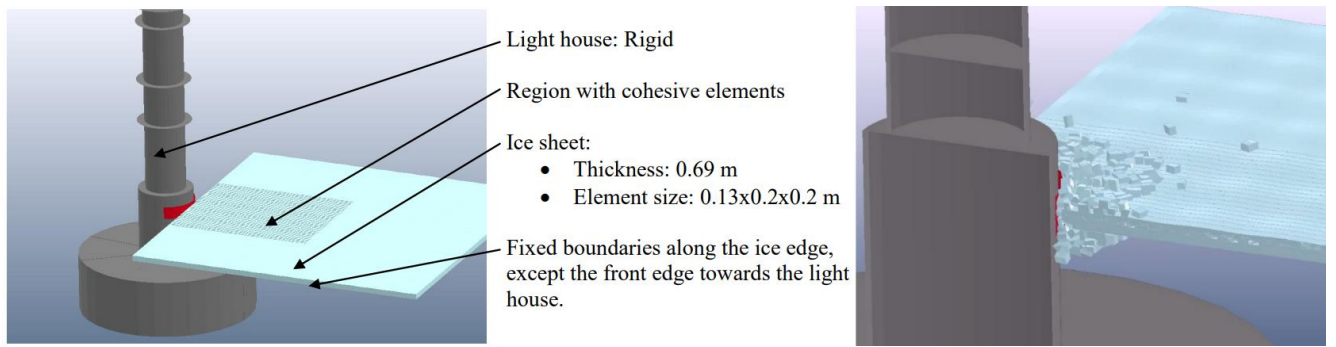
Figure 1.42 – Simulation of ice-structure interaction process using CEM [32]

In these researches authors defined cohesive element traction-separation law also called Tvergaard-Hutchinson law (Figure 1.43) for cohesive elements and elastic-plastic material with softening for ice bulk elements to achieve the macroscopic ice crushing behavior. The Mises material model was used for bulk elements. Cohesive element law is characterized through its piecewise continuous curve with softening. Cohesive properties are different in vertical and horizontal direction to accommodate anisotropy of fracture of sea ice. In all these studies, the von Mises yield criterion was used to describe the plasticity of the ice material in bulk elements.
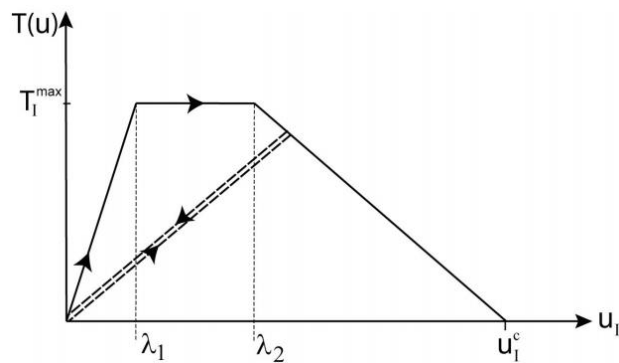

Figure 1.43 – Cohesive element traction-separation law defined in [29, 30, 31, 32]

For monotonic loading in fracture mode-I, the fracture energy, i.e. the area under the cohesion law curve can be written as [30]:

$$G_I^C = 0{,}5 T_1^{max} u_1^c (1 - \lambda_1 + \lambda_2), \qquad (1.65)$$

where T_1^{max} – peak traction accommodated by the material in the fracture process zone;

λ_1, λ_2 – separation values on cohesive traction-separation curve (Figure 1.43);

u_1^c – maximum allowable separation.

The issue of choosing values for the parameters of the materials used has been discussed many times. Difficulties arise because today there are no qualitative test data that determine the values of fracture parameters. The situation is complicated by the fact that the energy fracture parameters are highly dependent on the mesh size, so in some cases they had to be scaled tens of times [29, 31]. The values of material properties used in these papers are shown in Table 1.13.

Table 1.13 – Values of material properties used in [29, 30, 31, 32]

Paper title	Bulk element properties	Cohesive element properties
Numerical simulation of ice action to a lighthouse / Gürtner et al. (2009)	von Mises yield criterion $E = 1000$ GPa; $\rho = 910$ kg/m^3; $\mu = 0.3$; $\sigma_y = 0.0007$ MPa;	$G_{IC} = 20$ J/m^2 (vert.); $G_{IIC} = 28$ J/m^2 (vert.); $G_{IC} = 52$ J/m^2 (horiz.); $G_{IIC} = 52$ J/m^2 (horiz.); $\lambda_1 = 0.08$ (vert.); $\lambda_2 = 0.45$ (vert.); $\lambda_1 = 0.10$ (horiz.); $\lambda_2 = 0.55$ (horiz.)
Numerical modelling of a full scale ice event / Gürtner et al. (2010)	von Mises yield criterion $E = 5$ GPa; $\rho = 910$ kg/m^3; $\mu = 0.3$; $\sigma_y = 1,5$ MPa	$T_{max} = 1$ MPa (vert.); $T_{max} = 1.1$ MPa (horiz.); $G_C = 5200$ J/m^2; $\lambda_1 = 0.02$; $\lambda_2 = 0.55$ (vert.); $\lambda_2 = 0.45$ (horiz.) $u^c = 6.8$ mm (vert.); $u^c = 7.1$ mm (vert.);
Simulation of ice action loads on offshore structures / Hilding et al. (2011)	von Mises yield criterion $E = 5$GPa; $\rho = 910$ kg/m^3; $\mu = 0.3$; $\sigma_y = 2$ MPa	$T_{max} = 1$ MPa (vert.); $T_{max} = 1.1$ MPa (horiz.); $G_C = 5200$ J/m^2
Simulation of Loads from Drifting Ice Sheets on Offshore Structures / Hilding et al. (2012)	von Mises yield criterion $E = 5$GPa; $\rho = 910$ kg/m^3; $\mu = 0.3$; $\sigma_y = 2$ MPa	$T_{max} = 1$ MPa (vert.); $T_{max} = 1.1$ MPa (horiz.); $G_C = 5200$ J/m^2
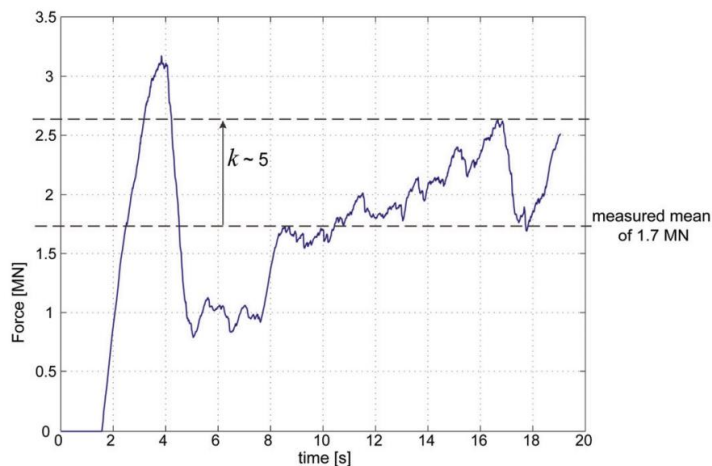
Figure 1.44 – Simulated horizontal global ice force on the lighthouse foundation and comparison to measured loads according to Gürtner et al. (2009) [30]

This modeling method (CEM) shows close to real behavior and the destruction of the ice cover when exposed to a vertical structure. Features such as the appearance of radial cracks, cyclic loading and ice extrusion can be observed. However, in my opinion it is impossible to speak of a good agreement

between the results and field data, especially because results of modeling in these papers were often compared with only a few field cases (most often with one). Numerical experiments in these papers have several disadvantages. The authors did not perform a qualitative selection of constitutive model and parameters of the ice material, which led to a large difference between the model and the real picture of the interaction. As it usual for almost all simulations, the authors did not consider the dependence of strength on the strain rate, temperature, as well as the ductile behavior of ice before fracture. The big assumption is the use of von Mises plasticity for bulk elements. This plasticity model does not take into account the influence of hydrostatic (mean) stress on total ice strength. This effect was described earlier in subsection 1.3. So, we can say that there is no qualitative material modeling of ice in these papers.

One of the latest investigations in the field of ice-structure interactions was made by **Wang et al.** (2019) [79]. In these paper authors also used the cohesive element method to model the ice actions on Norströmsgrund lighthouse with new modeling techniques. First of all, some ice bulk elements with random numbering are deleted to simulate natural ice sheet with initial defects. Then, the elastic modulus was calculated by the empirical formula and assigned to the ice elements. Thirdly, cohesive elements are inserted in ice sheet model which is meshed with tetrahedron elements. According to the authors the use of hexahedral elements will cause "zig-zag" crack paths that are not applicable for the cohesive zone method. A structured mesh with rectangular elements will create a 45° crack which will travel 2 times longer than the actual one, leading to an extra energy consumption. The numerical model used in calculations is presented in Figure 1.45. Ice element is assumed as elastic-perfect plastic material.
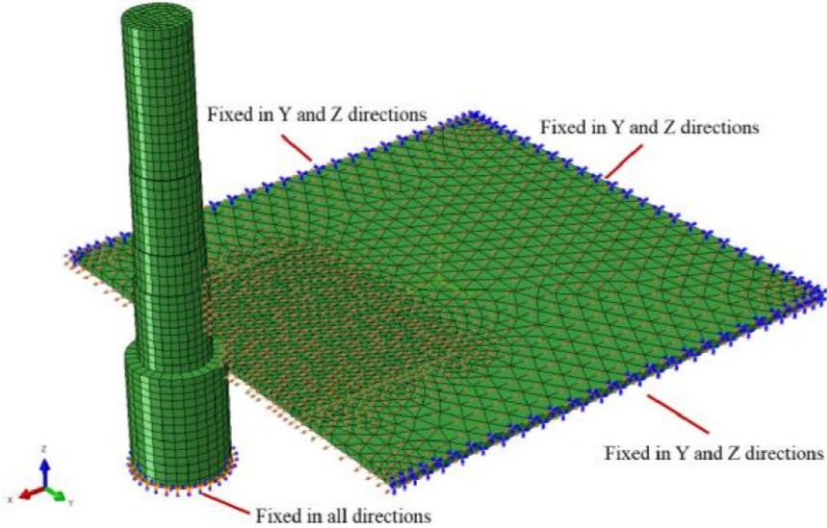
Figure 1.45 – Numerical model of ice sheet and lighthouse used in [79]

In general **Wang et al.** considered 3 different design cases: ice sheet without any initial defects, ice sheet has only initial defects and ice sheet has initial defects and changed elastic modulus. Horizontal force on the lighthouse and failure process of ice sheet are analyzed and compared with field data measured on lighthouse. All of three cases showed different failure pattern as shown in Figure 1.46. Values of simulated ice forces and comparison with field data is presented in Table 1.14.

Figure 1.46 – Ice failure patterns in three cases according to [79]

Table 1.14 – Comparison of the simulated mean horizontal forces with the measured data [79]

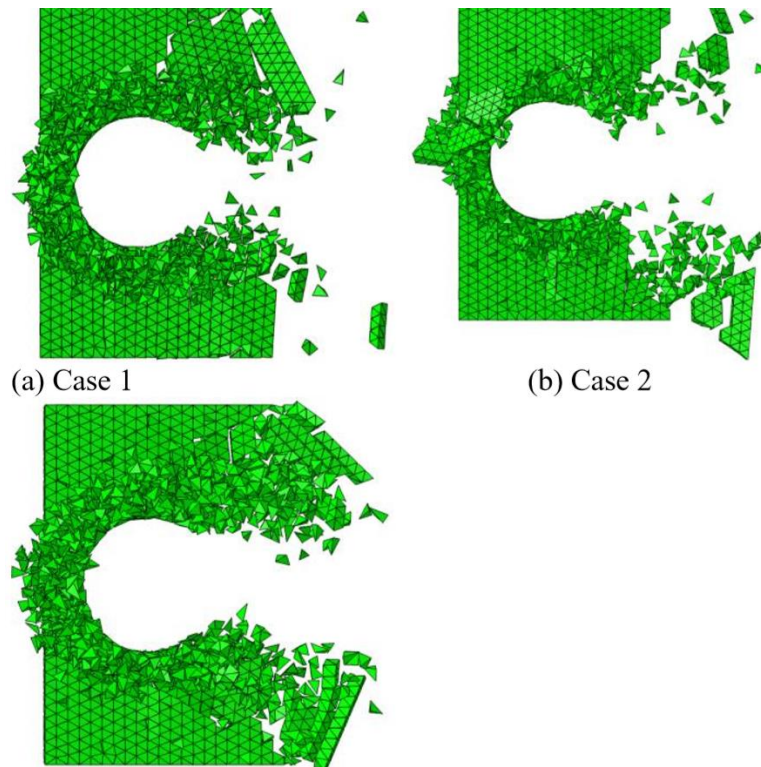| Case	Mean horizontal force, MN	Error
Case 1	3.21	15.5%
Case 2	2.59	6.8%
Case 3	2.92	5.7%
Measured results	2.78	-

Again, as in previously reviewed articles and theses, the same assumptions and disadvantages are present. The Mises model was used as a model of plasticity, which in my opinion cannot be applied as material model for such complex material as ice. Also, the authors did not take into account the influence of temperature, strain-rate effects. As can be seen from Figure 1.45, a more or less good-quality ice field mesh was made only in a small area near the interaction region. Away from this region, there is a rapid enlargement of the finite element mesh up to 1 element in the ice field thickness, which in my opinion leads to an incorrect distribution of stresses. Given all of the above, along with the fact that the comparison is made only for 1 case of interaction, it cannot be said that the error values given in Table 1.14 correspond to reality.

Nevertheless, the authors used some interesting methods. For example, they used a special subroutine to account for the buoyance and gravity forces, acting only on spalled elements. Preliminary removal of elements from the model to generate initial damage is also an interesting solution.

Good results in the field of numerical studies of the interaction of ice structures were obtained by **Sand (2008)** [63]. In modeling, the author used the finite element method in conjunction with the technique of removing elements and studied the effect of ice on both inclined and vertical structures. Sand in his thesis considered the applicability of some failure surfaces for ice modeling. Among the examined, the author identified the following:

- Hill yield criterion;

- Parisau parabolic criterion;

- Reinicke and Remer's failure criterion

- Horrigmoe and Zeng's failure criterion

According to Sand, criterion Horrigmoe and Zeng's failure criterion is most appropriate, because this orthotropic criterion contains not only a quadratic terms in stresses, but also linear terms in stresses and has the dependence of the yield strength on the mean stress. The search for the values of the parameters included in this criterion was performed by approximating the results of field experiments data from papers of Schulson. Resulting failure surface used in numerical calculations is presented in Figure 1.47. Moreover, the author noted that the obtained values can also be used in the Hill criterion.
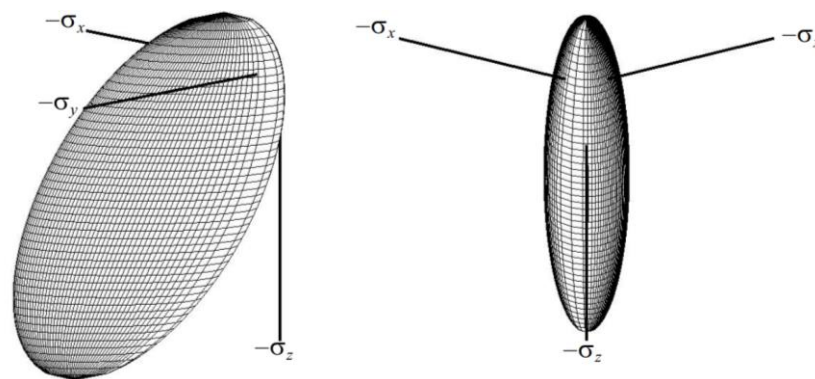

Figure 1.47 – Fitted three-dimensional plots of Horrigmoe and Zeng's failure criterion [63]

The behavior of the crushed or cracked ice was taken into account by replacing the "undamaged" finite elements with the "damaged" ones with changed properties. This is so-called transformation of state method that is shown in Figure 1.48. As in paper presented higher only elastic behavior of ice before crushing was considered, and author did not take into account the dependence of strength on the strain rate and temperature.

In terms of modeling the ice-vertical structure interaction problem, good results were obtained. Author conducted several simulations of ice actions of Norströmsgrund lighthouse which was mentioned before. Sand compared global ice forces with measured field data and considered failure patterns. One can notice the occurrence of radial and longitudinal cracks during simulation as presented in Figure 1.49. Comparison of the ice pressure distribution obtained by finite element computations with the measured ice pressure distribution according to Sand showed similar trends.
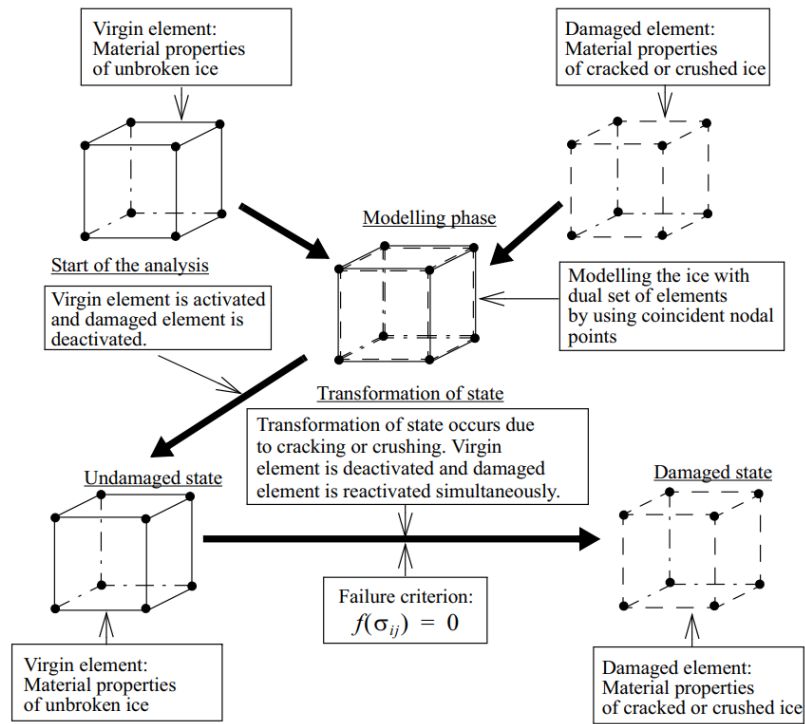
Figure 1.48 – Transformation of state method used by Sand B. [63]

$P_H^{num} = 3.86$ MN, $u_y = 6.00$ mm. $P_H^{num} = 4.34$ MN, $u_y = 7.00$ mm.

$P_H^{num} = 4.61$ MN, $u_y = 8.13$ mm. $P_H^{num} = 4.09$ MN, $u_y = 11.00$ mm.
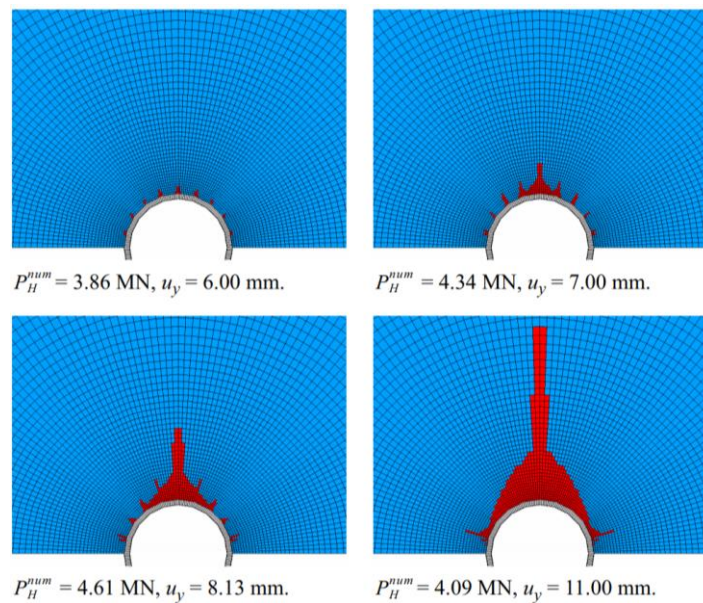
Figure 1.49 – Calculated failure pattern and distribution of ice pressure obtained by Sand (2008) [63]

Despite the widespread use of the finite element method, there is experience using other numerical methods. An example of numerical experiments of ice-structure interaction using the discrete element method is article of **Liu et al. (2016) [45]**. Authors presented ice load simulations for fixed and floating structures, i.e. jack-up legs and the Kulluk floating drilling platform. They also compared the computation time of a model using a computer processor Performing calculations using the GPU significantly reduces the calculation time (up to 36 times).

Ice sheet in simulations was modeled using contacted spherical particles bonded together using a

parallel bond model, as the bonding disk (Figure 1.50). The maximum tensile and shear stresses acting on the bonding disk are calculated based on the beam theory. In order to calibrate the relationship between the bonding strength parameters assumed in the DEM model and realistic ice strength terms, general ice sample tests of uniaxial compression test and 3-point bending test were simulated.
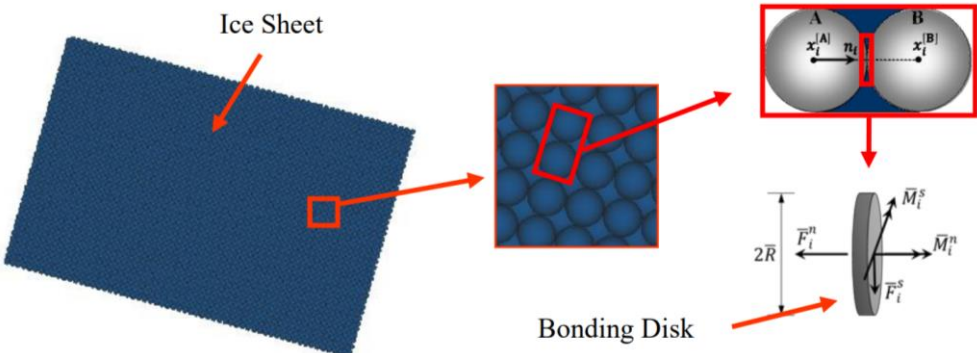

Figure 1.50 – Modeling the ice sheet using spherical bonded elements in Liu et al. (2016) [45]

Regarding vertical structures in this article the authors investigated the influence of the shape of the structure and the mutual influence of several supports on the ice load. Example of ice-structure interaction modeling with circular shape in this paper is presented in Figure 1.51. Results were compared with calculations of the ice load using ISO 19906 recommendations.
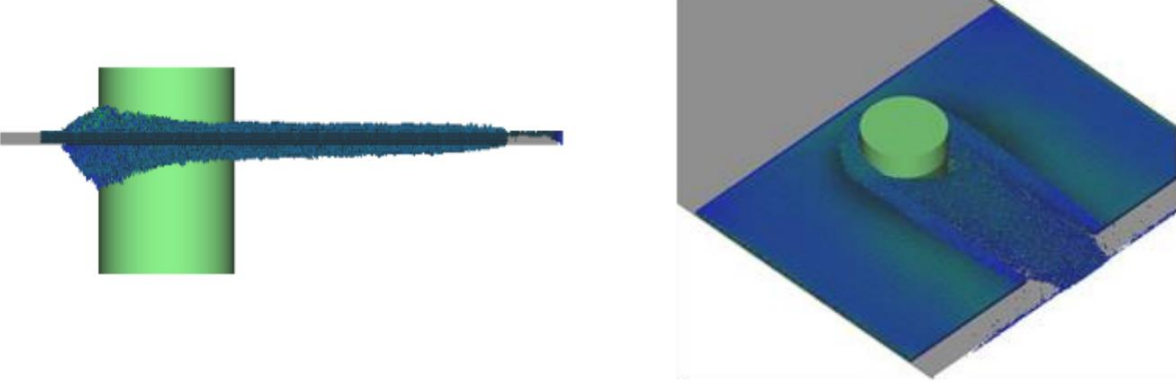
Figure 1.51 – Snapshots of DEM simulations of an ice sheet moving through circular support performed by Liu et al. (2016) [45]

The simulated ice force was less than 60% of the ISO 19906 formula value for the broadside direction case. The average and maximum peak ice forces simulated by DEM are both larger for the broadside case compared with the diagonal and round geometries but ISO 19906, which is based on projected area, suggests otherwise. The DEM simulation results presented in this paper are promising, but the accuracy and reliability of the tool still requires more validation studies and developments.

We can say that the simulation results in this paper showed poor convergence with analytical methods for determining ice load. Along with the lack of proper consideration for the non-uniform properties of ice and the high computational cost of calculations, the question of the applicability of using the discrete element method in modeling ice effects remains open.

1.6 Section conclusions

The problem of assessing ice impacts on the offshore structures is becoming more global and relevant in connection with the development of the energy complex and an increase in the rate of hydrocarbon production in the Arctic zone. The impact of ice on structures is a multifactorial phenomenon. The magnitude of ice loads depends not only on the climatic conditions, but also on the characteristics of the ice itself, the interaction conditions at the contact and many other factors.

Sea ice is a complex material consisting of hard ice, brine, gas, the ratio of which depends on temperature, texture, growth conditions, etc. Ways to describe the properties of ice have been developed and improved since the second half of the 20th century. Thus, the studies of Russian and foreign authors are based on a large number of field and laboratory experiments. Processing the results of these experiments allowed to obtain analytical dependencies of the components of sea ice (fresh ice, water and salts) on various properties. These properties vary greatly and depend on the area of research, methods of conducting experiments and the age of the ice. Nevertheless, as a result of their work, researchers managed to obtain many dependencies of ice parameters on various factors. As a rule, all parameters show a strong dependence on ice temperature. The salinity, porosity and texture of ice also play a significant role.

Comparison of methods for calculating the salinity of ice, brine volume, elastic modulus and compressive strength is shown in Figure 1.52-Figure 1.55. In Figure 1.54 curve named "Gammon P. H et al. (1983) + Weeks and Assur (1967)" means that values of elastic modulus of pure ice were selected from Table 1.5, corrected using equation (1.43) and values for sea ice was calculated using equation (1.48).
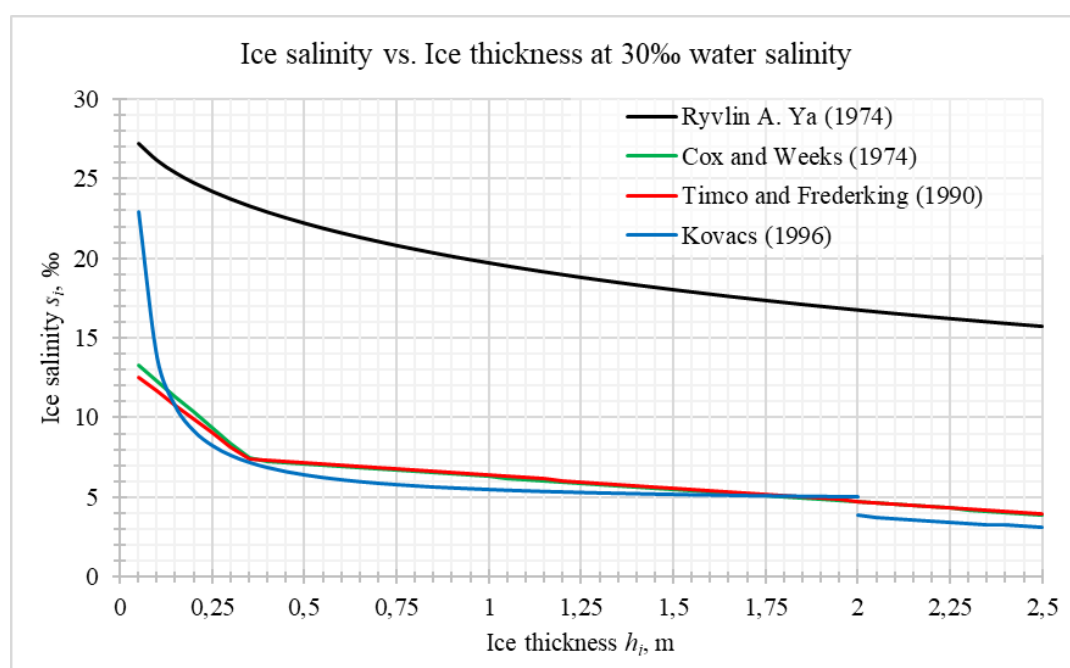

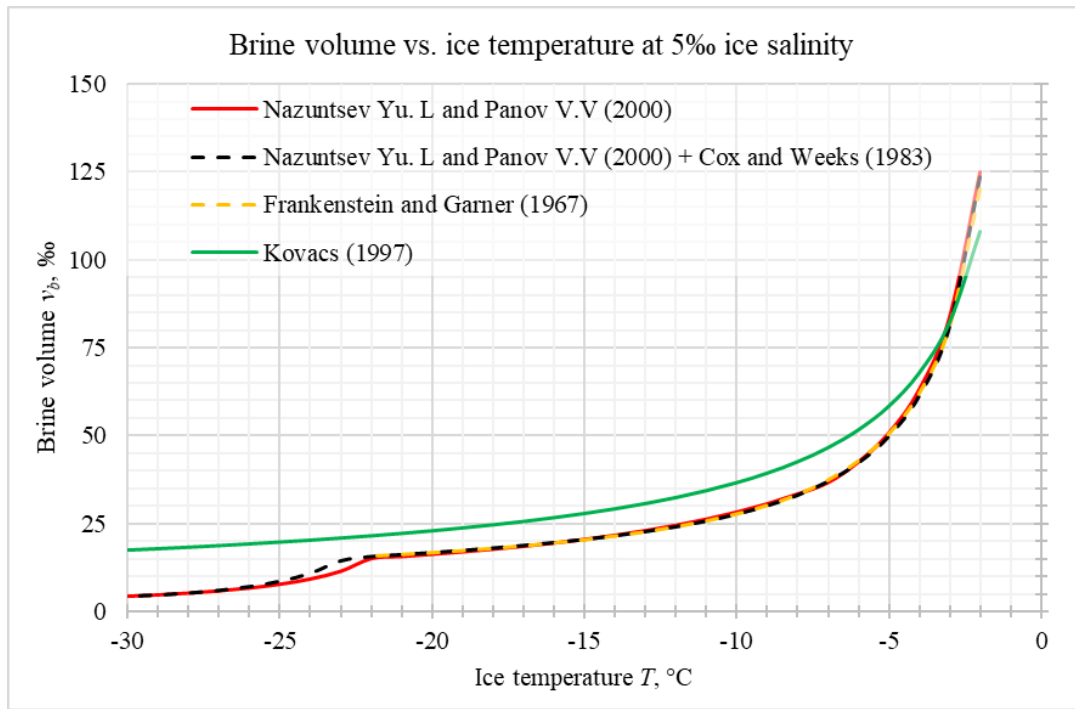Figure 1.52 – The dependence of the salinity of ice on its thickness by various methods

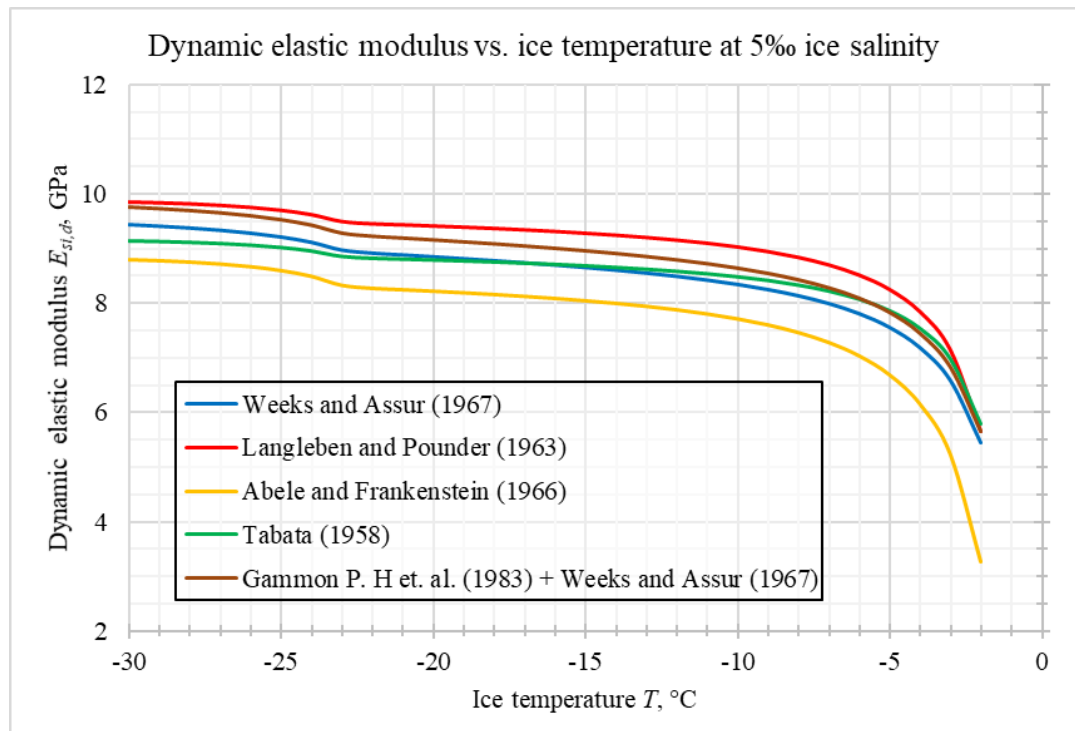Figure 1.53 – The dependence of the brine volume on ice temperature by various methods

Figure 1.54 – The dependence of the dynamic elastic modulus on ice temperature by various methods
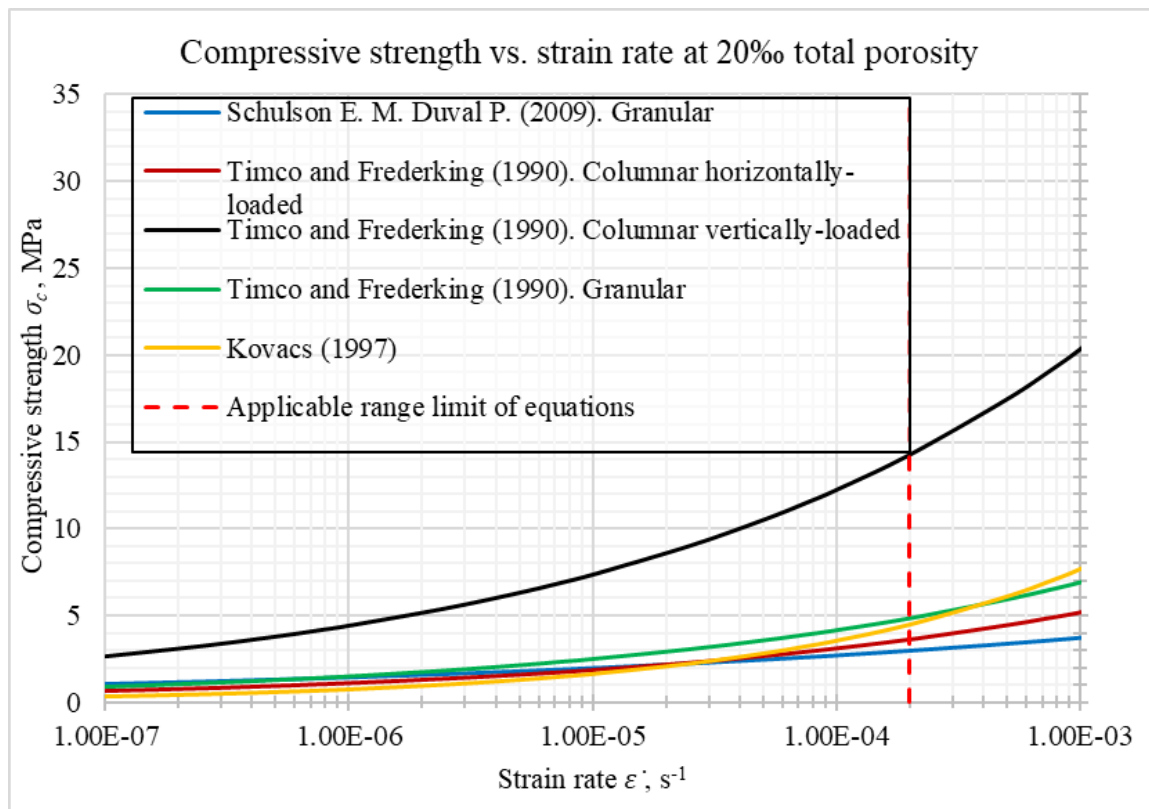
53

Figure 1.55 – The dependence of the compressive strength of ice on strain rate

A significant scatter of data appears between different methods. The selection of appropriate method should be done considering the testing approach that was used during experiments, age of researches and applicability range of equations. The most important features of ice as material that must be considering in numerical analysis are as follows:

- strong dependence of ice properties on temperature, salinity and its texture. Since during ice-structure interaction process different conditions can appear at the same time, especially on contact with structure, applied modeling methodology should have possibility to automatic recalculation of ice properties based on current conditions (temperature, mean stress, strain rate, etc.);

- growth and texture forming conditions. Anisotropy of ice polycrystals has strong dependence on ice texture. Thus, ice with random orientation of c-axes, for instance, granular ice, can be considered as isotropic material. But in case of columnar ice, which has more or less ordered directions of c-axes, polycrystal show clear anisotropic strength and elastic properties. So, the best way to describe this feature is to consider columnar type of ice as transversely isotropic or orthotropic material;

- plastic-brittle transition of ice behavior based on interaction strain rates. Since this feature of ice has not yet been taken into account by the authors earlier, this is an unresolved problem in modeling of ice actions, which will ensure the scientific novelty of this thesis.

In case of mechanism of ice-structure interaction it can be said that li limit stress mode of interaction is the most dangerous since has the highest forces. Crushing of ice is rapidly changing process

with occurrence of so-called high-pressure zones. To qualitatively take into account the influence of these zones on the total ice effect, it is necessary to study the issue of modeling of ice destruction process in details.

As for the worldwide experience of numerical modeling of ice impacts, a large number of papers have been performed using various numerical methods and approaches. The most promising in my opinion is the finite element method using the cohesive element method. In most cases, the authors do not pay due attention to the selection of constitutive models suitable for describing the plastic behavior and failure of ice. The considered papers of various authors do not take into account such features of ice, as the dependence of its properties on temperature, strain rate, pressure-hardening (except Sand [63]) and texture. In this regard, it is difficult to talk about the correspondence of the results of numerical models to real conditions.

Of great practical importance are the tools for optimizing the parameters of a material model for specific conditions (for example, for experimental data). Solving the inverse problem, pre-setting some restrictions, it is possible to numerically determine some empirical parameters of the material model.

2 Formulation of the problem and methodology of numerical modeling of ice impacts

2.1 Formulation of the problem

Offshore facilities on the continental shelf are unique facilities of increased responsibility, which requires appropriate careful assessment of the effects of external factors. Proper design of such objects ensures the reliability of structures and helps to prevent emergencies that may arise as a result of the destruction of the structure.

Ice impacts are one of the most complex factors evaluated during design. This is directly related to the spatio-temporal variability of the ice cover, the great variability of the physicomechanical properties of ice, the influence of other environmental factors on the ice formations, such as waves, currents, wind, etc. Therefore, it can be said that ice loads have stochastic nature, and load estimation methods used today in the design of offshore structures use a number of significant assumptions that can distort the real picture that arises in reality.

Numerical modeling methods can to some extent eliminate the difficulties that arise when taking into account the random nature of the values of ice parameters, which significantly increases the reliability of the magnitude of the ice load. In addition, as already mentioned, the destruction of ice formations during their interaction with vertical structures depends on many factors (Section 1) and has a strong influence on the formation of ice load. Thus, the assessment of the interaction of ice formations with vertical structures using numerical modeling considering the process of ice destruction will allow us to avoid several assumptions that affect the result.

In view of the above, to carry out a numerical simulation of the interaction of ice formations with vertical structures, taking into account the destruction of ice, it is necessary to:

- analyze the methods for calculating ice parameters and determine their dependence on temperature, salinity, strain rate, etc. (section 1);

- perform analysis and selection of constitutive models of plasticity and fracture, taking into account their applicability for modeling ice impacts;

- to establish a single principle for creating a numerical model, that includes certain considered environmental parameters, boundary conditions, geometry of ice formations, etc.;

- to make an algorithm for creating a numerical model that takes into account the above features.

- to establish parameters used in constitutive model to obtain the nature and picture of interaction, close to realistic.

The best way to verify the model would be to reproduce (simulate) field and laboratory experiments on ice impacts with identical conditions, such as dimensions of ice formation, its speed, temperature gradient, structure width and shape etc.

If the results of numerical simulation are consistent with the experimental results to an acceptable

extent, the next step will be to simulate the effects of ice with the structure under different scenarios. The most interesting and investigated feature of the interaction process is the effect of the complex stress-strain state of ice on the magnitude of the ice load, as well as the effect of ice destruction on it. Taking into account the destruction of ice upon contact will also allow to consider the process of occurrence of high-pressure zones described earlier.

The solution of the above problems will ultimately allow to develop a methodology and describe an algorithm for assessing ice impacts in real engineering tasks using numerical modeling.

2.2 Methodology of numerical simulation of ice impacts

2.2.1 Numerical method selection

Today, there is a wide selection of numerical simulation methods used to solve many engineering problems. Among the most famous, the following methods will be discussed as possible methods for simulation of ice-structure interaction.

Discrete element method (DEM). This numerical method was developed by Cundall and Strack (1978) [16] and mainly used for modeling granular media (such as soils), consisting of a large number of particles. The simulated medium is represented in the form of a set of individual particles that have their own properties (density, elastic modulus, velocity, etc.). Particles can be presented in various shapes and sizes. DEM allows to simulate the interaction between all particles, but usually it has significant computational cost.

In ice problems, the method was mainly used to simulate the interaction of ice formations with each other or with structures on a large scale as presented in Figure 2.1. In this case, ice formations (fields, glaciers, icebergs) are modeled as separate particles interacting with each other. Moreover, in most cases, it is assumed that the formations are indestructible. For example, the studies of Kim J-H. and Kim Y. (2019) [37] and Richard and McKenna (2013) [57] can be distinguished.
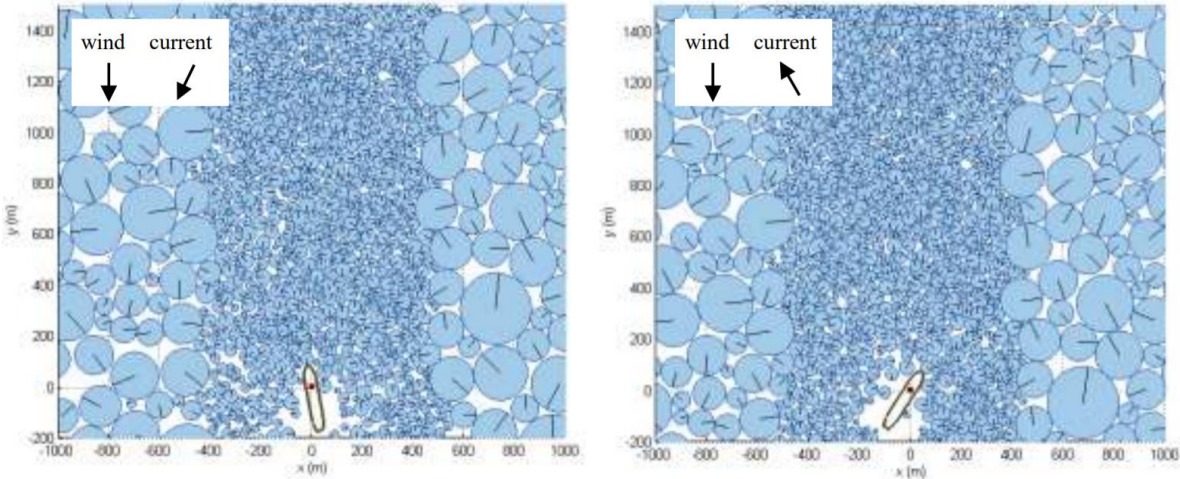

Figure 2.1 – Simulation of the movement of vessel through discontinuous ice [57]

DEM has also been used to model the interaction of ice and structures on a more detailed scale. In this case, the ice field is represented as a set of particles located in several layers as presented in Figure 1.51. The interaction between particles allows one to take into account the destruction, ridging and moving of ice on the structure, which is very useful in modeling the actions of ice on inclined structures. For example, the studies of Lu et al. (2012) [46] and Liu et al. (2016) [45] that was described earlier (subsection 1.5) can be distinguished. However, this method has several significant disadvantages:

- the particles themselves are almost non-deformable and cannot be destroyed;

- the destruction of the ice field can only occur between particles, which imposes restrictions on the path of conditional cracks;

- this method requires greater computing power compared with other considered numerical methods;

- DEM is not widely used among software systems if compare with FEM and is more suitable for modeling granular media than for solving a continuous medium problem.

Finite element method (FEM). To model the actions of ice formations, the finite element method is most often used. This method has received the greatest distribution among methods of numerical modeling and is actively developing today, because it has a wide range of advantages. The method is based on the concept of partition of unity and widely used to solve problems of solid mechanics, heat transfer, hydrodynamics and electrodynamics.

Using this method, all bodies are represented as they are, close to real geometry. Then the bodies are discretized into finite elements – a mesh of each body is created. Finding a solution at finite element nodes leads to solving a system of algebraic equations. The smaller the size of the finite elements (i.e., the more elements in the model), leads to a greater number of algebraic equations solved by the solver and the greater the computational cost.

When modeling the ice-structure interaction using the finite element method, the ice formation is often represented as a solid body. Usually the following two methods are used to simulate the destruction of ice: *cohesive element method* and *element erosion technique*.

Cohesive element method. In this method, the simulated body is discretized using conventional bulk elements, as well as special cohesive elements of zero thickness as presented in Figure 2.2. Bulk elements are used to model the process of ice deformation, and destruction occurs due to the loss of strength of the cohesive elements. Thus, it is assumed that the cohesive elements are possible paths for the formation and development of cracks. The behavior of the cohesive elements is subject to predefined traction-deformation rules. This method was widely used to model ice impacts on structures with taking into account the ice destruction process. Among the studies considered before, the following can be distinguished: Gürtner et al. (2010) [29], Li Liang (2014) [44], Salganik (2014) [62]. Among the disadvantages of this method, one can distinguish the high computational cost, as well as the difficulty

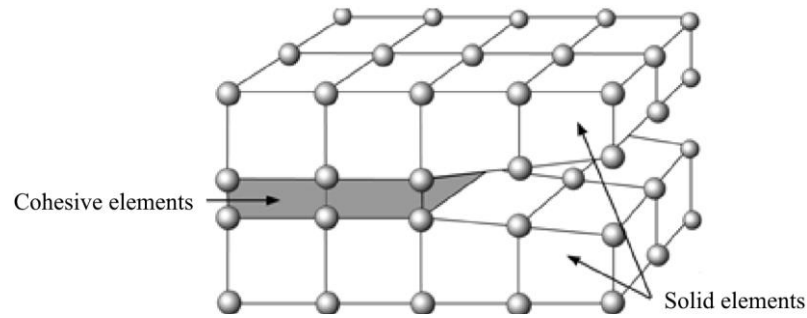of using in the case of complex geometry of ice formation.

Figure 2.2 – Mesh when using the cohesive element method

Element erosion technique. This method is also widely used to model ice-structure interaction problems but is easier to use than the previous cohesive element method. In this case, the ice formation is modeled as a completely continuous body using solid elements. To describe the behavior of ice under loads, special material models are used, which describe:

- the yield criteria (yield surface) and flow rule;
- the damage initiation criteria;
- the damage evolution law.

The life cycle of the finite element in this method is as follows. First, the behavior of the material completely depends on a predetermined constitutive model, then when a certain failure criterion is reached, the destruction of the material begins according to the damage evolution law. When the degree of damage reaches 100%, the material is considered destroyed and the finite element is removed from the model. The following studies of several authors described earlier use this method: Sand (2008) [63], Politko V.A. (2018) [56]. This method has high efficiency from the point of view of computation time, however, a significant disadvantage is the strong dependence on the mesh size (the size of the cracks is essentially connected with the size of the finite elements).

Moreover, when solving ice problems, two different formulations of finite elements can be used. The *Lagrangian-based* finite element simulations is one of the most frequently used continuum mechanics. This method relates the mesh and the material, which might cause excessive distortion and, hence, numerical instability problems in which the material is deformed greatly. The *ALE* method combines the methods of Lagrange and Euler (in the latter case, the mesh is fixed in space, and the material flows through it). It takes advantage of both integration methods: the computational efficiency of the Lagrange method and the ability to allow a significant deformation of the Euler method.

Extended Finite Element Method (XFEM). This method is an extension of the conventional finite element method. It can model cracks and other discontinuities by enriching the degrees of freedom in the model with additional displacement functions that account for the jump in displacements across the discontinuity. In this way, cracks modeled by this method are independent of the mesh (mesh-free), so the method is widely used in the fracture analysis. Nevertheless, it is practically not used to simulate

the interaction of ice with vertical structures, due to the difficulties in determining the position of the initial crack and a small degree of integration into CAE software.

As an example of the application of the extended finite element method to solve ice problems, the study of Lu et al. (2018) [47] in which authors performed the numerical modeling of ice destruction during interaction of ice floe with icebreaker as presented in Figure 2.3.
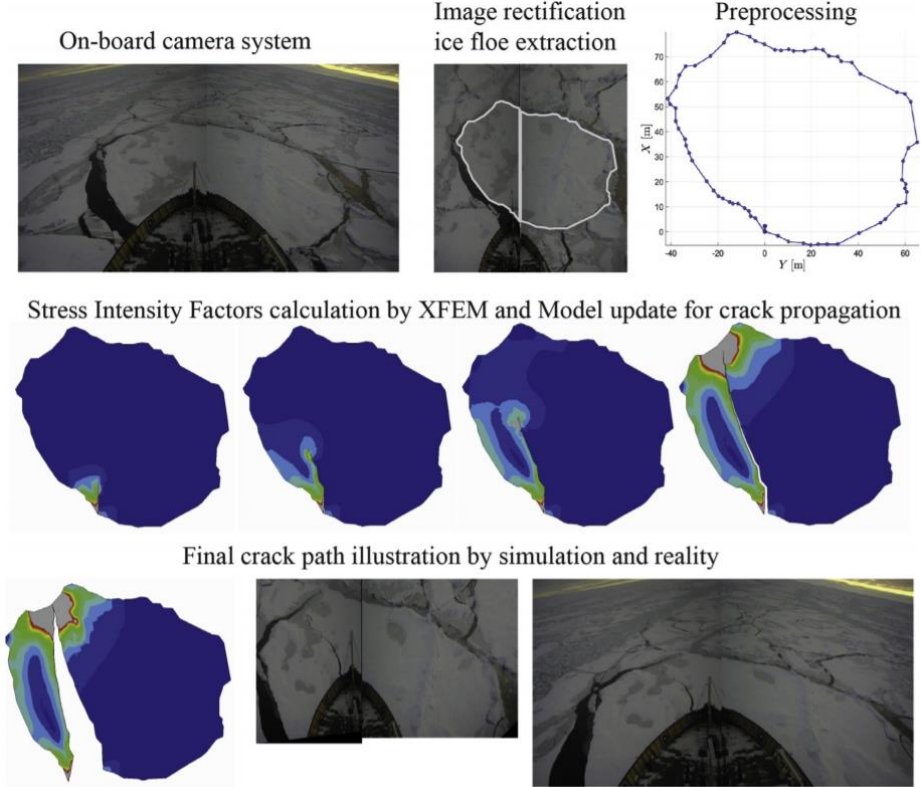

Figure 2.3 – Crack path within the selected ice floe before and after the fracture in both the simulation and reality according to Lu et al. (2018) [47]

After analyzing the considered methods of numerical modeling, it was decided to use the **finite element method in combination with cohesion element method**. This method has the following advantages compared to other methods:

- wide distribution and integration into a large number of software systems;
- relative ease of use and setting model parameters;
- clear and understandable interpretation of calculation results;
- good applicability for solving problems of solid mechanics;
- good agreement of results with field data (according to several authors).

A study of the effect of various material parameters on ice load using CEM was performed by **Feng et al.** [22]. According to this study it was found that the structural response is highly sensitive to the change of fracture energy rather than the cohesive strength used for defining the curve of cohesive elements. The change of the shape or the initial slope of the curve has little effect on results. Also, the stress-strain curve of the bulk elements has remarkable influence on simulations.

The solution comes down to solving the main equation of motion of the finite element method, which has the following form:

$$[M]\{\ddot{x}\} + [C]\{\dot{x}\} + [K]\{x\} = \{F\}, \tag{2.1}$$

where $[M]$, $[C]$ and $[K]$ – global mass, damping and stiffness matrixes respectively;

$\{\ddot{x}\}$, $\{\dot{x}\}$ and $\{x\}$ – nodal acceleration, velocity and displacement vectors respectively;

$\{F\}$ – applied load vector.

To perform numerical experiments, the SIMULIA Abaqus software package for finite element analysis will be used. SIMULIA Abaqus – universal software system of finite element (FEM) analysis, existing and developing over the past 40 years, is quite popular with specialists in the field of computer-aided engineering (CAE) and linear and non-linear, stationary and non-stationary problems of mechanics of a deformable solid and structural mechanics (including non-stationary geometrically and physically non-linear contact problems interaction of structural elements). Also, it can be used for solving the problems of fluid dynamics, heat transfer, electrodynamics, topology optimization and others.

2.2.2 Integration method selection

To simulate dynamic processes, including the impact of ice formations on a structure, two methods for integration of motion are used: explicit and implicit methods.

In practice, implicit methods are usually used to simulate relatively long-running processes, ranging from a few tenths of a second to several years (for example, the calculation of building structures considering creep). Implicit methods are reduced to a series of solutions of quasistatic problems with time-dependent loads. The time step may not be very small, since at each step a solution of the system of equations is performed and balancing iterations associated with matrix operations are carried out.

Explicit methods are methods for solving equations of motion that are not related to solving systems of equations, but using recurrence relations that express displacements, velocities, and accelerations at current step through their values in the previous steps. To obtain a stable solution, the time step in the calculations is very small compared to implicit methods. Such small steps allow to calculate taking into account all the non-linearities and to thoroughly track the behavior of structures.

In general, the choice of integration method is based on the time duration of the simulated process, as shown in the Figure 2.4.

Despite the fact that the process of ice interaction with structures is relatively lengthy, for the correct consideration of the nonlinear properties of ice in the process of deformation, it is necessary to use small time steps. In this regard, in this thesis **the explicit integration method will be used** for a more detailed and quick assessment of the behavior of the ice during deformation.
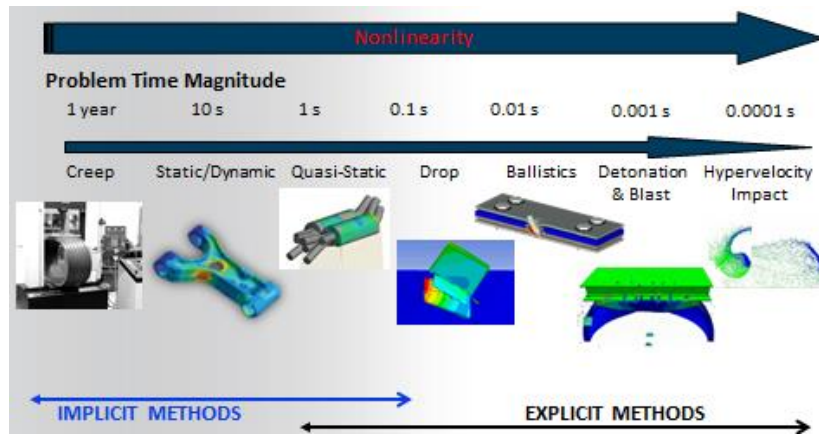
Figure 2.4 – The application boundaries of implicit and explicit methods [6]

Explicit dynamics procedure solves every problem as a wave propagation problem. Out-of-balance forces are propagated as stress waves between neighboring elements. As mentioned earlier, the time increment in explicit dynamics procedure is very small to achieve system stability. A bounded solution is obtained only when the time increment Δt is less than the stable time increment Δt_{min}. The stable time increment is the minimum time that a dilatational (i.e., pressure) wave takes to move across any element in the model. Its value for each element in the model can be calculated as follows:

$$\Delta t_{min} = \frac{L_e}{c_d}, \tag{2.2}$$

where L_e – characteristic length of element;

c_d – the dilatational wave speed:

$$c_d = \sqrt{\frac{E}{\rho}}, \tag{2.3}$$

where E – is the Young's modulus of material;

ρ – current material density.

Thus, decreasing element dimensions, increasing material stiffness, decreasing material compressibility and decreasing material density can reduce the stable time increment and increase the computational cost of solution.

Explicit method uses a central difference rule to integrate the equations of motion explicitly through time, using the kinematic conditions at one increment to calculate the kinematic conditions at the next increment. Initially, the solution comes down to defining accelerations at the beginning of the current increment that can be expressed from equation (2.1) as follows

$$\{\ddot{x}\} = [M]^{-1}(\{F\} - ([C]\{\dot{x}\} + [K]\{x\})) \tag{2.4}$$

Thus, the acceleration of any node is determined completely by its mass and the net force acting on it. Then the accelerations are integrated through time using the central difference rule, which calculates the change in velocity assuming that the acceleration is constant. This change in velocity is

added to the velocity from the middle of the previous increment to determine the velocities at the middle of the current increment:

$$\dot{x}_{\left(t+\frac{\Delta t}{2}\right)} = \dot{x}_{\left(t-\frac{\Delta t}{2}\right)} + \frac{\left(\Delta t_{(t+\Delta t)} + \Delta t_{(t)}\right)}{2} \ddot{x}_{(t)} \tag{2.5}$$

The velocities are integrated through time and added to the displacements at the beginning of the increment to determine the displacements at the end of the increment:

$$x_{(t+\Delta t)} = x_{(t)} + \Delta t_{(t+\Delta t)} \dot{x}_{\left(t+\frac{\Delta t}{2}\right)} \tag{2.6}$$

The solution process of this method of integration of the equations of dynamics is shown in Figure 2.5 and briefly can be explained following steps:

a) the motion of the node points produces deformation in the elements of the mesh;

b) the deformation results in a change in volume (hence density) of the material in each element;

c) the rate of deformation is used to derive material strain rates using various element formulations;

d) constitutive laws take the material strain rates and derive resultant material stresses;

e) the material stresses are transformed back into nodal forces using various element formulations;

f) external nodal forces are computed from boundary conditions, loads and contact (body interaction);

g) the nodal forces are divided by nodal mass to produce nodal accelerations;

h) the accelerations are integrated explicitly in time to produce new nodal velocities;

i) the nodal velocities are integrated explicitly in time to produce new nodal positions;

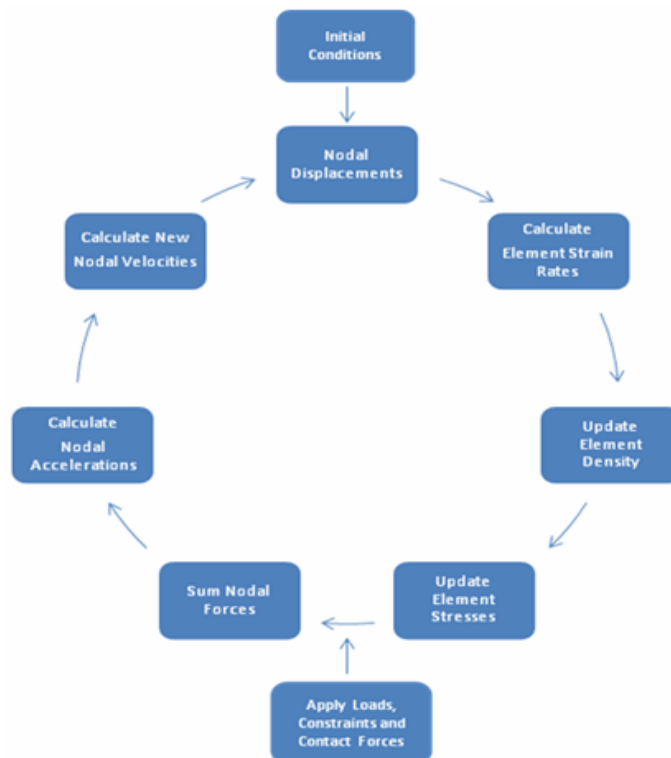g) the solution process (cycle) is repeated until a user defined time is reached.

Figure 2.5 – Solution process of explicit method [7]

2.2.3 General modeling techniques

Geometry of ice formations and structures. Of greatest interest in terms of the shape of vertical structures are single-cylinder cylindrical supports, due to their wide distribution in the construction of offshore structures. Structures of other forms in the plan are also available, but much fewer are built. In this regard, in this dissertation, the impacts of ice formations on **circular structures** will be investigated.

Among the various forms of ice formations, according to the methods of calculating ice load, they distinguish level-ice sheets, hummocks and icebergs. The most common case of impact is the impact of level ice. Its thickness can reach several meters and, in the case of multi-year ice, have a very heterogeneous structure in thickness (Figure 1.4). The dependence of the ice load on the thickness in real conditions is indirect, due to the variable properties through the thickness. In modern analytical calculation methods, today, the dependence of the load on the ratio d/h is considered, where d – width (diameter) of the structure and h is thickness of level-ice sheet. For offshore structures, this ratio usually has a value of more than 5. Lower ratios (with small diameters) are more likely to correspond to various port structures (for example, piers and berths). Thus, cases of ice-structure interactions with **ratios of d/h greater than 5 will be considered**.

As mentioned earlier, the case of interaction with limit stress mode is the most dangerous and therefore of great interest. Thus, the numerical modeling will be performed under the assumption of the **infinite ice field conditions**. Shape of ice sheet in plan is applied as rectangular. To reduce the influence of boundary conditions, the **dimensions of the ice field with respect to the structure diameter d are taken as follows:**

- ice field width in the direction of movement – $6d$;
- width of front face – $12d$.

These dimensions are assigned based on the assumption that stresses propagate over a width of $4d$ (interaction zone). This fact has been investigated by researchers earlier [38] and is adopted in the current national codes [68].

Applied physical and mechanical properties of ice. The importance of taking into account the anisotropic properties of ice over the thickness of the ice field is described in Section 1. To consider the heterogeneous structure of the ice field, the **simulated ice body is divided into 2 connected bodies with a thickness ratio of 1:3** according to SP 38.13330.2018 [68]. This division of the ice field is shown in the Figure 2.6.

It is assumed that the upper body is granular ice layer with random *c*-axes orientations and therefore with isotropic properties. The lower body is taken as a columnar layer with orthotropic properties. For this case the most convenient way to describe ice properties is to accept the fact that the ice field has S2 texture type (Table 1.6) at which *c*-axes are randomly oriented in X_1–X_2 plane (horizontal

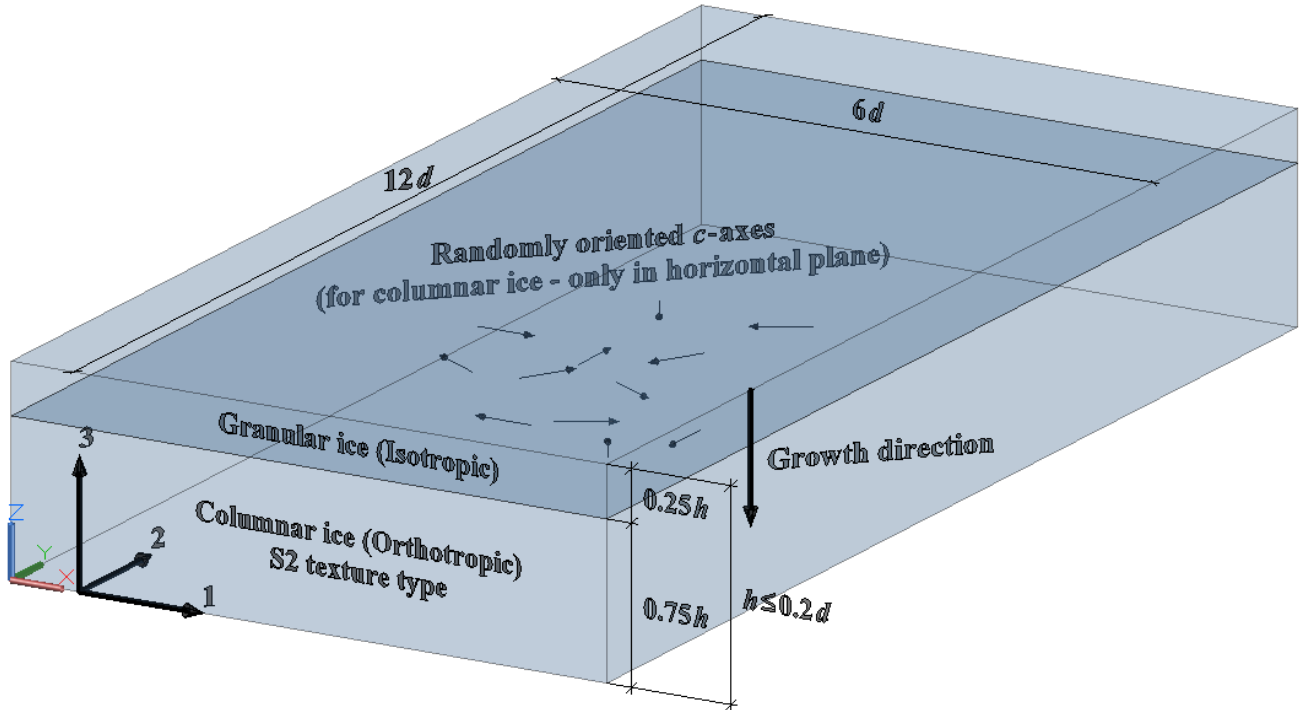plane) and X_3 is parallel to the direction of growth of the ice field.

Figure 2.6 – Geometric dimensions and texture assignments of modeled ice sheet (vertical dimension is scaled by 5 times)

The temperature gradient in ice is assumed linear. The initial temperatures of the ice field are generated by a preliminary steady-state thermal analysis. The temperature calculation results are then integrated into the main model. The boundary temperatures are: on the top face of the ice field – ambient temperature; on the bottom face of the ice field – the freezing temperature of sea water, determined according to SP 38.13330.2018 as follows [68]:

$$t_b = -0{,}057 s_w, \tag{2.7}$$

where s_w – water salinity, ‰.

All equations of physical and mechanical properties of ice, which will be used in this thesis, are presented in Table 2.1. Thus, the initial independent physical properties are temperature at the upper boundary of the ice field, water salinity and ice thickness. Other physical and mechanical properties depend on each other.

Meshing and boundary conditions. Since the cohesive element method shows significant dependence on mesh size, the appropriate mesh settings must be applied. The main work in the interaction of ice on the structures is done by the material near the contact. This region is discretized into the smallest finite elements and has dimensions of about $2d$. Further, the finite elements of the ice field will gradually increase in size up to the boundaries of the simulated ice body. To optimize the time of the model creation process, as well as reduce the distortion of finite elements, their number in thickness is taken equal for the whole body.

Table 2.1 – Equations for determining the physical and mechanical properties of ice

Ice properties	Equation	Equation number	Reference	Additional information
Ice salinity	$s_i = 4{,}606 + \left(\dfrac{91{,}603}{h_i}\right)$	(1.35)	Kovacs (1996) [40]	Used in ISO/DIS 19906:2019 Will be used for ice thickness up to 2 m
Ice density	$\rho_i = 0{,}917 - 1{,}403 \cdot 10^{-4}T$	(1.39)	Cox and Weeks (1983) [14]	-
	$\rho_{si} = (1 - \nu_a)\dfrac{\rho_i \cdot F_1(T)}{F_1(T) - \rho_i \cdot s_i \cdot F_2(T)}$	(1.40)		
Brine salinity, mass and volume	$m_b = s_i \dfrac{1 + (\beta T + l)}{\alpha T + k}$	(1.16)	Nazintsev and Panov (2000) [51]	Used in SP 38.13330.2018
	$s_b = \dfrac{\beta T + l}{1 + \beta T + l}$	(1.18)		-
	$\nu_b = \dfrac{\rho_{si} s_i}{F_1(T)}$	(1.21)	Cox and Weeks (1983) [14]	
Elastic properties	$E_{si} = E_i(1 - \nu_b)^4$	(1.48)	Weeks and Assur (1967) [81]	Used in ISO/DIS 19906:2010
	$E(T) = E(T_r) \cdot \left(1 - a(T - T_r)\right)$	(1.43)	Gammon et al. (1983) [25]	Based on measurements using Brillouin spectroscopy
	$G(T) = G(T_r) \cdot \left(1 - a(T - T_r)\right)$			
	$\mu_{i,s}(T) = \mu_{i,s}(T_r) \cdot \left(1 - a(T - T_r)\right)$			
Compressive strength	$\sigma_c = 37(\dot{\varepsilon})^{0{,}22}\left(1 - \sqrt{\dfrac{\nu_t}{270}}\right)$	(1.57)	Timco and Frederking (1990) [75]	Used in ISO/DIS 19906, ANSI API RP 2N-2015, CSA/S471-04
	$\sigma_c = 160(\dot{\varepsilon})^{0{,}22}\left(1 - \sqrt{\dfrac{\nu_t}{200}}\right)$	(1.58)		
	$\sigma_c = 49(\dot{\varepsilon})^{0{,}22}\left(1 - \sqrt{\dfrac{\nu_t}{280}}\right)$	(1.59)		

The effect of the mesh pattern on the result will be later explored in this thesis. To simulate the conditions of an infinite ice field, all the faces of the body except the frontal one are constrained from movements in the direction orthogonal to the direction of motion. The initial velocity is also assumed constant on these faces. Destroyed ice in the process of interaction continues to affect the structure. Crushed ice increases the contact area, and also adds some vertical component acting on the ice field. In this regard, the forces of gravity and buoyance cannot be neglected. Gravity is taken into account very simply, by adding the appropriate load object to the bulk elements through the interface of the Abaqus software. Buoyancy can be modeled in several ways.

The first is a Coupled Eulerian-Lagrangian (CEL) approach. In this case the two formulations of finite elements (Eulerian and Lagrangian) are used simultaneously. Ice field and structure are modeled by finite elements in Lagrangian formulation (material and mesh are interconnected). Water medium is modeled by Eulerian domain in which the mesh doesn't move during the analysis and water material "flow" through the mesh. For this approach water material is usually modeled using equations of state (EOS) that represents the hydrodynamic behaviour. Since this approach significantly increases the computational cost of calculations, the **second method of modeling buoyancy will be used**.

The main idea of the second method is to reproduce the water pressure acting on the external faces of bulk elements. If we assume that the vertical z-axis in the model is directed up, then buoyancy pressure p, Pa, in the node of submerged finite element can be calculated as follows:

$$p = \rho_w g(z_0 - z), \tag{2.8}$$

where ρ_w – density of sea water, kg/m³;

g – gravitational acceleration, m/s²; $g \approx 9{,}81\ m/s^2$;

z_0 – coordinate of water surface in vertical direction (z-axis), m;

z – coordinate of node in vertical direction, m;

In the toolkit of the Abaqus software package, there is no way to add a pressure depending on the distance, the value of which will be updated every time increment. To add such pressure load the following **subroutine was created in the Fortran programming language**, which was then initialized at the beginning of each calculation time increment:

```
      subroutine vdload (nBlock, ndim, stepTime, totalTime, amplitude,
     & curCoords, velocity, dirCos, jltyp, sname, value)
! General subroutine settings
       include 'vaba_param.inc'

       dimension curCoords(nBlock,ndim), velocity(nBlock,ndim),
     1  dirCos(nBlock,ndim,ndim), value(nBlock)
       character*80 sname
! User-defined parameters
       parameter (WaterDens = 1020, Gravity = 9.81, Zmax = 0, IceH = 1,
     *       IceDens = 930)
! WaterDens - approximate water density
! Gravity - gravity acceleration
! Zmax - z-coord (in vertical direction) of ice bottom
```

```
! Ice dens - approximate ice density (average)

    parameter (iX    = 1,
  *          iY    = 2,
  *          iZ    = 3)
! Subroutine main
! Repeat every time increment
    do i = 1, nBlock

     if(curCoords(i,iZ) .Le. Zmax) then
       Pressure = WaterDens*Gravity*(IceH*IceDens/WaterDens+Zmax
  *           - curCoords(i,iZ)) ! Calculated buoyancy pressure
      value(i) = Pressure
     else
      value(i) = 0.d0
     endif
    end do
    return
    end
```

2.2.4 Selection of constitutive models for ice material

Sea ice, as described earlier, is an extremely complex material. It can exhibit both plastic and brittle properties. Moreover, depending on the structure, ice formations can be considered as isotropic or orthotropic bodies. In this thesis, granular ice located mainly in the upper layers are assumed to be isotropic, since, as mentioned above (subsection 1.3), it has a random orientation of single crystals. In the case of columnar ice, the principle of isotropy cannot be applied, since the properties of such ice are very different in different directions. A good solution would be to consider columnar ice polycrystals as an orthotropic material.

To describe complex material behavior constitutive model are used. Constitutive model of material is a set of mathematical relationships which describes the material behavior under different loading conditions. Today there are a huge number of different models of materials that mathematically describe their various features. To model the actions of ice on vertical offshore structures, it is necessary to describe the behavior of the ice at all its stages up to destruction. For this, elasticity models, plasticity models, as well as the damage initiation (failure) criteria and damage evolution laws, will be considered.

Elasticity model. As basic parameters for modeling, elastic properties are used. These properties can be defined via the corresponding elasticity models. In this thesis, **isotropic and orthotropic elasticity** is used to model ice material behavior where the stress versus strain relationship is linear and the loading is kept within the elastic range. The models follow Hooke's law (equation 1.42), so assumes that the stretch or compression remains in the elastic range of the material and the model will return to its original shape after unloading. The elastic properties of polycrystals of isotropic and orthotropic ice are presented in Table 1.5 and Table 1.6, respectively. The temperature dependence of the characteristics is determined by the equation (1.43).

In case of cohesive elements, the constitutive response is defined in terms of traction versus-separation law. It assumes a linear elastic traction-separation law prior to damage. The elastic behavior is written in terms of an elastic constitutive matrix that relates the nominal stresses to the nominal strains across the interface. The nominal stresses are the force components divided by the original area at each integration point, while the nominal strains are the separations divided by the original thickness at each integration point. The default value of the original constitutive thickness equal to 1.0 will be used, which ensures that the nominal strain is equal to the separation. The elastic behavior can then be written as [71]

$$t = \begin{Bmatrix} t_n \\ t_s \\ t_t \end{Bmatrix} = \begin{bmatrix} E_{nn} & E_{ns} & E_{nt} \\ E_{ns} & E_{ss} & E_{st} \\ E_{nt} & E_{st} & E_{tt} \end{bmatrix} \begin{Bmatrix} \varepsilon_n \\ \varepsilon_s \\ \varepsilon_t \end{Bmatrix}, \tag{2.9}$$

where t_n – normal component of nominal traction stress vector, Pa;

t_s and t_t – shear components of nominal traction stress vector, Pa;

E_{ij} – corresponding elastic (or shear) modulus, Pa;

ε_n, ε_s, ε_t – normal and two shear components of strain vector respectively:

$$\varepsilon_i = \frac{\delta_i}{T_0}, \tag{2.10}$$

where δ_i – corresponding separations, m;

T_0 – original constitutive thickness of cohesive element; since $T_0 = 1$ the strains and separations are equal.

However, a simplified formulation can be used in which the behavior of the cohesive elements in the normal and tangent directions is uncoupled. In this case each traction component t_i depends only on its conjugate nominal strain ε_i:

$$t = \begin{Bmatrix} t_n \\ t_s \\ t_t \end{Bmatrix} = \begin{bmatrix} E_{nn} & 0 & 0 \\ 0 & E_{ss} & 0 \\ 0 & 0 & E_{tt} \end{bmatrix} \begin{Bmatrix} \varepsilon_n \\ \varepsilon_s \\ \varepsilon_t \end{Bmatrix}, \tag{2.11}$$

Plasticity model. To describe the plastic properties of ice, it is necessary to choose a plasticity model. Typically, plasticity models consist of three main components [4]:

- the yield criterion that defines the material state at the transition from elastic to plastic behavior;

- the flow rule that determines the increment in plastic strain from the increment in load;

- the hardening (or softening) rule that gives the evolution in the yield criterion during plastic deformation.

The following yield theories with corresponding materials models are most widely used in structural analysis: von Mises yield theory, Tresca theory, Mohr-Coulomb theory and Drucker-Prager theory. High usability of these models is associated with the ease of use – the parameters needed to determine the yield surface can be obtained from standard material tests (yield strength, internal friction angle, adhesion).

Von Mises yield criterion is isotropic and independent of hydrostatic pressure, which can limit its applicability to microstructured materials and materials that exhibit plastic dilatation such as steels. This material model as mentioned before was used by such researchers as Gürtner et al. (2009) [30], Gürtner et al. (2010) [29], Hilding et al. (2011) [31], Hilding et al. (2012) [32] and Wang et al. (2019) [79]. It includes an associated flow rule. Yield surface in axes of principal stresses is presented in Figure 2.7, a. The von Mises yield criterion is [4]:

$$F = \sigma_e - \sigma_y = 0, \tag{2.12}$$

where σ_y – yield strength of material;

σ_e is the von Mises equivalent stress, also known as the von Mises equivalent stress:

$$\sigma_e = \sqrt{3J_2}, \tag{2.13}$$

J_2 – second deviatoric stress invariant:

$$J_2 = \frac{(\sigma_{11} - \sigma_{22})^2 + (\sigma_{22} - \sigma_{33})^2 + (\sigma_{33} - \sigma_{11})^2}{6} + \sigma_{12}^2 + \sigma_{23}^2 + \sigma_{31}^2, \tag{2.14}$$

where $\sigma_{11}, \sigma_{22}, \sigma_{33}, \sigma_{12}, \sigma_{23}, \sigma_{31}$ are stress components of Cauchy stress tensor $\boldsymbol{\sigma}$:

$$\boldsymbol{\sigma} = \begin{bmatrix} \sigma_{11} & \sigma_{12} & \sigma_{13} \\ \sigma_{21} & \sigma_{22} & \sigma_{23} \\ \sigma_{31} & \sigma_{32} & \sigma_{33} \end{bmatrix}.$$

The Tresca theory suggests that the material goes into a plastic state when the maximum shear stress τ_{max} reaches the shear yield strength σ_{shear}. Yield surface in axes of principal stresses is presented in Figure 2.7, a. The Tresca yield criterion is [4]:

$$F = \tau_{max} - \sigma_{shear} = 0, \tag{2.15}$$

The above criteria do not consider the effect of hydrostatic stress on the condition of the transition of the material into plastic behavior. Some materials show the influence of the hydrostatic stress component on yielding onset: the higher the hydrostatic stress (confinement pressure) the higher the yield strength. The two simplest models that take this feature into account are the Mohr-Coulomb and the Drucker-Prager models.

The Mohr-Coulomb material model is used to represent the behavior of aggregate materials. Aggregate materials such as soil, rock and concrete begin to plastically deform when the shear stress exceeds the internal friction resistance between the material particles. The friction resistance is a function of the normal force between the particles. The model defines yielding when the combination of pressure and shear stress reaches the cohesion of the material particles. Mohr-Coulomb yield criterion was used as fracture criterion by Politko (2018) [56]. Yield surface in axes of principal stresses is presented in Figure 2.7, b. Yielding occurs when the shear stress τ on any plane in the material reaches this criterion:

$$\tau = c - \sigma_m \tan \varphi, \tag{2.16}$$

where c – material cohesion;

φ – angle of internal friction;

σ_m – hydrostatic stress:

$$\sigma_m = \frac{\sigma_{11} + \sigma_{22} + \sigma_{33}}{3} \qquad (2.17)$$

The classic Drucker-Prager model is used for modeling the granular materials such as soils, rock, concrete and uses the outer cone approximation to the Mohr-Coulomb law. This yield surface is a circular cone with the material parameters chosen such that it corresponds to the outer apices of the hexagonal Mohr-Coulomb yield surface as presented in Figure 2.7, b. Yield criterion of classic Drucker-Prager model is [5]:

$$F = 3\beta\sigma_m + \sqrt{J_2} - \sigma_y = 0, \qquad (2.18)$$

where β and σ_y – material model parameters;

J_2 – second deviatoric stress invariant expressed in equation (2.14);

σ_m – hydrostatic stress expressed in equation (2.17).
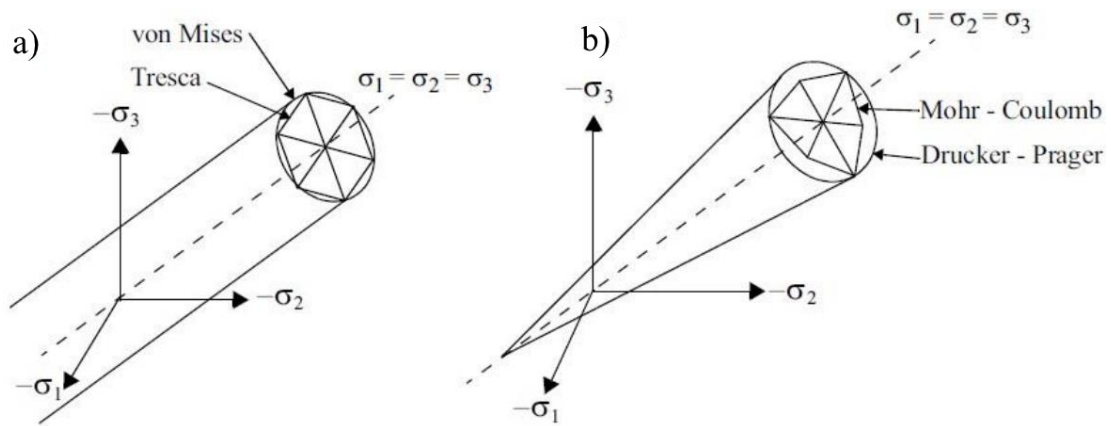

Figure 2.7 – Yield surfaces in axes of principal stresses: a) von Mises and Tresca; b) Mohr-Coulomb and classic Drucker-Prager [56]

Among the other plasticity models that were used in different papers the following can be distinguished: Extended Drucker-Prager models, Hill plasticity, Johnson-Cook, Orthotropic Yield model, Horrigmoe and Zeng's model and others. Some description of these models and discussion about their applicability for modeling ice problems are described in [48].

For isotropic ice **Linear Drucker-Prager criteria will be used** for modeling the yielding of pressure-dependent granular ice with different values of tension and compression yield stresses. Yield surface shown in Figure 2.8 provides for a possibly noncircular form in the deviatoric plane (π-plane) to match different yield values in triaxial tension and compression, associated inelastic flow in the deviatoric plane, and separate dilation and friction angles. The linear Drucker-Prager criterion is written as

$$F = t - p\tan\varphi - c = 0, \qquad (2.19)$$

where p – pressure stress:

$$p = -\sigma_m \qquad (2.20)$$

71

φ – the slope of the linear yield surface in the p–t stress plane and is commonly referred to as the friction angle of the material;

t – value determined by the following equation:

$$t = \frac{1}{2}\sigma_e \left(1 + \frac{1}{K} - \left(1 - \frac{1}{K} \right) \left(\frac{J_3}{\sigma_e} \right)^3 \right), \tag{2.21}$$

where K – the ratio of the yield stress in triaxial tension to the yield stress in triaxial compression and, thus, controls the dependence of the yield surface on the value of the intermediate principal stress;

J_3 – third deviatoric stress invariant:

$$\frac{2}{27}I_1^3 - \frac{1}{3}I_1 I_2 + I_3, \tag{2.22}$$

where I_1, I_2 and I_3 – first, second and third stress invariants, respectively:

$$I_1 = \sigma_{11} + \sigma_{22} + \sigma_{33}, \tag{2.23}$$

$$I_2 = \begin{vmatrix} \sigma_{22} & \sigma_{23} \\ \sigma_{32} & \sigma_{33} \end{vmatrix} + \begin{vmatrix} \sigma_{11} & \sigma_{13} \\ \sigma_{31} & \sigma_{33} \end{vmatrix} + \begin{vmatrix} \sigma_{11} & \sigma_{12} \\ \sigma_{21} & \sigma_{22} \end{vmatrix}, \tag{2.24}$$

$$I_3 = \begin{vmatrix} \sigma_{11} & \sigma_{12} & \sigma_{13} \\ \sigma_{21} & \sigma_{22} & \sigma_{23} \\ \sigma_{31} & \sigma_{32} & \sigma_{33} \end{vmatrix} \tag{2.25}$$
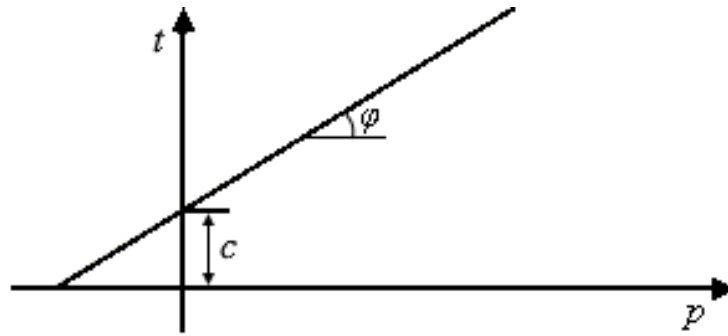

Figure 2.8 – Yield surface of linear Drucker-Prager criterion in the meridional plane

The input parameters when using Simulia ABAQUS software are the angle of internal friction φ, as well as the stress $\bar{\sigma}_0$, which determine the initial shape of the yield surface (at zero values of plastic strains $\bar{\varepsilon}^{pl}$). The yield strengths described above also depend on the strain rate and temperature.

In Simulia ABAQUS, the stresses $\bar{\sigma}_0$, which determine the initial yield surface, as well as the equivalent stresses $\bar{\sigma}$, with the corresponding plastic strain values $\bar{\varepsilon}^{pl}$, which determine the hardening, can be interpreted by the user as the yield strength under uniaxial compression, tension or pure shear. It is obvious that the most convenient is the determination of hardening through uniaxial compression stresses, since in most cases the data on the nonlinear nature of ice deformation were obtained by the authors through uniaxial compression tests. On the other hand, for brittle materials, including ice, the cohesion c can be interpreted as the yield stress on pure shear, but when determining the hardening through compression stresses, the cohesion value c will be automatically calculated in the model

depending on the angle of internal friction β, defined by the user, according to the following equation [72]:

$$d = \left(1 - \frac{1}{3}\tan\beta\right)\bar{\sigma} \tag{2.26}$$

In addition, the angle of internal friction β for brittle materials is a conditional characteristic, and for a material such as ice, the selection of the optimal value is a difficult task. In this regard, the following algorithm for modeling ice using the linear Drucker-Prager model in the Simulia ABAQUS software package will be used [48]:

1) Determination of values of the ultimate strength of ice for uniaxial compression σ_c and shear σ_τ, corresponding to several values of temperature t and strain rate $\dot{\bar{\varepsilon}}^{pl}$.

2) Assuming that $\bar{\sigma} = \sigma_c$, and $c = \sigma_\tau$, the calculation of the angle of internal friction values β by the equation

$$\beta = \tan^{-1}\left(\frac{3 \cdot (\sigma_c - \sigma_\tau)}{\sigma_c}\right) \tag{2.27}$$

Thus, the shape of the yield surface will most accurately describe the strength characteristics of the simulated ice. When the stress level in the volume element of the compressive strength is reached, its deformation will continue as perfectly plastic.

Failure criterion and post-fracture behavior. To determine the conditions under which the material is destroyed, the failure criteria are used. When using the damage evolution laws fracture criteria are also called "damage initiation criteria". Often, fracture criteria are represented as failure surfaces in the space of principal stresses. In the structural analysis of structures, the behavior of materials after destruction is usually not considered, since structures are designed from the condition of preventing their destruction. However, in this thesis, the process of ice load formation is considered taking into account ice destruction. In the simple case, it can be accepted that the ice is destroyed after failure. In this way, *instantaneous failure* is modeled. Bur after the appearance of cracks and partial destruction, the ice is still able to affect the structure up to complete destruction. The so-called damage evolution laws can be used to describe the behavior of ice after failure. In this way, *gradual failure (damage)* is modeled. Fracture energy-based damage models are commonly used for this purpose.

Many criteria determine the destruction of the material when the value of plastic deformation $\bar{\varepsilon}^{pl}$ reaches a critical value $\bar{\varepsilon}^{pl}_{max}$. In most cases, the fact is accepted that the destruction of the material occurs when it reaches a yield surface (for example, when calculating steel structures). This is especially valid when describing the fracture of brittle materials such as rock, concrete and ice. In this case, it can be accepted that the condition of fracture onset is the appearance of plastic deformations ($\varepsilon_{pl} > 0$). These criteria work well when describing the fracture of ductile materials such as metals. Estimation of optimal value of critical strains is a very difficult task, since in experiments even among samples with similar

parameters, critical strains vary greatly However, in order to maintain the stability of the system and prevent excessive distortion of the finite elements, the criterion of critical plastic strains will be applied to bulk elements. A plastic strain value of 1 will be used as a criterion for the removal of elements for the first modeling iterations. This value is several times higher than the possible real values for ice and, accordingly, will not affect the ice-structure interaction process.

In subsequent numerical experiments, the main process of destruction of ice is modeled using cohesive elements. So, the traction of cohesive elements is not infinite and have limits. In Abaqus software there are several failure models that can be applied to cohesive elements. The initial response of the cohesive element is assumed to be linear as discussed above. However, once a damage initiation criterion is met, material damage occurs according to a damage evolution law also called traction-separation law (Figure 2.9). The cohesive elements do not undergo damage under pure compression.
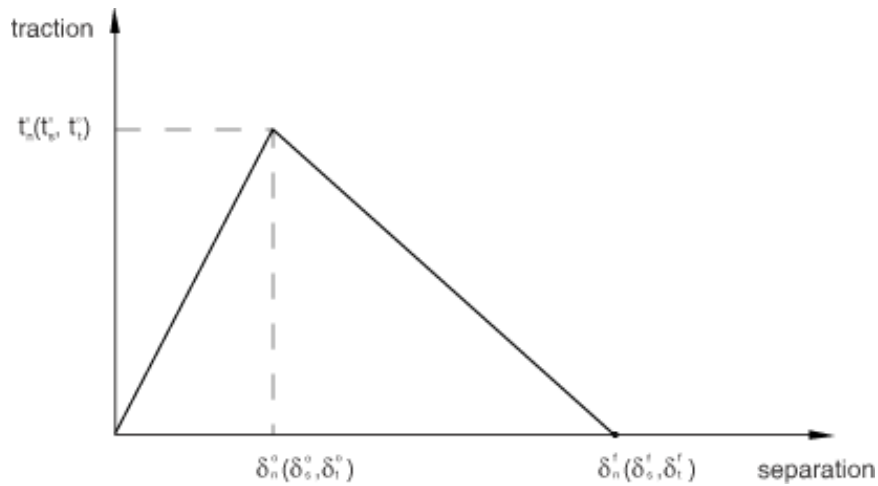

Figure 2.9 –Typical traction-separation response of cohesive elements [71]

Damage initiation refers to the beginning of degradation of the response of a material point. The process of degradation begins when the stresses satisfy the following damage initiation criteria:

$$max \left\{ \frac{\langle t_n \rangle}{t_n^0}, \frac{t_s}{t_s^0}, \frac{t_t}{t_t^0} \right\} = 1, \tag{2.28}$$

where t_n^0, t_s^0 and t_t^0 – maximum values of corresponding tractions.

The damage evolution law describes the rate at which the material stiffness is degraded once the corresponding initiation criterion is reached. The stress components of the traction-separation model are affected by the damage according to:

$$t_n = \begin{cases} (1-D)\bar{t}_n, & \bar{t}_n \geq 0 \\ \bar{t}_n, & \bar{t}_n < 0 \end{cases} \tag{2.29}$$

$$t_s = (1-D)\bar{t}_s, \tag{2.30}$$

$$t_t = (1-D)\bar{t}_t, \tag{2.31}$$

where $\bar{t}_n$, $\bar{t}_s$ and $\bar{t}_t$ are the stress components predicted by the elastic traction-separation behavior for the current strains without damage;

D – scalar damage variable represents the overall damage in the material and captures the combined effects of all the active mechanisms. It initially has a value of 0. Then the value of *D* monotonically evolves from 0 to 1 upon further loading after the initiation of damage.

In the case of an orthotropic material, individual strength limits for compression, tension and shear in all three directions can be considered.

2.3 Section conclusions

Thus, the advantages and disadvantages of numerical methods were considered. The finite element method with an approach to modeling ice fracture by the method of cohesive elements was chosen as a tool for solving the tasks described above. Numerical modeling will be performed using the Simulia ABAQUS software and for integration of general equation of motion (2.1) explicit method will be used.

The basic principles of creation a numerical model were also identified, as well as constitutive models for modeling ice material. To use the above principles in numerical modeling, it is necessary to follow the certain algorithm, starting with a description of the simulated situation (the size and shape of the ice formation and structure, the speed of ice formation, temperature) and ending with the interpretation of the calculation results (history of ice load, cyclic movement of the structure). Typical scheme for performing numerical experiments is presented in Figure 2.10.
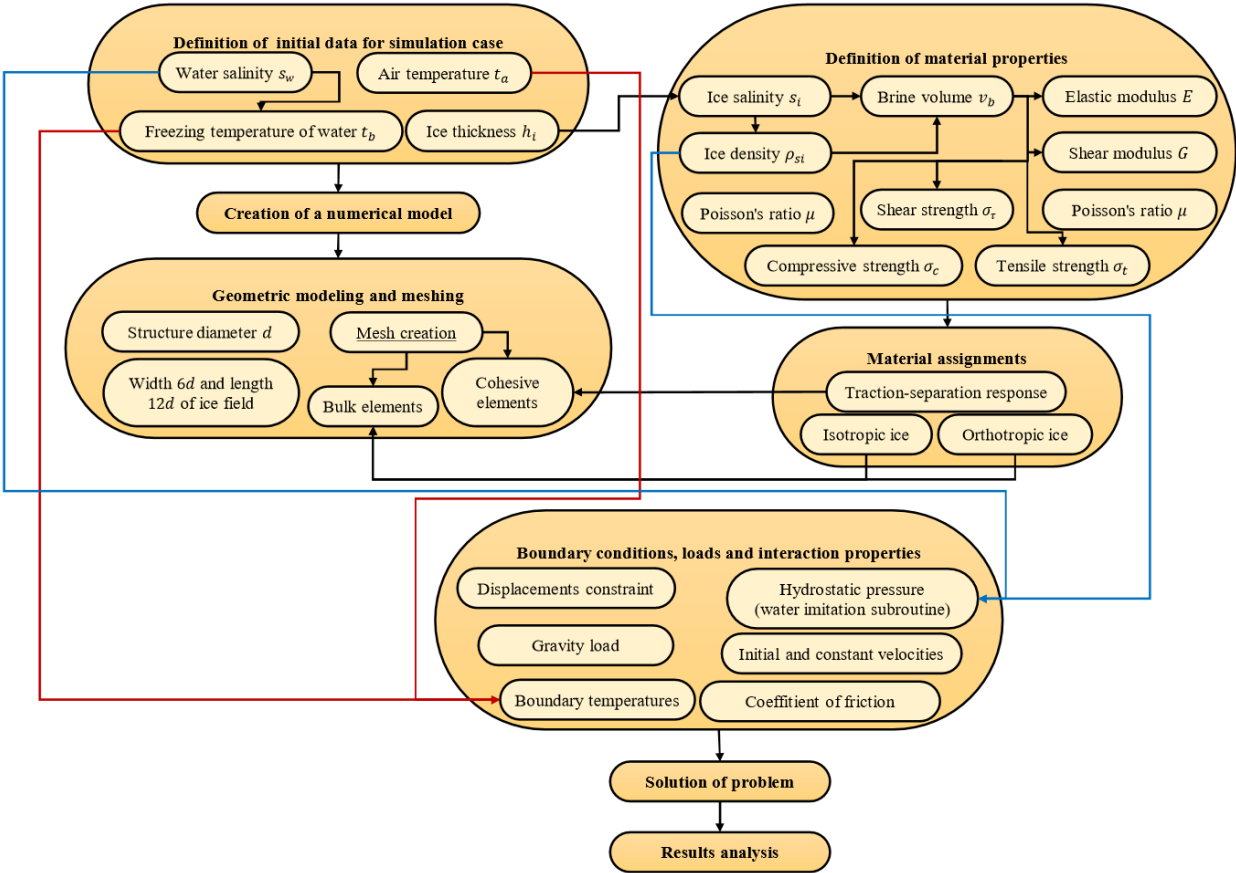

Figure 2.10 – Typical calculation algorithm

In the numerical model there is a joint work of bulk elements modeling the deformability of ice, as well as cohesive elements modeling its destruction. The parameters of a model with such a complex interaction require additional justification. Thereby, to analyze the applicability of the developed model it is necessary to perform numerical experiments. The main goal of experiments is to study the developed model of the ice-structure interaction by varying its parameters and assessing the quality of the interaction picture. Subsequent simulations will be performed according to following plan:
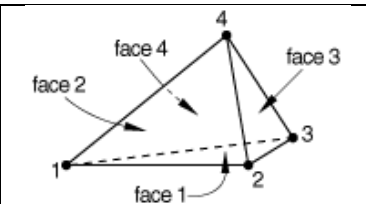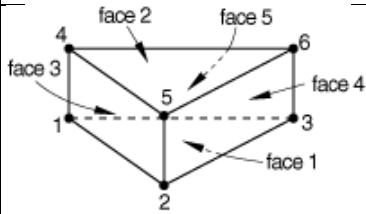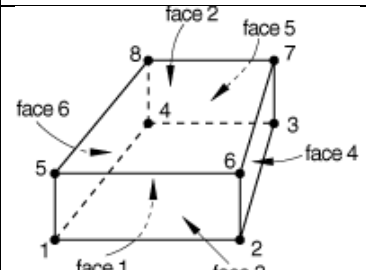
1. Studying the influence of a mesh pattern;

2. Studying the influence of the size of bulk elements;

3. Selection of the optimal value of critical strains at which bulk elements are removed;

4. The study of correspondence of the plasticity response and the pattern of deformation of bulk elements to real conditions;

5. Examination of the formation of a complex stress-strain state and its effect on the ice load value.

3 Numerical experiments on the impacts of ice formations on vertical structures and development of the model
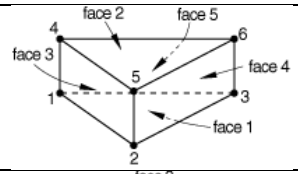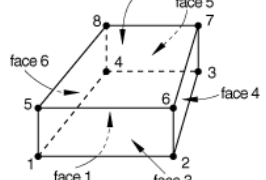
3.1 Assessment of the influence of mesh pattern

Since the solution of the tasks is performed by the numerical finite element method, it is necessary to evaluate the effect of the finite element mesh on the modeling results. This assessment is especially important when using the cohesive element method since the faces of bulk elements are possible crack paths. There are several types of finite elements in the library of the Abaqus/Explicit module, with which the volumetric body of an ice field can be discretized. They differ in geometric order, degrees of freedom, the presence of hourglass control and other functions. Since connected finite elements can only be of low geometric order and the ice field mesh must be conformal, quadratic bulk elements are not considered further. Available cohesive and linear bulk finite elements with temperature degree of freedom in the Abaqus/Explicit module are presented in Table 3.1.

Table 3.1 – Available types of finite elements for modeling of ice field

Code name	Description	Picture
Bulk elements		
C3D4T	A 4-node thermally coupled tetrahedron, linear displacement and temperature	
C3D6T	A 6-node thermally coupled triangular prism, linear displacement and temperature	
C3D8T	An 8-node thermally coupled brick, trilinear displacement and temperature	

Continuation of Table 3.1

Cohesive elements		
COH3D6	A 6-node three-dimensional cohesive element	
COH3D8	An 8-node three-dimensional cohesive element	

Thus, four mesh patterns will be compared: unstructured tetrahedral mesh using C3D4T and COH3D6 elements, unstructured prism mesh using C3D6T, COH3D6 and COH3D8 elements, structured hex mesh using C3D8T and COH3D8 elements, unstructured hex mesh using C3D8T and COH3D8 elements. Finite element models for all 4 cases are presented in Figure 3.1. Minimum and maximum mesh sizes are the same for all cases and equal to 0.25 m and 1.5 m respectively. Only four "layers" of elements in thickness are created to reduce calculation time.
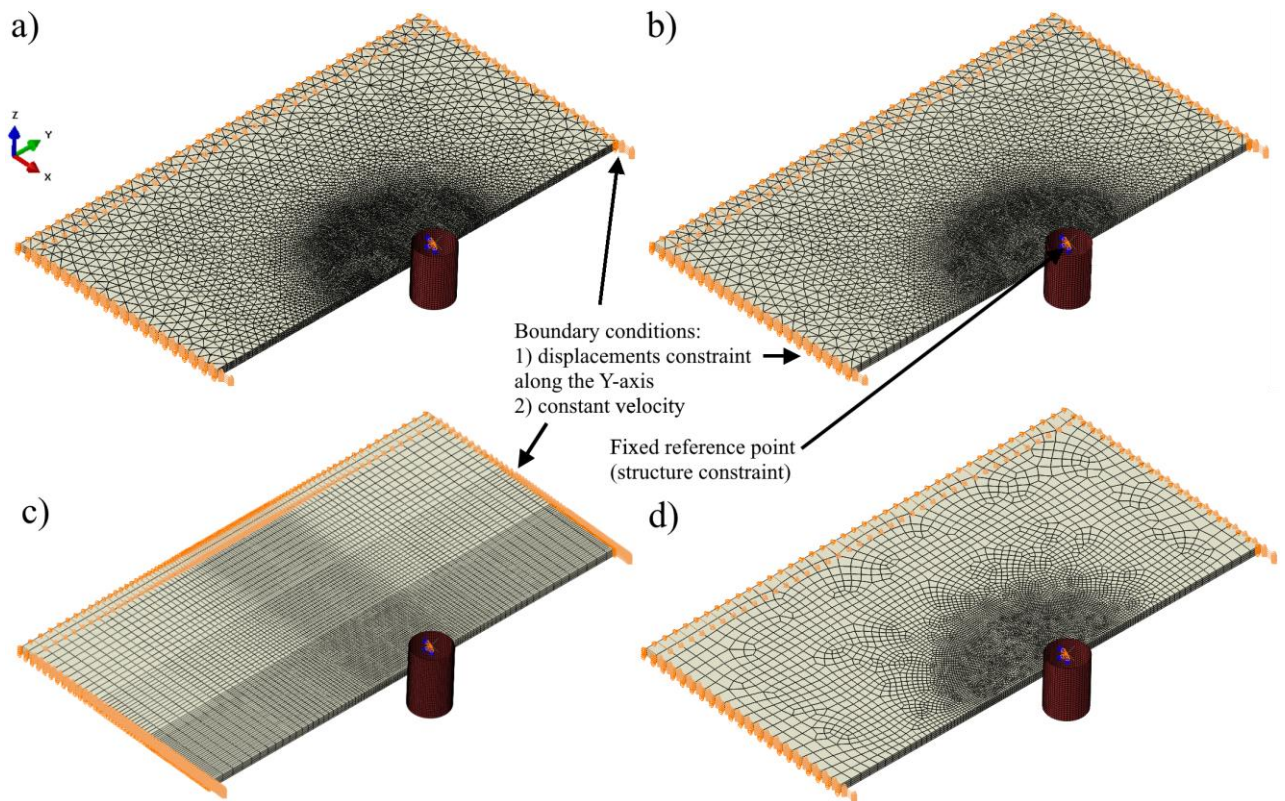

Figure 3.1 – Finite element models with different mesh patterns: a) tetrahedral mesh; b) prism mesh; c) structured hex mesh; d) unstructured hex mesh

To perform this study, a model is created with the following parameters:

- diameter of the structure d equal to 5 m;

- ice sheet dimensions 60x30x1 m;

- drift velocity v equal to 0.5 m/s;

- water salinity s_w equal to 20 ‰;

- air temperature t_a equal to -20 °C;

- only isotropic ice and linear behavior will be considered.

Other physical and mechanical properties are determined according to the accepted methodology (section 2). The time of simulation is assumed to be 5 seconds, so that the structure crashes into the ice field to full width. As an evaluation criterion, the general picture of ice destruction, as well as the history of ice load during the simulation, are used.

In Table 3.2 the information is presented about the components of the computer on which all calculations are performed.

Unfortunately, in the current version of the ABAQUS software package it is impossible to use a graphic card to perform calculations with explicit time integration. All calculations are performed on CPU. General modeling information is presented in Table 3.3. Ice load history in the direction parallel (*x*-axis) and orthogonal to the direction of movement (*y*-axis) is presented in Figure 3.2 and Figure 3.3.

Table 3.2 – Computer specifications

Component	General information
Motherboard	GigabyteX570 Aorus Ultra (rev. 1.0) PCI Express 4.0
Central processing unit (CPU)	AMD Ryzen 9 3900x, 12 cores 4.1 GHz, 24 threads
Random-access memory (RAM)	DDR4 DIMM 16x4 GB (64GB total) 3200 MHz
Storage device	Sabrent 1TB Rocket NVMe 4.0 Gen4 PCIe M.2 Internal SSD Extreme Performance Solid State Drive (SSD); Read speed 5000 MB/s; Write speed 4400 MB/s

Table 3.3 – General modeling information

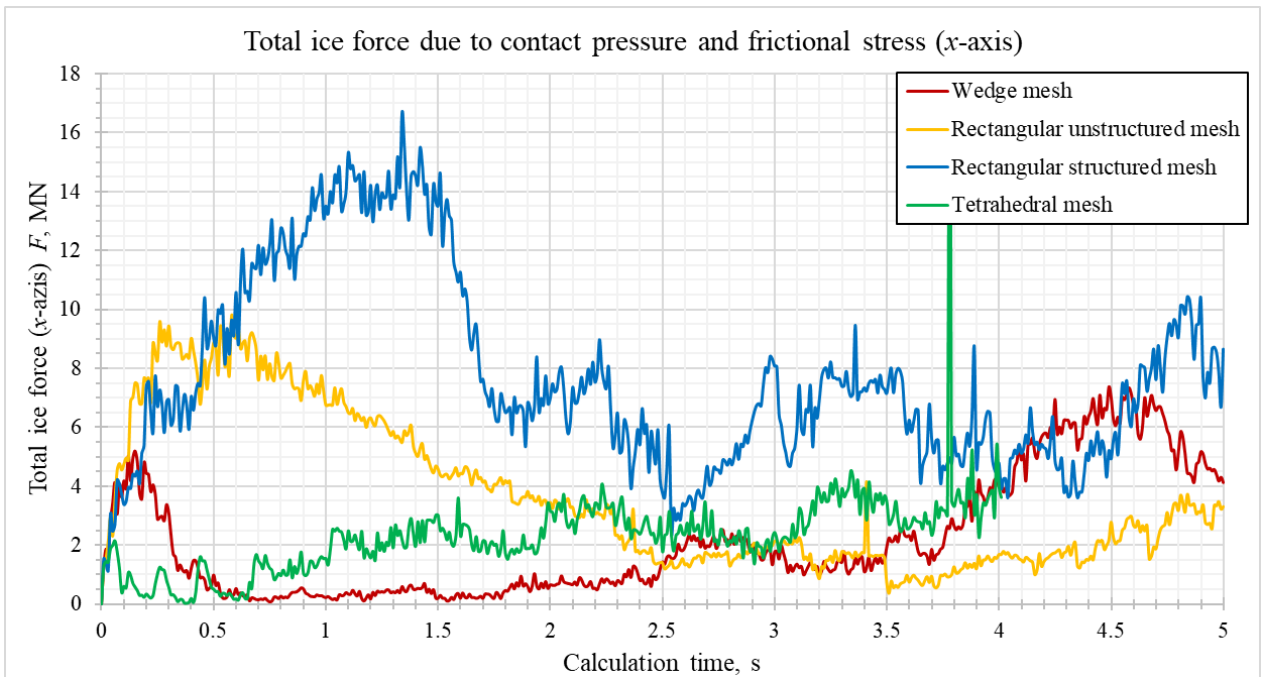| Case	Number of finite elements (bulk / cohesive)	Total calculation time, hours	Peak total ice force along direction of motion F_x^{tot}, MN
Tetrahedral mesh	124 261 / 236 075	48.63 (4.01 s out of 5)	-
Prism mesh	46 272 / 103 672	12.61	7.358
Unstructured hex mesh	26 312 / 71 918	4.88	9.785
Structured hex mesh	29 808 / 81 264	2.25	6.224

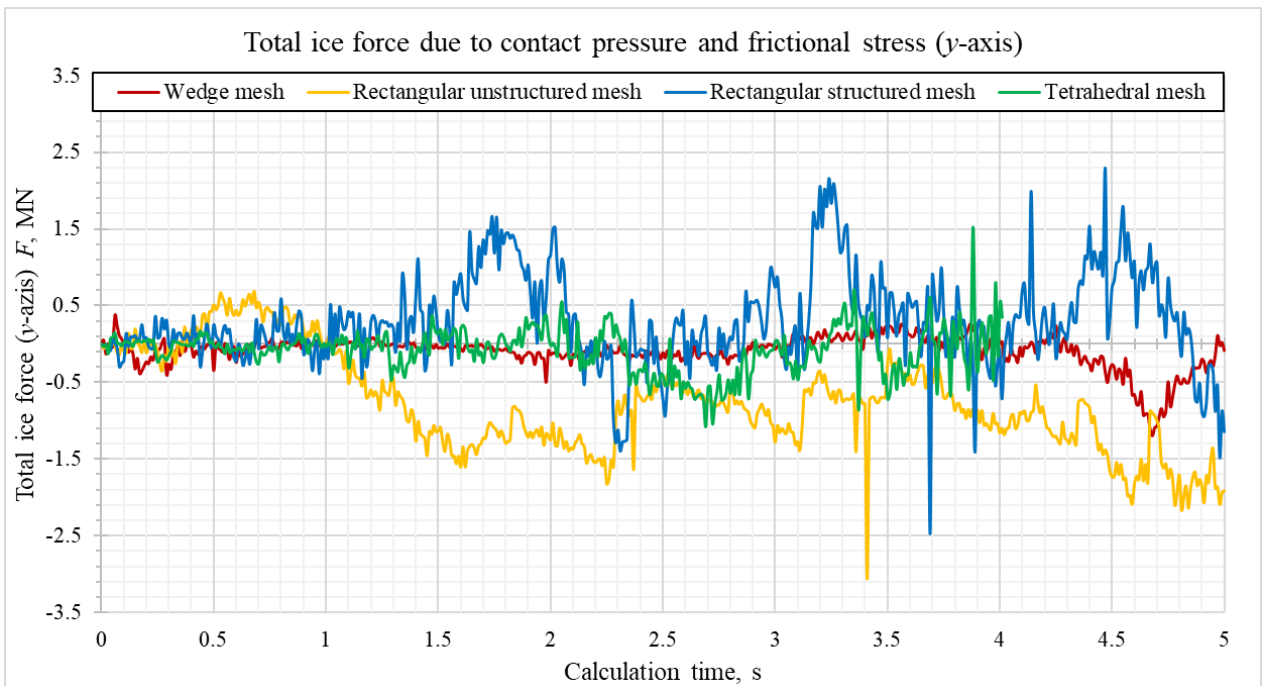Figure 3.2 – Load history with different mesh patterns (along *x*-axis)

Figure 3.3 – Load history with different mesh patterns (along *y*-axis)

As we can see mesh patterns showed quite different results. First, let us consider the *structured hex mesh* case. In my opinion this type of mesh showed the worst result. Peak force with extremely large value of 16.676 MN occurs at 1.34 s of calculation time, which corresponds to a depth of penetration of the structure of 0.67 m, and then decreases to average values around 6.23 MN. Obviously, this does not correspond to the real mechanics of the ice-structure interaction. Also, these values are several times higher than other cases. The picture of ice destruction at the end of the calculation is presented in Figure 3.4.
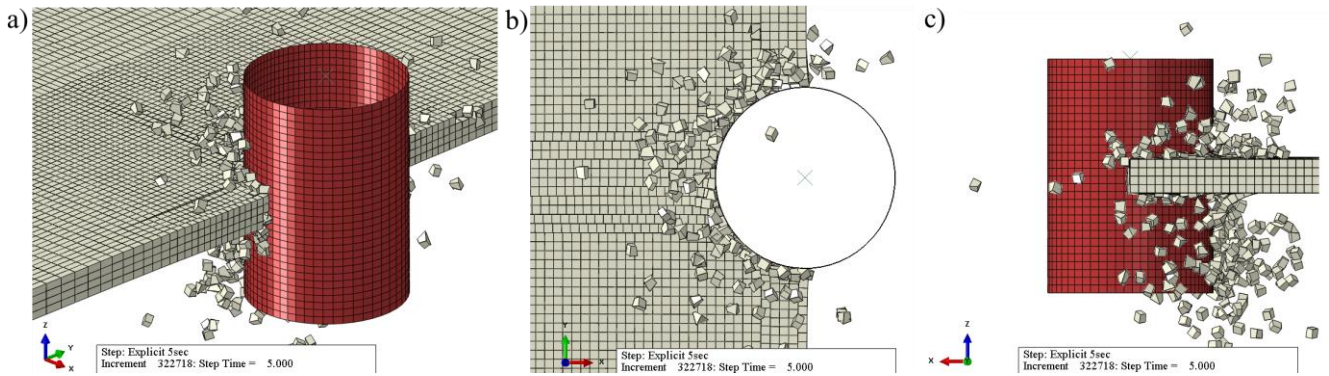
Figure 3.4 – Ice crushing during impact of ice field in case of structured hex mesh: a) general view; b) top view; c) side view

As we can see, the vertical cohesive elements destroyed along several parallel faces of the central finite elements. To understand the reason, it is necessary to consider the very beginning of the interaction. Figure 3.5 shows that, at first, the two closest finite elements to the structure begin to interact with it. Then, shear stresses τ_{xz} arise on the lateral faces of these elements. Since the mesh is structured, the propagation of stresses passes deep into the field in a straight line without any bulk elements in the pass. The cause of the unrealistic destruction of vertical cohesive elements is the rapid propagation of shear stresses τ_{xz}, while cohesive elements orthogonal to them are not working. This is clearly seen when looking at the fracture pattern presented in Figure 3.6.
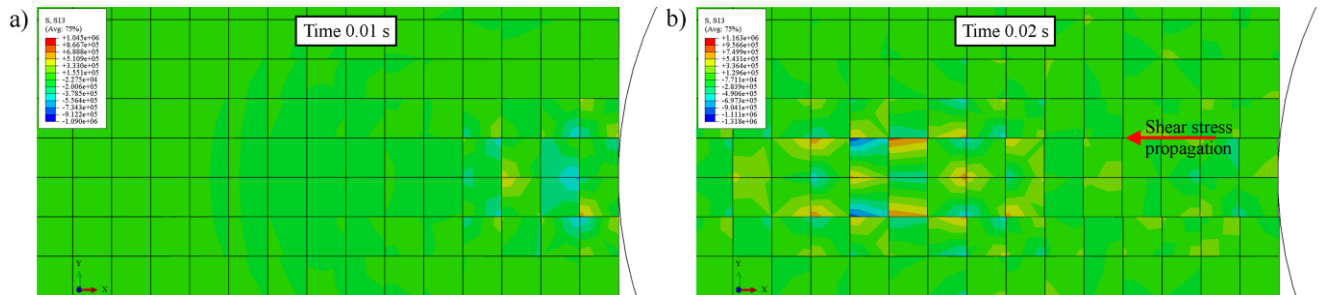

Figure 3.5 – Propagation of shear stress τ_{xz} in structured hex mesh: a) at time 0.01 s; b) at time 0.02 s
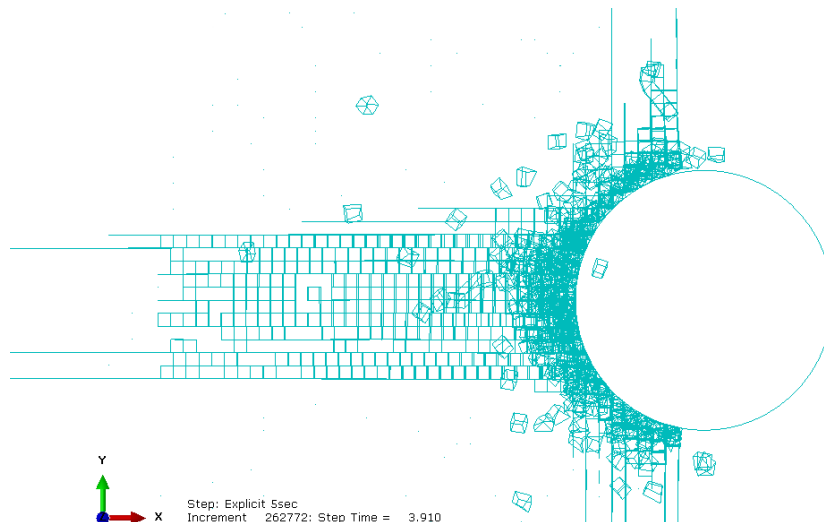

Figure 3.6 – Fracture pattern at time 5 s (structured hex mesh)

Some similarities can be seen with the splitting failure mode described in section 1 and presented in Figure 1.25, but this is not the right case, since longitudinal separating cracks form on the faces of each row of finite elements. Also, the horizontal load along *y*-axis shows very unstable behavior. Some rapidly changing peaks can be seen from time 1 s. Thus, for the correct description of the destruction process, **the use of a structured hex mesh is not allowed.**

The second type of mesh to consider is *unstructured hex mesh.* The result of the calculation at the last second of the interaction is presented in Figure 3.7. As for the general picture of the interaction it is obvious that the asymmetric destruction occurs with the breaking away of large parts of the ice field. Although the presence of an unstructured mesh made it possible to avoid the propagation of shear stresses over the entire width of the modeled field, there are still small regions consisting of "direct" parallel faces of elements form weak zones (Figure 3.8) along which the field is destroyed and which are the cause of the asymmetric interaction picture. Reducing the mesh size in the case of a hexagonal mesh will only worsen the situation, since a decrease in the size of the elements leads to a straightening of the boundaries of elements and the mesh tends to become structured.
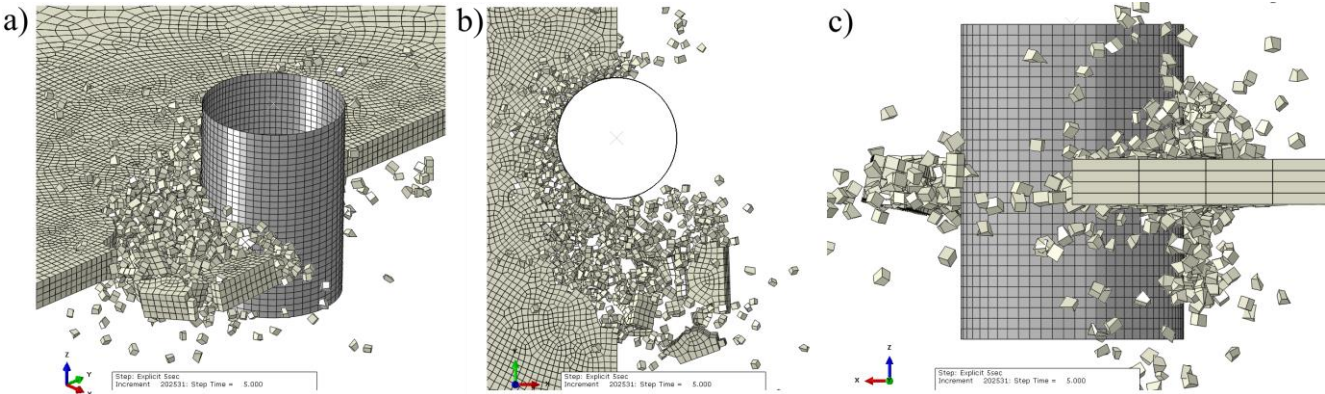

Figure 3.7 – Ice crushing during impact of ice field in case of unstructured hex mesh: a) general view; b) top view; c) side view
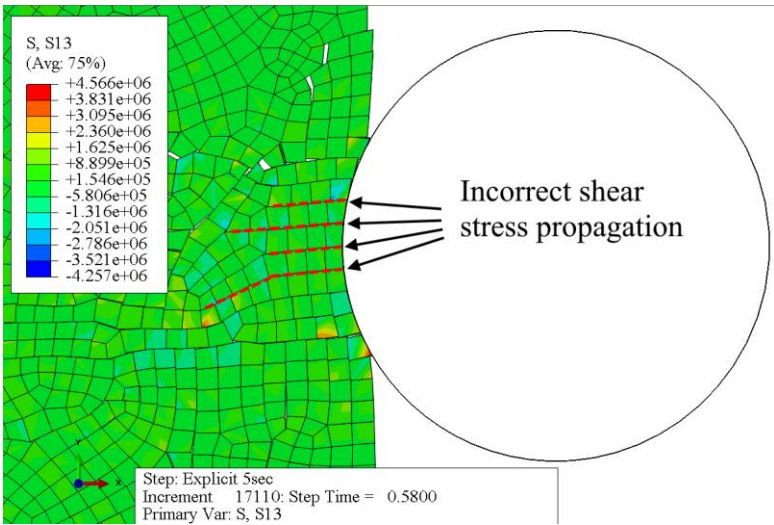

Figure 3.8 – Shear faults at time 0.58 s in case of unstructured hex mesh

The ice load in this case rapidly increases to high values (about 9.785 MN), and then gradually decreases to values of about 1,5 MN. The maximum value corresponds to the beginning of interaction (time range 0.3-0.6 s), that is obviously not correct. The effect of asymmetric fracture can also be seen by looking at the load history in the *y* direction (Figure 3.3). After splitting off a large fragment of the field, there was no contact with solid ice on this side. In this regard, the horizontal load from ice on the other side of the structure along the *y*-axis was significant throughout almost the entire calculation time. Fracture pattern is shown in Figure 3.9. Given all the above, we can conclude that despite the efficiency of computing, the **use of a hexagonal mesh at all is unacceptable** when modeling the impact of ice on structures.
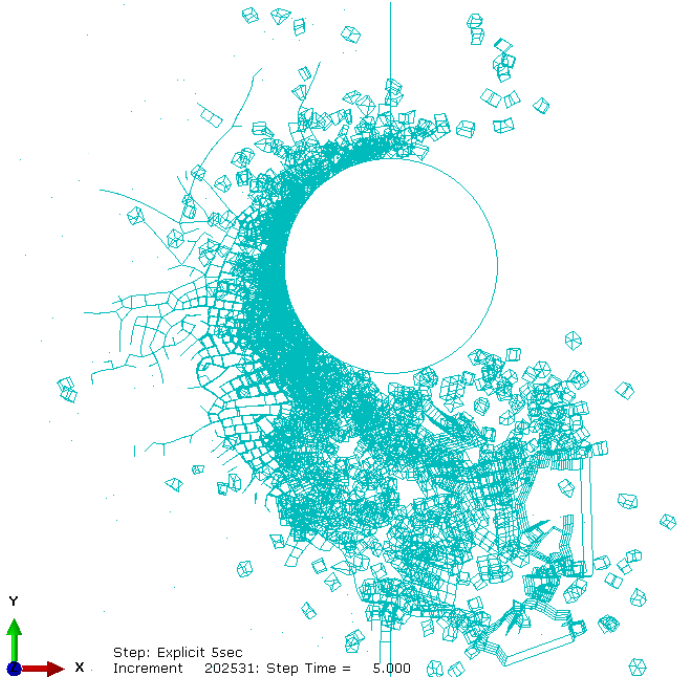

Figure 3.9 – Fracture pattern at time 5 s (unstructured hex mesh)

Next, consider the *prism mesh* case. The result of the calculation at the last second of the interaction is presented in the Figure 3.10. This case shows more realistic picture. Spalls and slight hummocking are present. An interesting fact is the periodic formation of "wing" fracture surfaces in an ice field. For example, as can be seen in Figure 3.11 (a), at the beginning of the interaction, the mean (hydrostatic) stresses have increased values in the region of future cracks. With further interaction, the ice fails mainly on these surfaces, then the process repeats Figure 3.11 (b). For clarity, the fact of the formation of such cracks is shown in the Figure 3.12.

As for the ice load, then, as in the past case, it quickly increases at the beginning of the interaction to the value 4.398 MN at 0.15 s, and then decreases to average values of about 0.318 MN. However, further behavior shows a different result then previous one. From about 1.8 s, the load begins to slowly increase and reaches its peak value of 7.358 kN at a time of 4.49 seconds, which corresponds to almost full-diameter penetration of the structure into the field. At a time of about 4.7 s, the horizontal load along

the y axis increased to 1.2 MN due to the destruction of ice on one side of the structure, but then quickly returned to low values.

The presence of a peak in ice load at the beginning of the interaction is connected with a small contact area and in my opinion is not correct. As can be seen from Figure 3.11, a, one finite element has a significantly higher level of stress than the other surrounding elements. This may be due to many factors, such as improper contact stiffness in the model, or the incorrect principle of a mesh creation in the contact zone. Therefore, additional studies of the applicability of this pattern are required.
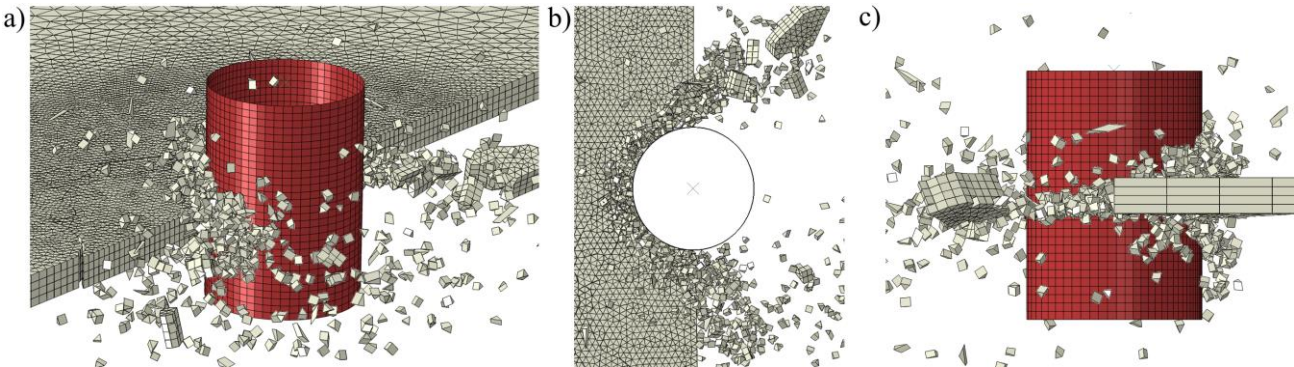

Figure 3.10 – Ice crushing during impact of ice field in case of prism mesh: a) general view; b) top view; c) side view
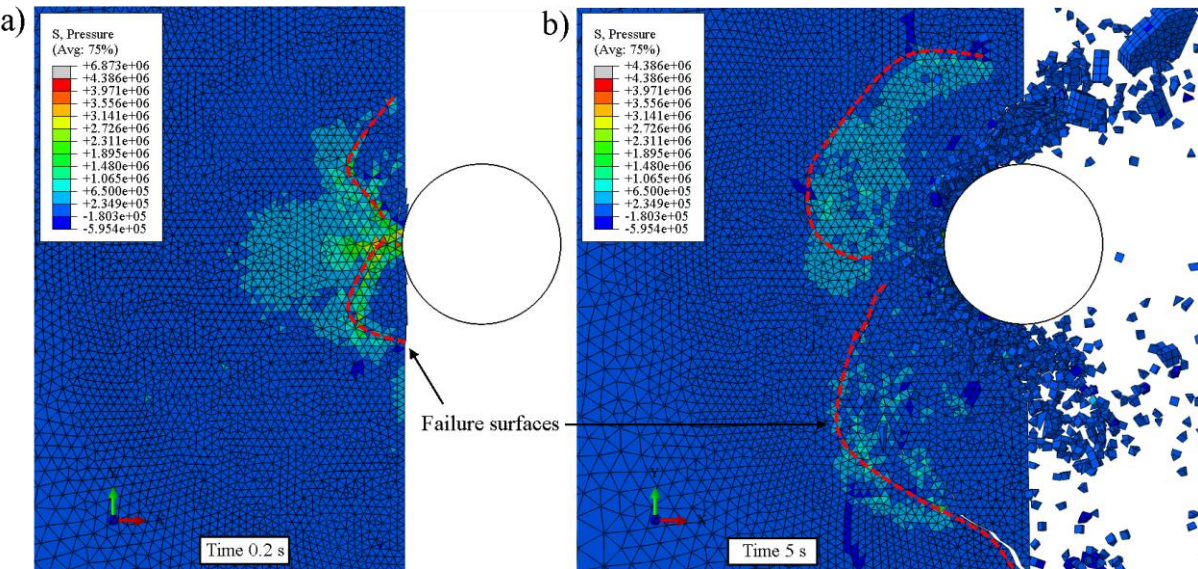

Figure 3.11 – Formation of "wing" failure surfaces in ice field in case of prism mesh pattern: a) at time 0.2 s; b) at time 5 s

The disadvantages of this type of finite elements can be seen by considering the central section of the model (Figure 3.13). Although the destruction pattern is acceptable in top view, in this section there is a complete discrepancy with real observations of ice impacts. With the current drift velocity and the diameter of the structure, the type of interaction should correspond to crushing failure mode of the ice field at the contact. Bekker's monograph [9] describes the process of field destruction in thickness for

this mode. In nature, in the upper and lower layers of ice spalls are formed along inclined surfaces, contributing to the concentration of stresses in the central part of the ice field. However, the Figure 3.13, c, shows that after partial crushing of the ice, the horizontal connected finite elements are destroyed simultaneously over the entire thickness, due to which the ice field is more or less equally vertically stressed. With an increase in the number of finite elements in thickness, a different picture may be observed, however, a decrease in the size of the finite elements may not be practical in comparison with the use of tetrahedral finite elements.
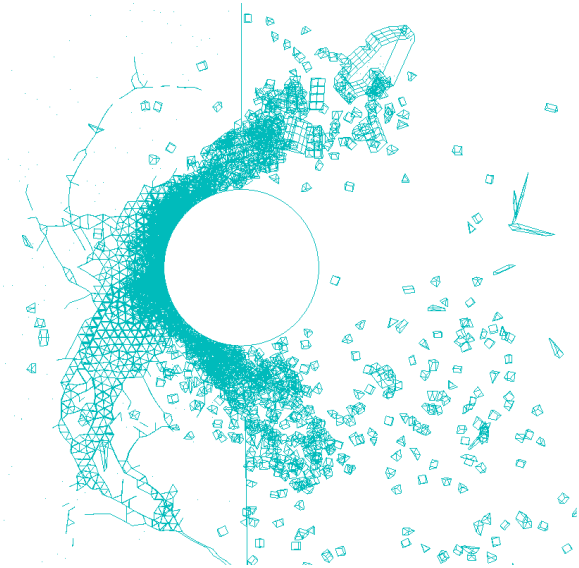

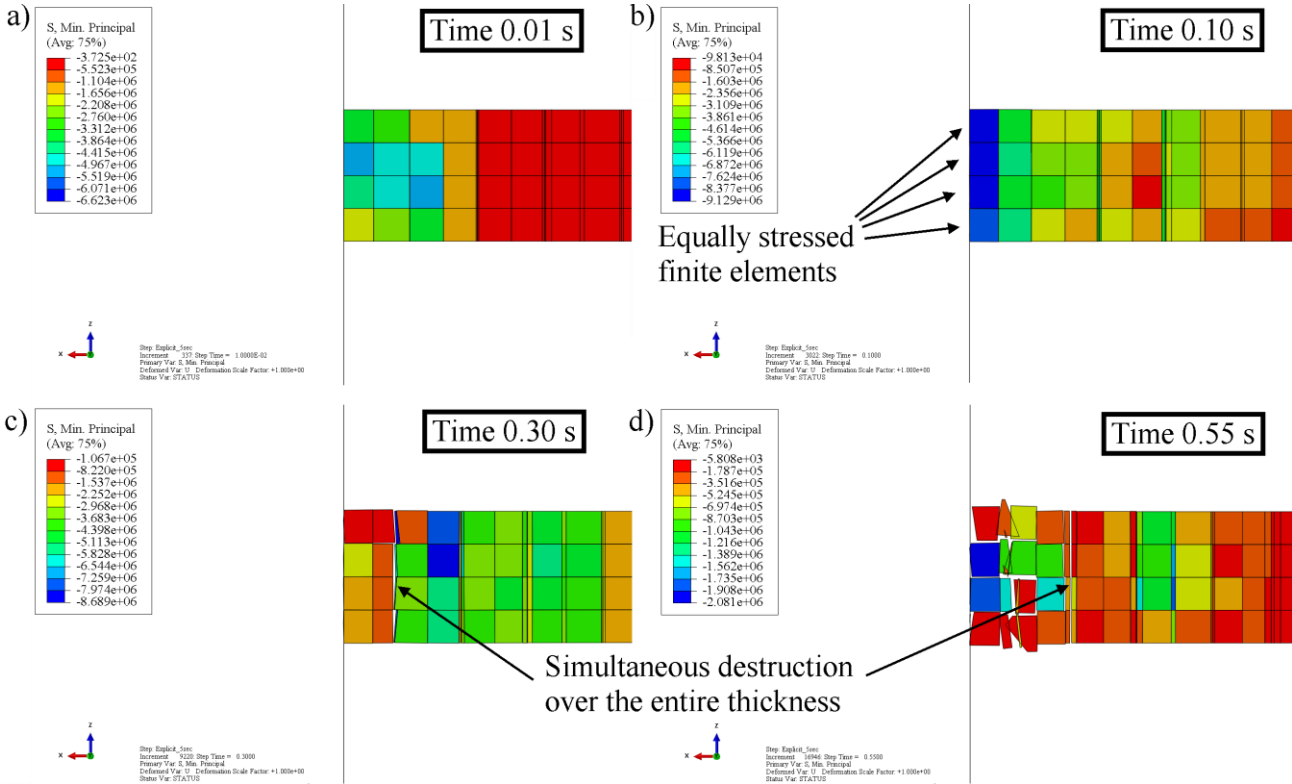Figure 3.12 – Fracture pattern at time 5 s (prism mesh)

Figure 3.13 – Central vertical section of model during interaction (prism mesh): a) at 0.01 s; b) at 0.1 s; c) at 0.25 s; d) at 0.55 s

Modeling of ice with a prismatic mesh requires significantly longer calculation time than in the case of a hexagonal mesh, but such a mesh allows to take into account the uneven development of cracks in the vertical plane to a good extent.

The last case to consider is a *tetrahedral mesh*. This case is considered the most expensive in terms of computation cost. This is due to the much larger number of finite elements needed to discretize the model with the same size settings. The calculation was not completed until the end, since at a time point of 4.01 s in the simulation, the time increment became very small, possibly due to strongly deformed elements. As a result, to calculate a model with the same initial conditions using the tetra mesh, almost 6 times more time is required than in the case of prism mesh. The simulation result for time in model equal to 4.01 s is shown in Figure 3.14. The deformation pattern in this case is quite different from the previous ones. The fracture pattern is shown in Figure 3.15.
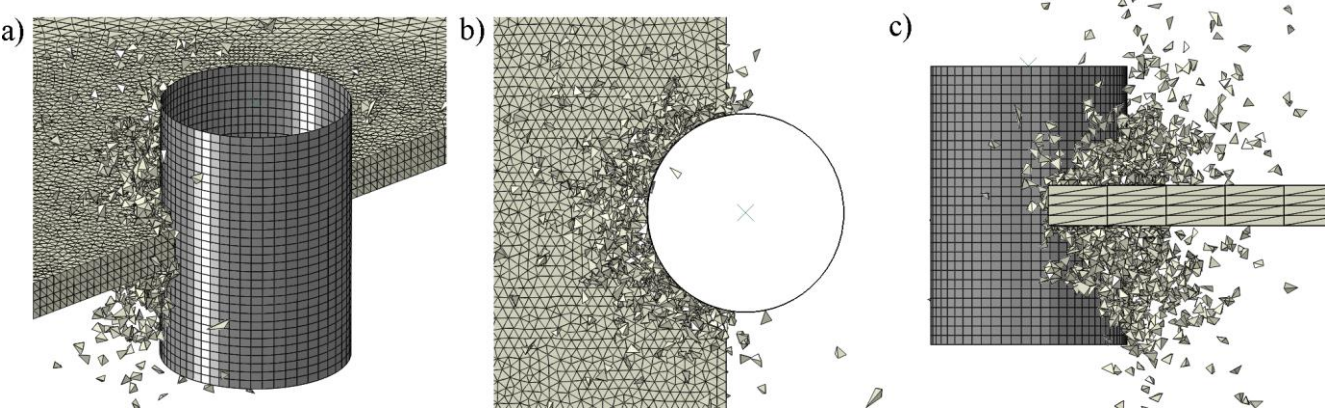

Figure 3.14 – Ice crushing during impact of ice field in case of tetrahedral mesh: a) general view; b) top view; c) side view
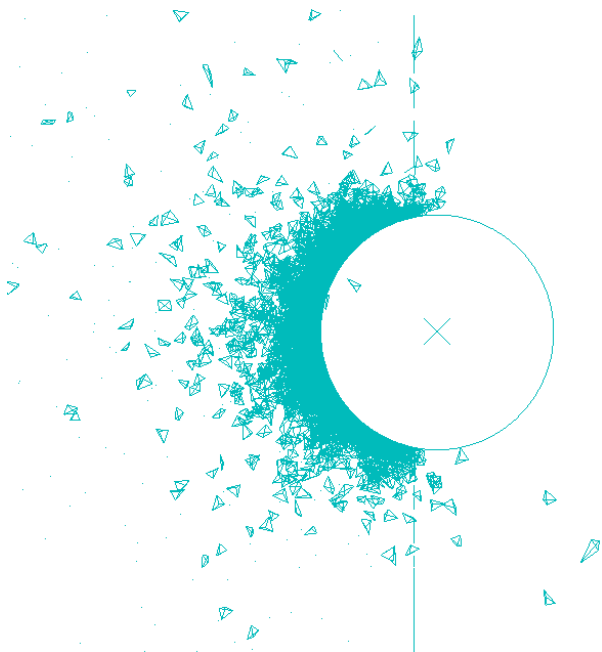

Figure 3.15 – Fracture pattern at time 4.01 s (tetra mesh)

In this case, there are no large chipped pieces as well as cracks propagation deep into the ice field. Figure 3.14, c shows a hummocking process, which has a much greater degree than in previous cases. This picture clearly corresponds to the real case of destruction, when a gradual and uniform destruction of ice at the contact is realized. The reason for the strong difference between the tetrahedral mesh and the prismatic one can be seen if we analyze the beginning of the interaction and the central vertical section of ice field.

As can be seen in Figure 3.16, a, at the very beginning (up to 0.1 s), the main destruction begins along the horizontal and vertical faces of the elements and the difference with the prismatic mesh is not noticeable. However, with further interaction Figure 3.16, c, the inclined faces of the tetrahedral elements are included in the work and serve as fracture surfaces.
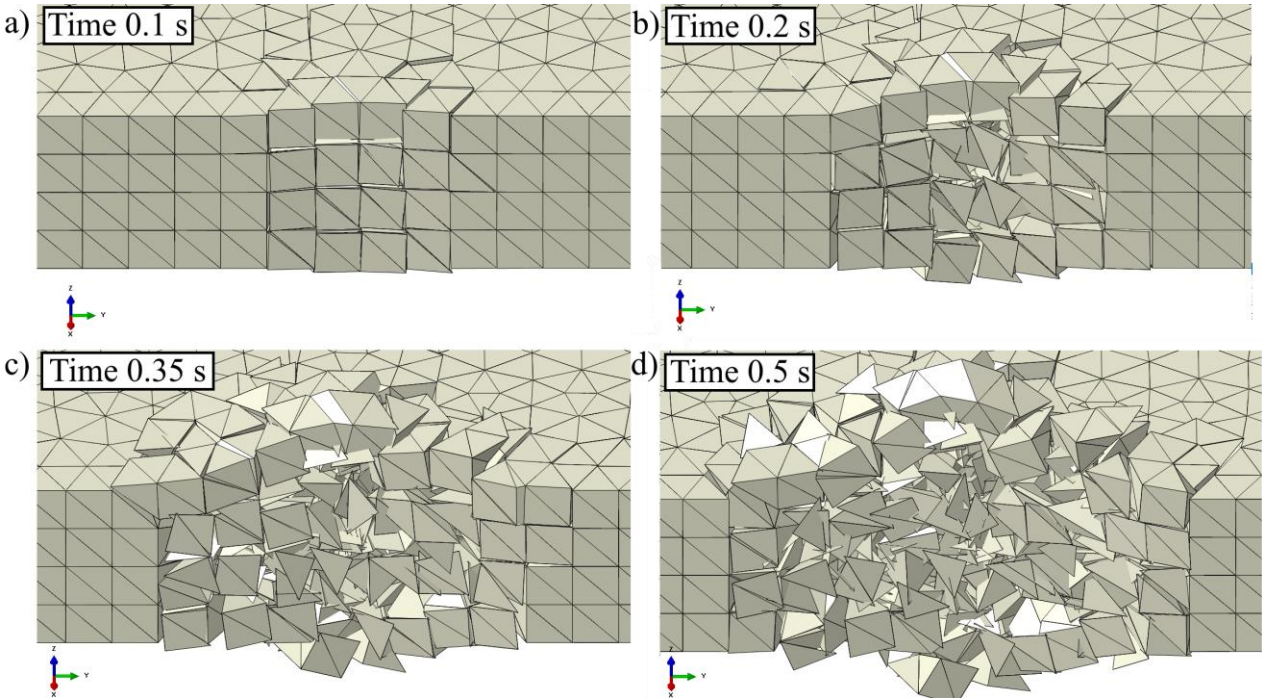
Figure 3.16 – The development of ice destruction at the contact: a) at 0.1 s; b) at 0.2 s; c) at 0.35 s; d) at 0.5 s

The qualitative picture of fracture, as in the case of a prismatic mesh, can be estimated by considering the interaction in the central section of the model. This section is presented in Figure 3.17. Unlike the case of a prismatic mesh, the pattern of destruction is more consistent with the process described by Bekker (2004) [9]. At the beginning of interaction (Figure 3.17, b) the central part of the ice field has the highest stress values, since spalls have occurred in the upper and lower parts. Uneven destruction of the ice field in thickness is clearly visible in the Figure 3.17, d. The lower part of the ice field is destroyed to a greater extent due to high ice temperatures and, accordingly, low ice strength. Thus, the fracture process in this case is periodic in nature with the formation of inclined fracture surfaces. This interaction physics will be better visible if the number of finite elements in the thickness of the ice field is increased.

Figure 3.17 – Central vertical section of model during interaction: a) at 0 s; b) at 0.01 s; c) at 0.05 s; d) at 0.25 s

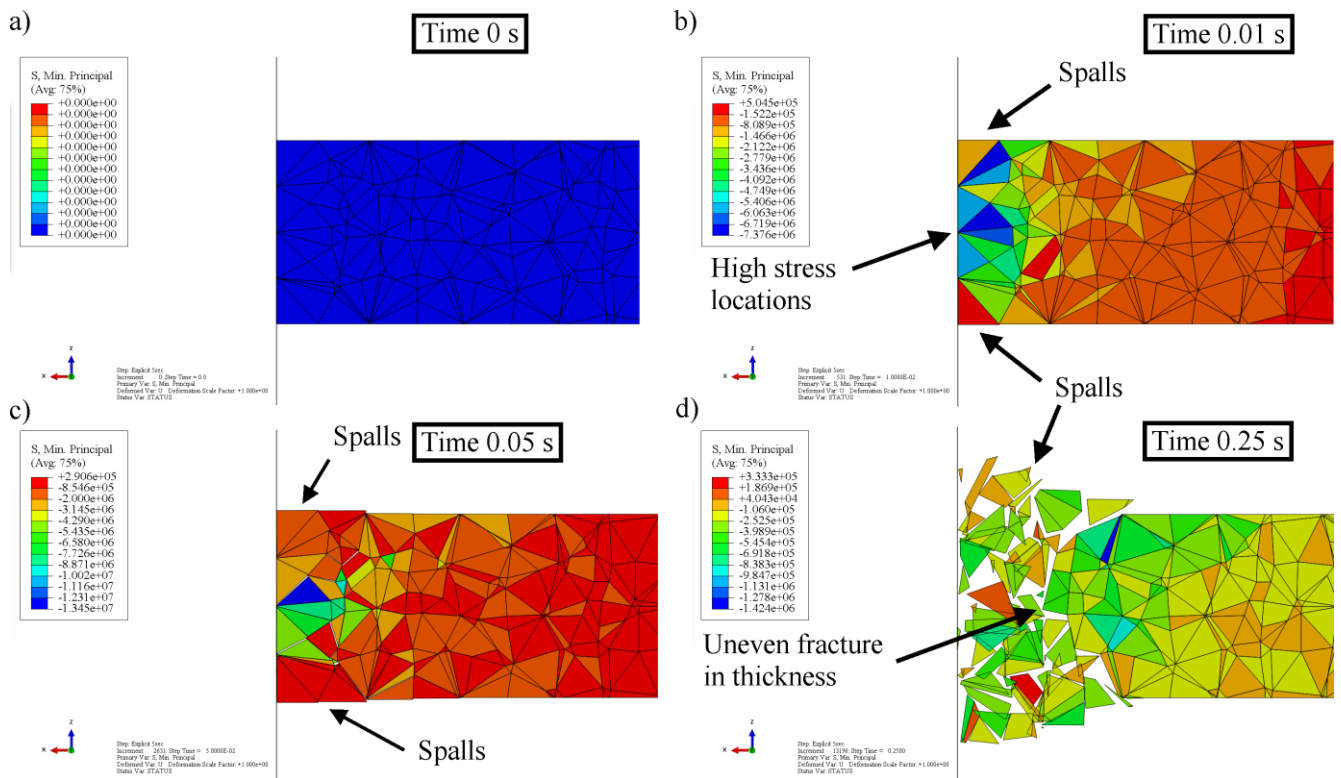As for the nature of the ice load, this pattern is the only one considered that has almost no peak load at the beginning of the interaction. The presence of this peak can also be due to the influence of inclined faces and spalls, that are destroyed and reduce the contact area. Also, load is increasing in slow manner during analysis. Unfortunately, it was impossible to estimate the load when embedding the structure at full width, because the calculation was interrupted. An additional study of the criterion for the removal of bulk and cohesive elements can solve the problem of a strong decrease in the time step.

At the end of the study of the mesh pattern, the following conclusions can be drawn:

- the hexagonal mesh showed the highest value from the calculated loads;

- the presence of a structured mesh speeds up the calculation, but leads to an incorrect picture of the interaction and stress distribution in an ice field;

- the presence of inclined faces of finite elements significantly changes the pattern of destruction;

- the tetrahedral mesh has significantly higher computational cost;

- the tetrahedral mesh shows the most realistic picture of the interaction.

In my opinion, using a tetrahedral finite element would be the best solution, since this case has an acceptable picture of failure and the nature of the load. It has high computational cost, but this problem can be solved by using more powerful computers. As for the process of interaction with structures in the first seconds, a rapidly increasing load can be a problem of ensuring the correct initial contact.

3.2 Element size influence

At this stage of the model study, the influence of the size of finite elements on the final simulation result was considered. As the first case in a series of experiments, the model from the previous subsection (tetrahedral mesh pattern) was adopted. When creating a new model, all sizes and boundary conditions were preserved, but the size of the finite elements of the ice field was changed. Moreover, to optimize the calculation time, the field was divided into 4 zones as presented in Figure 3.18.
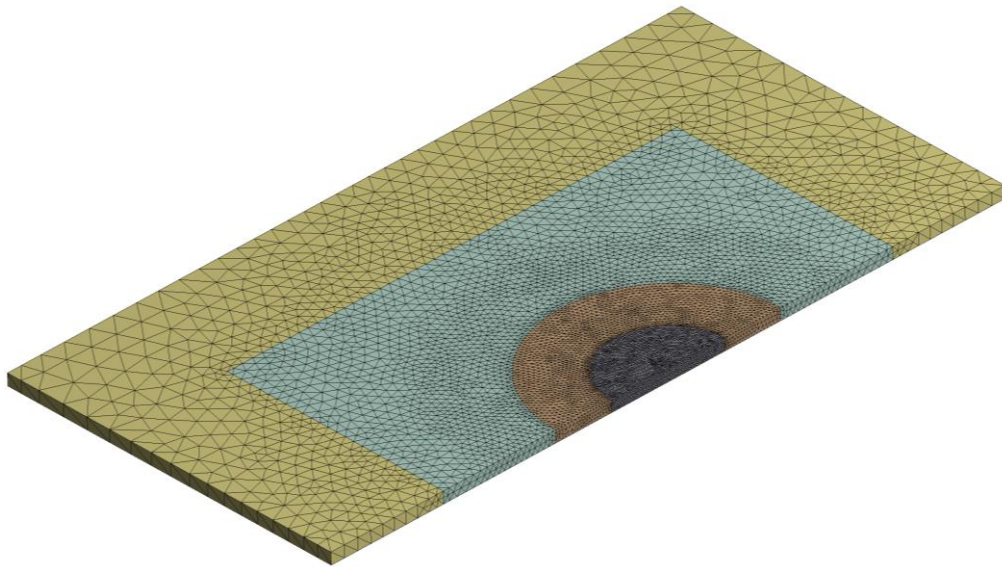

Figure 3.18 – Mesh zones with different element sizes

The first zone has a radius equal to the diameter of the structure and the minimum size of the finite elements is approximately 0.15 m. By thickness, the ice field is discretized into 8 layers. The second zone – two diameters with an approximate size of the finite elements equal to 0.3 m (4 elements in thickness). The third and fourth zones have 2 and 1 end elements in thickness, respectively, with a maximum size of about 2.2 m. This decision was made based on the destruction pattern presented in the Figure 3.15, namely, it is clear that zone of destroyed cohesive elements does not extend much deep into the field, when the field interacts almost over the full diameter. Thus, a more accurate description of contact with the structure was provided, and the total number of finite elements was increased by only 1.5 times. The calculation results are presented in the Table 3.4. The history of the load along and across the direction of movement is presented in the Figure 3.19 and Figure 3.20.

The nature of the load in the cases considered is, as expected, very similar, but for the case of the fine mesh, the vibrations are smoother. Moreover, with a decrease in the size of the elements, the load has higher values throughout almost the entire interaction time. The picture of destruction in the plan is shown in the Figure 3.21 and visually not much different. The central section of the model is shown in Figure 3.22.

Table 3.4 – General modeling information

Case	Number of finite elements (bulk / cohesive)	Total calculation time, hours	Peak total ice force along direction of motion F_x^{tot}, MN
0.30 m (4 elements in thickness)	124 261 / 236 075	48.63 (4.01 s out of 5)	-
0.15 m (8 elements in thickness)	195 904 / 378 476	141.68	10,096
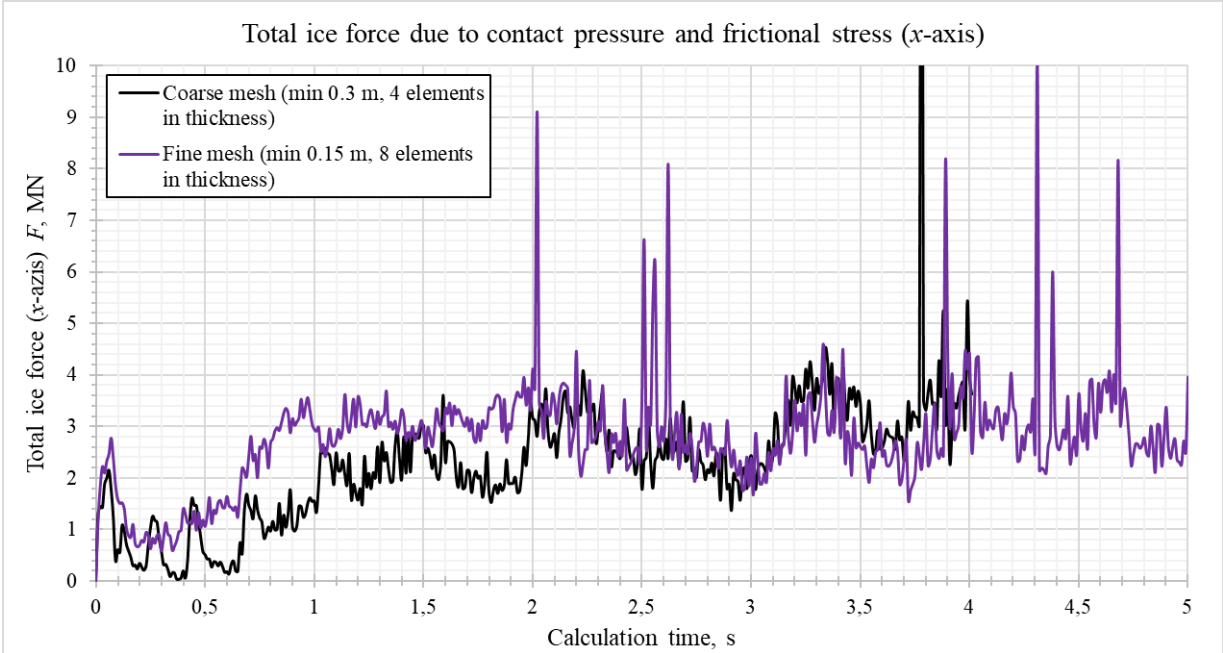
Figure 3.19 – Load history with different mesh sizes (along *x*-axis)
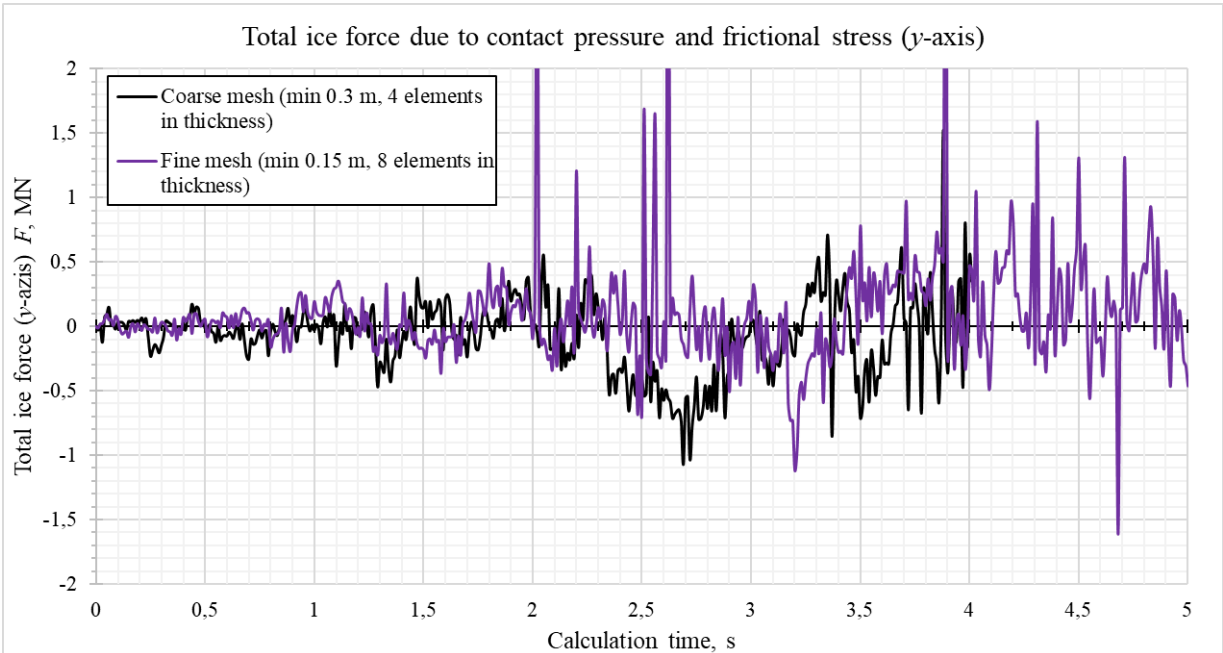
Figure 3.20 – Load history with different mesh sizes (along *y*-axis)
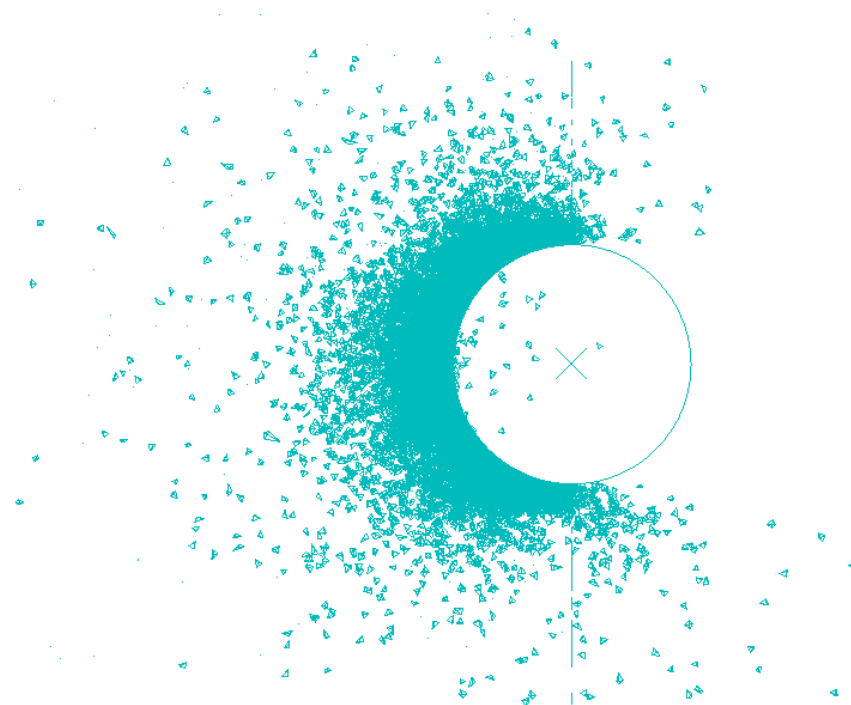
Figure 3.21 – Fracture pattern at time 5 s (model with fine mesh)
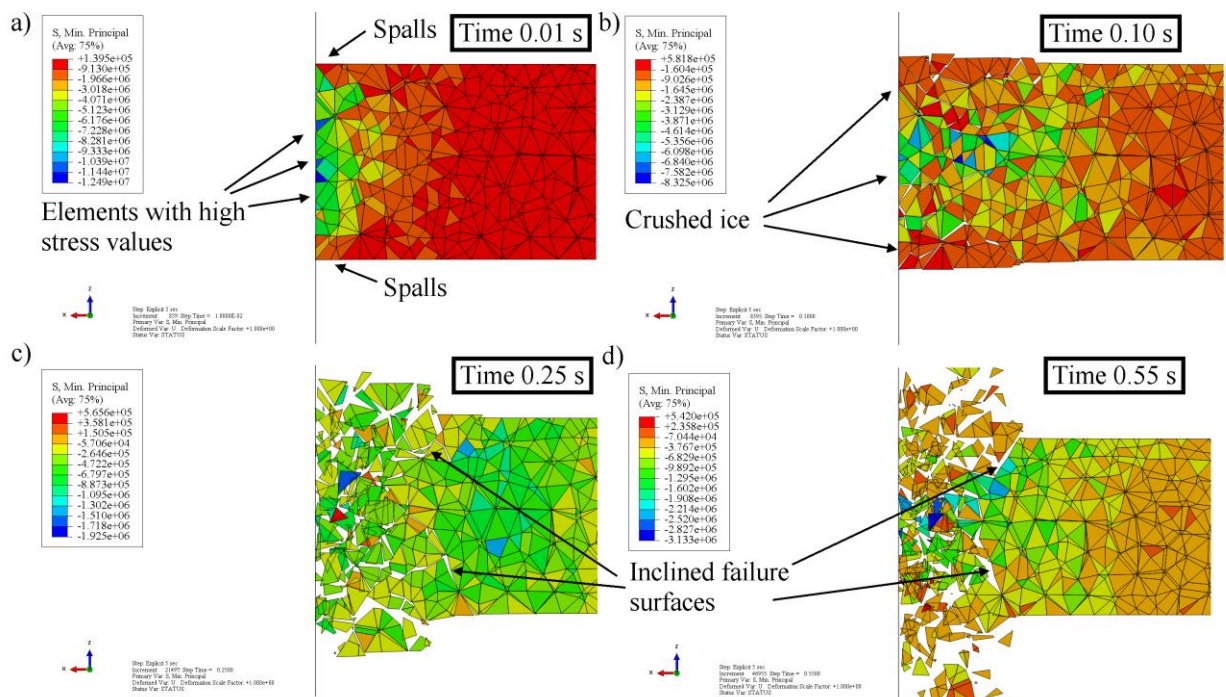
Figure 3.22 – Central vertical section of model with 8 elements in thickness during interaction: a) at 0.01 s; b) at 0.10 s; c) at 0.25 s; d) at 0.55 s

Noticeable improvements can be seen in the overall picture of the interaction. As in the case of a coarse mesh, at the beginning of the interaction, high compressive stresses are concentrated in the center of contact zone (Figure 3.22, a). A small peak of the load that occurs in the first fractions of a second is associated with the process of deformation and growth of stresses in bulk elements. Then the first spalling occurs, and the total ice force drops to low values. A further increase in the load is associated

with an increase in the contact area and, accordingly, the number of contacting elements. The inclined surfaces of destruction are now visible even more clearly (Figure 3.22, d).

Also in the process of destruction, there were moments when the destruction of the ice field did not occur along two, but along one inclined surface throughout the thickness as presented in Figure 3.23. Such a picture can also develop and is associated with low strength of the lower layers, which are destroyed earlier than the rest.
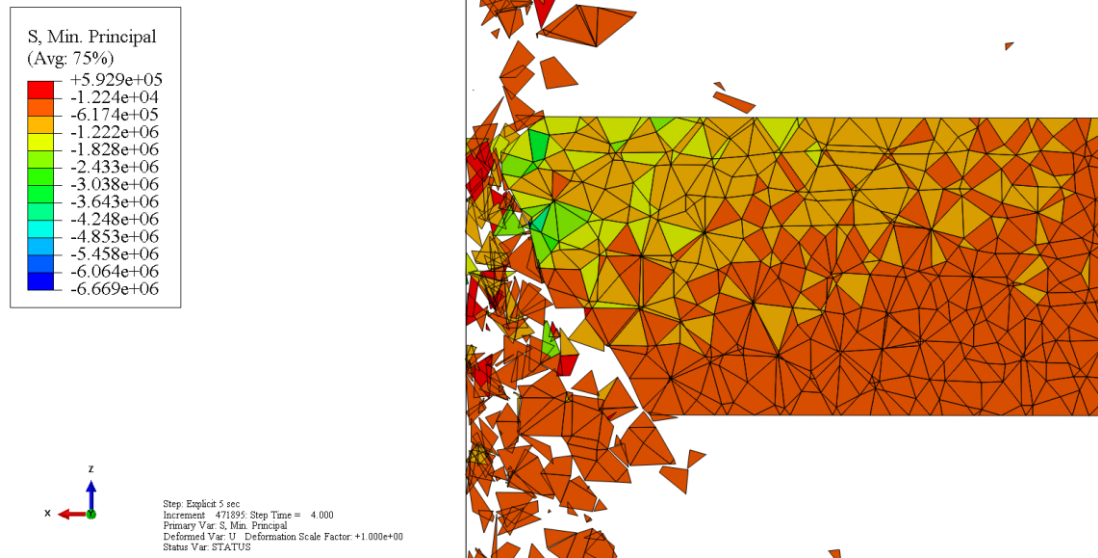
Figure 3.23 – Central vertical section of model with 8 elements in thickness at time 4.0 s

3.3 Section conclusions

The results of modeling the ice impacts on vertical structures according to the accepted method showed good results. As expected from the finite element method, the influence of various mesh patterns on the picture of ice field destruction is large. The presence of inclined cohesive elements leads to a more realistic picture of the interaction. Therefore, an ice field of tetrahedral bulk elements is the most acceptable option from the considered. The main problems when using tetrahedral elements are as follows:

- assignment of ice properties to inclined cohesive elements, since there is little information on the deformation and strength characteristics of ice along inclined axes;

- big time for calculating models, which can be solved by using a more powerful computer.

The dependence of the load on the size of the finite elements was weak for the considered case. However, the pattern of ice destruction at the contact is much better when using a fine mesh and coincides with the real observations of some authors.

The nature of the destruction of ice in general corresponds to the crushing failure mode in real conditions. Unequal destruction of the ice field in height during modeling is a significant factor that

confirms the relevance and reliability of the applied method. Also, this nature of the destruction is contrary to Gladkov's assumptions [27], on which the current methodology for determining ice loads in the regulatory document SP 38.13330.2018 [68] is based. In determining the values of the factor k_b, he admitted that all layers of the ice field are destroyed simultaneously.

To assess the possibility of applying the considered methodology for solving real engineering problems, it is necessary to verify it.

4 Verification of the methodology for modeling ice impacts on vertical offshore structures

4.1 Comparison of load with analytical methods of national codes

To confirm the efficiency of the model for solving real engineering problems, it is necessary to verify the used methodology of ice-structure interaction modeling. This can be done, for example, by methods such as analyzing the correspondence of the qualitative picture of ice destruction to recorded cases and comparing the magnitude of the impact with the measured in the field.

Another way is to compare the simulation results with the analytically calculated value of the load according to various theories. Although the analytical methods used to date have several disadvantages, they are still successfully used in the design of offshore structures. The first stage of verification will be the comparison of magnitude of the ice load obtained as a result of modeling with the load calculated by the methods described in the national codes below. Most of national standards require to take into account several limiting factors of ice load described earlier (section 1). The methods for calculating the corresponding scenarios of the interaction of ice formations and structures have large differences. However, since the principle of infinite ice field is applied in the modeling, a comparison with the load only for limit stress scenario will be performed.

SP 38.13330.2018 [68]. This regulatory document is a standard of the Russian Federation and contains requirements for the calculation, design, justification of the reliability and safety of hydraulic structures. In accordance with these standard, the ice load form drifting ice field on structures with a vertical front face in case of limit stress scenario $F_{b,p}$, MN, is determined by the modified Korzhavin's formula proposed by Gladkov M. G. [27]:

$$F_{b,p} = mk_b k_V Rbh, \tag{4.1}$$

where m – structure shape factor;

k_b – indentation factor taking into account the influence of complex stress-strain state of ice field on the ice strength limit;

k_v – factor taking into account the influence strain rate on the ice strength limit;

R – compressive strength of ice, MPa;

b – structure width, m;

h - ice thickness, m.

STO Gazprom 2-3.7-29-2005 [69]. This document is a standard of the Russian company Gazprom and contains methods for calculating the ice load, supplementing and clarifying the design requirements, and the provisions of Russian national codes. The load from the impact of ice formations is determined with the values of $d/h \geq 10$ according to following equation

$$F_{b,p} = mk_b Rbh, \tag{4.2}$$

The parameters in equation (4.2) are the same as in equation (4.1).

ND 2-020201-015 [52]. These rules of the Russian Maritime Register of Shipping establish requirements that are specific to floating drilling rigs and offshore stationary platforms, take into account the recommendations of the IMO Code for the design and equipment of floating drilling rigs adopted by the IMO Assembly on December 2, 2009. In this case ice load is determined by equation

$$F_{b,p} = mk_L k_v R b^{0.85} h^{0.9}, \tag{4.3}$$

where k_L – factor that takes into account the effect of ice field area and structure diameter on the load.

Other parameters in equation (4.3) are the same as in equation (4.1).

ISO/FDIS 19906:2019(E) [33]. This document was developed by the International Organization for Standardization (ISO) and establishes requirements, provides recommendations for the design, construction, transportation, installation and decommissioning of offshore structures associated with the activities of the oil and gas industry in the Arctic and cold regions. Based on this document the global ice load is determined as follows:

$$F_{b,p} = bhC_R \left(\left(\frac{h}{h_1} \right)^n \left(\frac{b}{h} \right)^m + f_{AR} \right), \tag{4.4}$$

where C_R – the ice strength coefficient, MPa;

n and m – empirical coefficients;

f_{AR} – empirical term given by

$$f_{AR} = e^{-b/3h} \sqrt{1 + 5\frac{h}{b}}, \tag{4.5}$$

CAN/CSA-S471-04 [11]. This document is Canada's national standard.

This standard use power-law dependencies of ice pressure on nominal contact area, which were obtained as a result of processing a large amount of ice pressure data on the hulls of the Kigoriak, Polar Sea, MV Arctic, Manhattan and Oden icebreakers in Canadian waters. The code recommends two different formulas for calculating the ice load depending on the ratio of the width of the structure to the thickness of the ice field.

If the global ice load $F_{b,p}$ is determined as follows:

$$F_{b,p} = \begin{cases} C_p A_N^{(D_p+1)}, & b/h < 10 \\ C_p h^{(D_p - E_p + 1)} \cdot b^{(E_p+1)}, & b/h \geq 10 \end{cases} \tag{4.6}$$

where A_N – nominal contact area, m²;

C_p, D_p и E_p – empirical parameters.

Elforsk rapport 09:55 [24]. This report by the Swedish energy research company contains recommendations, a description of the ice load mechanisms and statistics from the Baltic Sea. In

accordance with the recommendations of this report, the ice load from the level ice fields acting on structures can be evaluated by the original Korzhavin's equation:

$$F_{b,p} = mk_c k_b Rbh,$$ (4.7)

where k_c – contact factor that covers the fact that ice under continuous crushing is not in contact with the whole nominal area.

GL 2005. IV-Part 6 [26]. These rules are a German national standard and are designed to evaluate the properties of sea ice and ice loads on offshore structures. Ice load is determined using the formula obtained by several authors at Iowa University based on small-scale tests:

$$F_{b,p} = kb^{0.5}h^{1.1}R,$$ (4.8)

where k – empirical factor.

As a simulated case of ice impact on structures, the case of a tetrahedral mesh, described in section 3.1 of this thesis, is accepted. The maximum load was considered in two ways: load surges were considered and not considered. This decision was made because the cause of these surges is unknown and their number is very small compared to other data points. Calculations using analytical methods were carried out strictly in accordance with all clauses of national standards. The strength of ice was calculated in accordance with the recommendations of each regulatory document. In the case when there is no indication in the codes on the strength of ice, then its value was taken equal to that calculated by the SP 38.13330.2018. A comparison of the results is presented in the Table 4.1 and in the Figure 4.1.

Table 4.1 – Comparison of ice load and difference with simulation results

Parameter	Modeling (with surges)	SP	MRS	ISO FDIS	CAN CSA	Elforsk	GL	Modeling (without surges)
Ice load, MN	10.10	7.83	11.44	9.36	3.94	1.59	4.17	4.59
Difference with modeled load (surges are considered), %	0.00	28.99	13.29	7.85	156.25	534.55	142.10	119.72
Difference with modeled load (surges are not considered), %	119.72	70.34	148.92	103.72	16.63	188.80	10.19	0.00

The magnitude of the ice load calculated by various analytical methods in some cases differs several times. If we compare these values with the values of the load obtained as a result of modeling we get a mixed result.
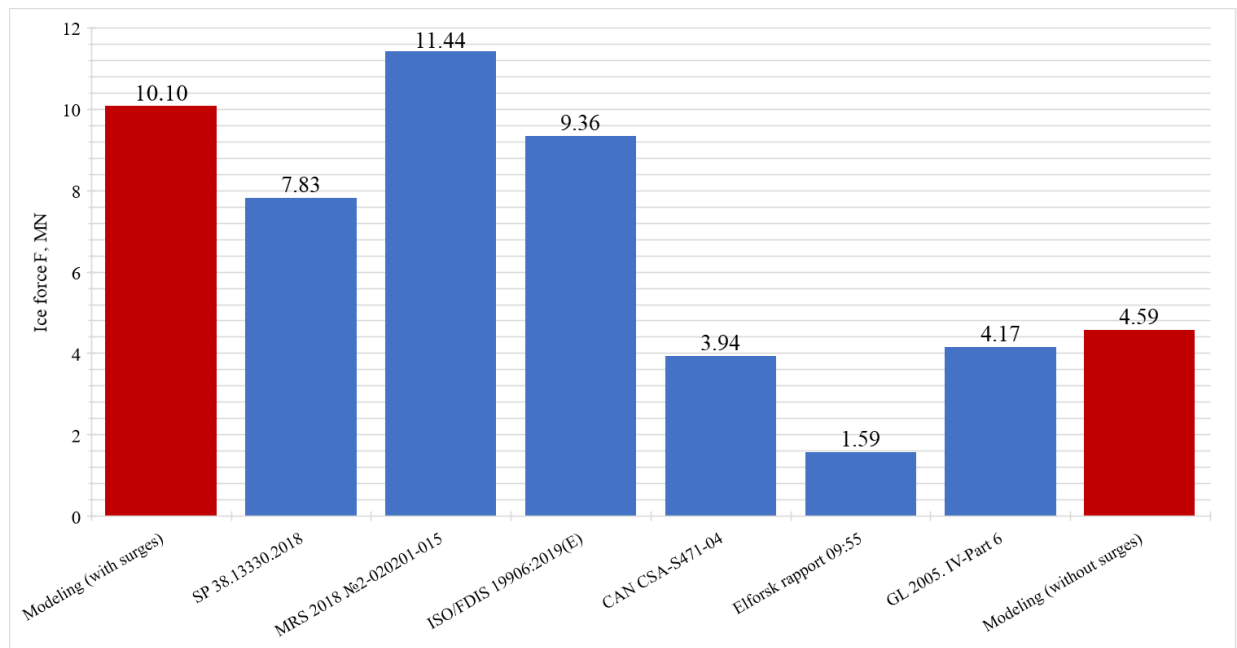
Figure 4.1 – Comparison of the ice load according to different codes with the result of numerical simulation

If we take into account surges, then the load has value that is close to calculated according to more modern standards (SP 38.13330.2018, MRS 2018 №2-020201-015, ISO/FDIS 19906:2019(E)). In this case the methodology of the ISO normative document showed the greatest convergence, but when compared with other standards, the difference reaches 534.55% for Elforsk rapport 09:55. This fact may also be a coincidence, therefore, it is impossible to judge the correctness of the ice load obtained during modeling. Analytical methods also have their own assumptions and disadvantages, so it is necessary to perform several iterations of calculations with different conditions, and then perform a comparison.

4.2 Modeling of uniaxial compression tests

Finally, the last approach to verify the numerical model is to simulate uniaxial compression tests. Such laboratory data are valuable, since the parameters of ice and load can be regulated during the experiment, and different cases can be considered. The author took part in a series of such experiments conducted in Laboratory of Ice Mechanics of Far Eastern Federal University (FEFU). One of the main goals of tests was to determine the compressive strength of sea ice at different strain rates.

Ice samples for testing were prepared as follows. First of all, ice cores were cut from ice in Novik Bay, located near the university using the core sampler (Figure 4.2, a). The ice thickness at the time of core sampling was approximately 25 cm. Then the cores were transported to the laboratory and placed in the refrigerator. Second, samples of 200 mm height were cut out from cores, their sizes and weights were measured. For the compression tests, 20 cylindrical samples with a diameter of 90 mm and a height

of 200 mm were prepared (Figure 4.2, b). The tests were performed using the Shimadzu press (Figure 4.2, c). The maximum possible load on the press is 100 kN. Apparatus has the possibility to control loading speed. Test were performed on following speeds: 0.1 mm/s, 0.5 mm/s, 1 mm/s, 1.5 mm/s, 2.5 mm/s using 5 samples in each case. After crushing the temperature of each sample was measured.
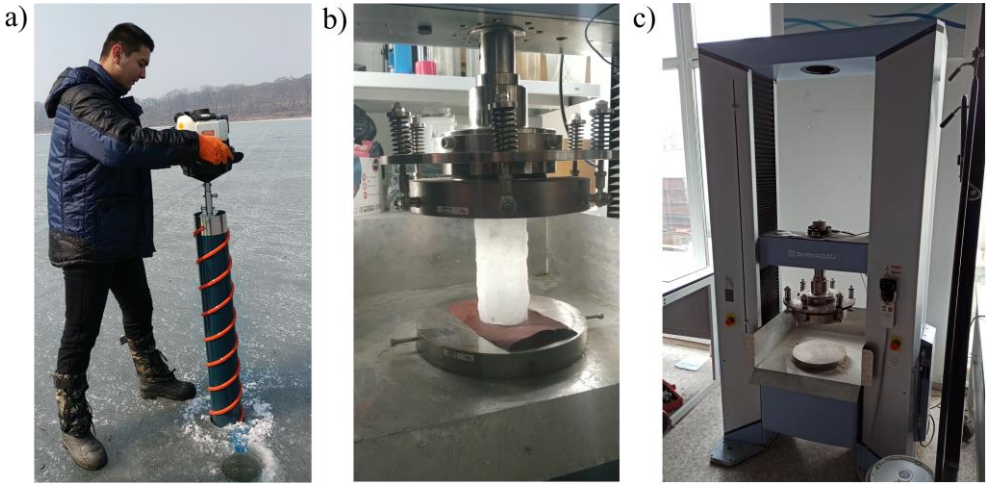
Figure 4.2 – Compression tests preparation: a) core sampling; b) sample setting; c) Shimadzu press

During the verification process, the reaction force magnitude of the upper plate, as well as the overall pattern of fracture of the samples will be compared with experimental data. The finite element model with boundary conditions is presented in Figure 4.3.

When creating a numerical model of experiments, the following assumptions were made:

- support and loading plates of the press are modeled using rigid shells;

- roughnesses in the surface of the samples are not taken into account;

- the size of the finite elements of the sample is taken equal to 12 mm;

- the coefficient of friction is taken equal to 0 to prevent the confining of displacements in the vicinity of plates.

Figure 4.3 – Finite element model in numerical experiments on uniaxial compression of ice samples

A comparison of forces in modeling and laboratory experiment is presented in the Figure 4.4. The results were mixed. On the one hand, the nature of the load is very different. for example, during

modeling, there are constant power surges throughout the entire time. The output frequency was assumed to be 0.01 second, as in a laboratory 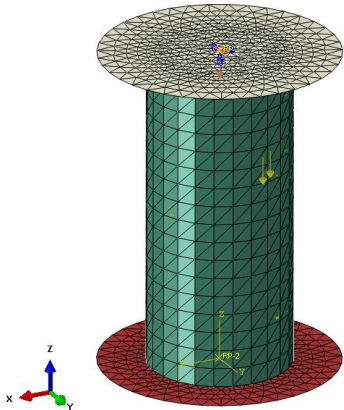experiment. On the other hand, the force graph obtained from the results of a laboratory experiment runs right through the upper points almost until the sample is destroyed. In my opinion, in general, the result is acceptable, because when evaluating the force along the upper boundary, as when comparing the ice load according to regulatory documents, there is a good agreement.
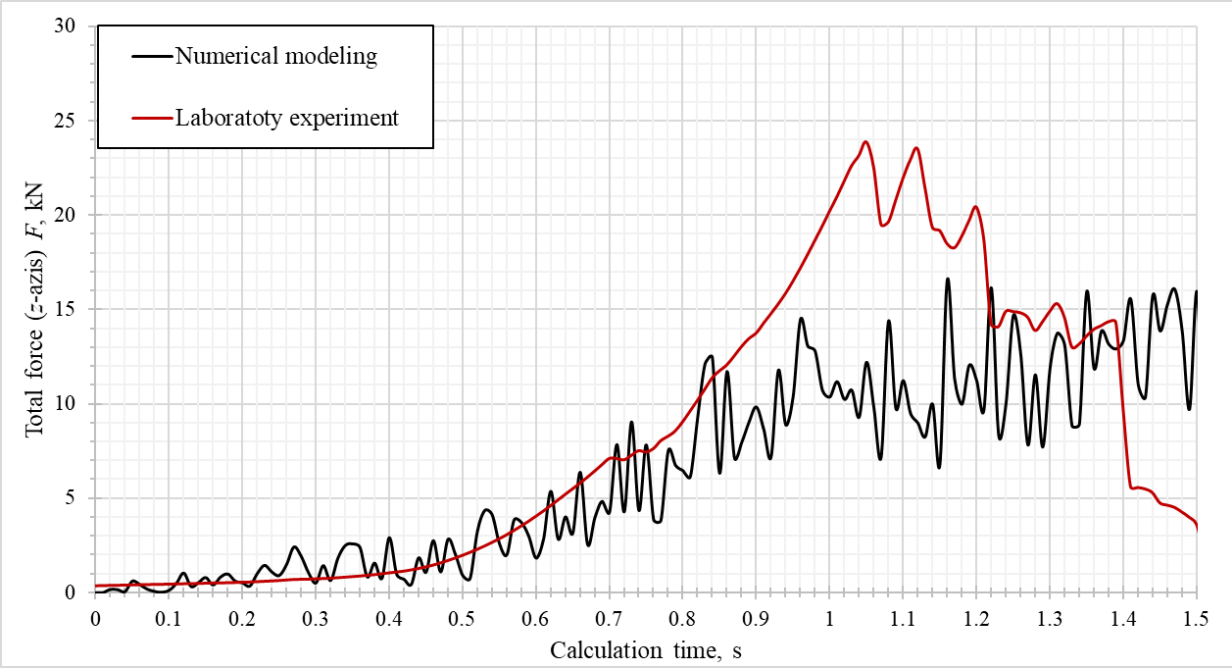
Figure 4.4 – Comparison of forces in modeling and laboratory experiment

4.3 Section conclusions

In this section, verification of the developed methodology for numerical modeling of the impact of ice formations on the vertical supports of structures was performed.

This modeling methodology showed a good correspondence of the load values to the load determined by the current documents. Even among themselves, the methods of various codes are very different from each other. For example, the very important fact that almost all foreign standards consider the regime of viscous-brittle fracture when the strain rate is within approximately $5 \cdot 10^{-4} \div 10^{-3}$ s^{-1}. Thus, such regulatory documents assume the maximum strength of ice during interaction. The only exceptions is the code GL 2005. IV-Part 6 [26] who propose using the empirical formula obtained by Kovacs (1997) [39] to calculate the strength of ice based on tests of ice samples from the Beaufort Sea. The Russian standards have a k_v factor which was first introduced in SNiP 2.06.04-82* at the proposal of M. G. Gladkov [27], although Korzhavin, when developing the original formula, also took into account the influence of the strain rate on the strength of ice. The proposed method takes into account the rate of ice deformation during the entire simulation time, which is an undoubted advantage over analytical methods.

As for verification using laboratory test data, the result is mixed. On the one hand, the general nature of the increase in load during modeling correlates well with the laboratory experiment. Also, the maximum force does not differ much from that obtained in the experiment. On the other hand, when modeling, there are multiple fluctuations in the force, although the frequency of the data corresponds to the frequency of recording the force of the press machine. This can be due to many factors and is one of the problems that can be solved with further research.

Conclusion

Summarizing the results obtained in this dissertation, the following conclusions can be drawn:

1. Based on the analysis of the current state of problem of assessing the impact of ice fields on structures, it can be concluded that this problem has been solved for a rather long time. In terms of determining the physicomechanical characteristics of ice, a significant amount of research has been performed. Numerical modeling is a promising way to solve this problem. To date, there are a number of works in this area. In almost all the reviewed articles and theses, the authors did not pay due attention to the selection and substantiation of constitutive models of ice material. Such features of ice as the strong dependence of the parameters on temperature, the complex stress-strain state, and also the strain rate were not taken into account.

2. A comprehensive study of methods for determining the parameters of ice, depending on many factors was made. An algorithm has been compiled to calculate the full set of necessary characteristics of ice, depending on some initial conditions.

3. As a method for solving the problem, a numerical finite element method is chosen. The solution tool is the SIMULIA Abaqus software package. As an integration method for the main equation of motion, an explicit integration method was justified and adopted. Tasks were set and a plan was drawn up for numerical experiments performed in the thesis. Initial numerical models of the interactions of the ice field with structures were created on the basis of some assumptions based on the known results of experimental studies of sea ice.

4. The statement of the problem based on the developed methodology of numerical modeling includes the following studies and improvements:

- the tetrahedral mesh pattern is accepted as the most optimal from the point of view of a qualitative picture of interaction;

- reducing the size of the finite elements does not lead to a significant change in the magnitude of the ice load, but contributes to a more detailed description of the process of ice loads formation and the formation of a more accurate picture of ice destruction;

- the accepted threshold in the criterion for the removal of bulk elements was found to be applicable

5. The numerical model of interaction with the introduced improvements was verified in two ways: comparison of load with analytical methods of national codes and modeling of uniaxial compression tests. As a result of verification calculations, numerical models showed good convergence with the reference data. The nature of the destruction of the ice field during modeling is in good agreement with field observation, for example, the formation of piles of ice fragments (hummocking) and uneven destruction of the ice field in thickness.

6. The developed methodology for numerical modeling of ice formations impacts can be used to

solve real engineering problems and will significantly improve the reliability and reduce the risk of offshore structures. The method will allow to evaluate the complex stress-strain state of structure under action of ice loads from drifting ice fields.

7. One of the main problems in using the developed modeling approach is the high computational cost. When solving real engineering problems, it is recommended to use powerful computers with a lot of CPU cores.

8. The model can be more deeply researched and improved in the following terms:

- improving methods for calculating the deformation and strength parameters of ice;

- taking into account the influence of deformations in mutually perpendicular directions in the material model of cohesive elements, i.e., a coupled traction model can be used;

- to study the influence of the general damping parameters of the model (linear and quadratic viscosity);

- searching for appropriate initial contact between finite elements of structure and ice field;

- assessment of the degree of influence of various water models on simulation result

- application of the Coupled-Eulerian-Lagrangian method in numerical model;

- verification of the model can be supplemented by modeling real recorded cases of ice impacts on structures.

References

1 **Albrektsen A.** Prediction of the response from ice forces to a lighthouse structure: master's thesis. - Trondheim : Department of Structural Engineering, NTNU, 2009.

2 **Aleksandrov A.V., Platonov V.V., Matantsev R.A.** Study of ice failure and deformation processes [Conference] // Proceedings of the ASME 2014 33rd International Conference on Ocean, Offshore and Arctic Engineering OMAE2014. - San Francisco : American Society of Mechanical Engineers, 2014.

3 **Alexandrov A.V., Matantsev R.A.** Primeneniye metodov komp'yuternogo modelirovaniya v reshenii zadach masshtabirovaniya ledovykh nagruzok [Application of computer simulation methods in solving problems of scaling ice loads] [Journal] // Trudy Krylovskogo gosudarstvennogo tsentra - Proceedings of the Krylov State Center. - St. Petersburg : FSUE Krylov State Scientific Center, 2017. - 379 : Vol. I. - pp. 70-77.

4 **ANSYS Documentation.** Mechanical APDL. Material reference. Chapter 4: Nonlinear material properties.

5 **ANSYS Documentation.** Mechanical APDL. Theory reference. Chapter 4: Structures with Material Nonlinearities.

6 **ANSYS Documentation.** Mechanical Applications. Explicit Dynamics Analysis Guide. Chapter 3: Transforming an Implicit Model to run in Explicit Dynamics.

7 **ANSYS Documentation.** Mechanical Applications. Explicit Dynamics Analysis Guide. Chapter 6: Explicit Dynamics Theory Guide.

8 **Assur A.** Flexural and Other Properties of Sea Ice Sheets: Condensed Version [Conference] // Physics of Snow and Ice : proceedings. - 1967. - Vol. 1. - pp. 557-567.

9 **Bekker A.T.** Veroyatnostnyye kharakteristiki ledovykh nagruzok na sooruzheniya kontinental'nogo shel'fa [Probabilistic characteristics of ice loads on the continental shelf structures] [Monograph]. - Vladivostok : Dalnauka, 2004.

10 **Bjerkås M. Meese A., Alsos H.** Ice Induced Vibrations – Observations of a Full Scale Lock-in Event [Conference] // Proceedings of the 23rd International Offshore and Polar Engineering. - Anchorage : International Society of Offshore and Polar Engineers (ISOPE), 2013. - pp. 1272-1279.

11 CAN/CSA S471-04. General requirements, design criteria, the environment and loads. - Ontario : Canadion standards association, 2004. - 116 p.

12 **Carney K., Benson D., DuBois P., Lee R.** A phenomenological high strain rate model with failure for ice [Journal] // International Journal of Solids and Structures. - 2006. - 43. - pp. 7820-7839.

13 **Cole D. M.** Strain-rate and grain-size effects in ice [Journal] // Journal of Glaciology. - [s.l.] : Cambridge University Press, 1987. - 115 : Vol. 33. - pp. 274-280.

14 **Cox G. F. N., Weeks W. F.** Equations for determining the gas and brine volumes in sea ice samples [Journal] // Journal of Glaciology. - 1983. - 102 : Vol. 29. - pp. 306-316

15 **Cox G. F. N., Weeks W. F.** Salinity variation in sea ice [Journal] // Journal of Glaciology. - 1974. - 67 : Vol. 23. - pp. 109-120.

16 **Cundall P. A. Strack O. D. L.** The distinct element method as a tool for research in granular media [Book]. - Minneapolis : Department of Civil and Mineral Engineering, University of Minnesota, 1978. - Vol. I.

17 **Daiyan H., Sand B.** Numerical Simulation of the Ice-Structure Interaction in LS-DYNA [Conference] // Proceedings of 8th European LS-DYNA Users Conference. - Strasbourg : [s.n.], 2011.

18 **Derradji-Aouat Ahmed** Explicit FEA and constitutive modelling of damage and fracture on polycrystalline ice - simulations of ice loads on offshore structures [Conference] // Proc., 18th Int. Conf. on Port and Ocean Eng. Under Arctic Conditions. - Canada : , 2005. - Vol. I. - pp. 225-238.

19 **Doronin Yu. P.** Fizika okeana [Ocean Physics] [Book]. - St. Petersburg : Russian State Hydrometeorological University, 2000. - 305 p. (in Russian).

20 **Doronin Yu. P., Kheisin D. E.** Morskoy lod [Sea ice] [Book]. - Leningrad : Gidrometeoizdat, 1975. - 320 p. (in Russian).

21 **Dykins J. E.** Tensile Properties of sea ice grown in a confined system [Conference] // Physics of Snow and Ice: proceedings. - Japan : Bunyeido Printing, 1967. - Vol. 1. - pp. 523-537.

22 **Feng D., Pang D. S., Zhang J.** Parameter Sensitivity in Numerical Modelling of Ice-Structure Interaction With Cohesive Element Method [Conference] // Proceedings of the ASME 2016 35th International Conference on Ocean, Offshore and Arctic Engineering (OMAE). - Busan : ASME, 2016.

23 **Frankenstein G., Garner R.** Equations for determining the brine volume of sea ice from -0.5 °C to -22.9 °C [Journal] // Journal of Glaciology. - 1967. - 48 : Vol. 6. - pp. 943-944.

24 **Fransson L. Bergdahl L** Elforsk rapport 09:55 // Recommendations for design of offshore foundations exposed to ice loads. - 2009. - 43 p.

25 **Gammon P. H., Kiefte H., Clouter M. J., Denner W. W.** Elastic constants of artificial and natural ice samples by Brillouin spectroscopy [Journal] // Journal of Glaciology. - [s.l.] : Cambridge University Press, 1983. - 103 : Vol. 29. - pp. 433-460

26 GL 2005 IV. Part 6 - Offshore Installations. Chapter 7 - Guideline for the Construction of Fixed Offshore Installations. - Hamburg : Germanischer Lloyd, 2005. - 29 p.

27 **Gladkov M. G.** Nagruzki i vozdeystviya l'da na morskiye gidrotekhnicheskiye sooruzheniya: dis. … dokt. tekh. nauk [Loads and impacts of ice on marine hydraulic structures. Dr. thesis (Eng.)]. - St. Petersburg : [s.n.], 1997. - 181 p.

28 **Gold L. W.** Engineering properties of fresh-water ice [Journal] // Journal of Glaciology. -

[s.l.] : Cambridge University Press, 1977. - 81 : Vol. 19. - pp. 197-212.

29 **Gürtner A. Bjerkås M., Forsberg J., Hilding D.** Numerical modelling of a full scale ice event [Conference] // Proceedings of 20th IAHR International Symposium on Ice. - Lahti : [s.n.], 2010.

30 **Gürtner A., Bjerkås M., Kühnlein W., Jochmann P., Konuk I.** Numerical Simulation of Ice Action to a Lighthouse [Conference] // Proceedings of the ASME 28th International Conference on Ocean, Offshore and Arctic Engineering (OMAE). - Honolulu : ASME, 2009.

31 **Hilding D., Forsberg J., Gürtner A.** Simulation of ice action loads on offshore structures [Conference] // Proceedings of 8th European LS-DYNA Users Conference. - Strasbourg : DYNAmore GmbH, 2011.

32 **Hilding D., Forsberg J., Gürtner A.** Simulation of Loads from Drifting Ice Sheets on Offshore Structures [Conference] // Proceedings of 12th International LS-DYNA Users Conference. - Detroit : Livermore Software Technology Corporation, 2012.

33 ISO/FDIS 19906:2019(E). Petroleum and natural gas industries — Arctic offshore structures. Final Draft. International Organisation for Standartization. ISO/TC 67/SC 7. - Vernier : ISO copyright office, 2019. - 583 p.

34 **Jones S. J.** The confined compressive strength of polycrystalline ice [Journal] // Journal of Glaciology. - [s.l.] : Cambridge University Press, 1998. - 98 : Vol. 28. - pp. 171-177.

35 **Jordaan I. J.** Mechanics of ice-structure interaction [Journal] // Engineering Fracture Mechanics. - [s.l.] : Elsevier, 2001. - 17 : Vol. 68. - pp. 1923-1960.

36 **Karulina M., Shkhinek K., Thomas G** Theoretical and experimental investigations of level ice interaction with fourlegged structures [Conference] // Proc. of 21st Int. Conf. on Port and Ocean Eng. under Arctic cond., POAC 11. - Montreal : Curran Associates, Inc, 2011. - Vol. 1. - pp. 235-246. - ISBN: 978-1-61839-225-1.

37 **Kim J-H., Kim Y.** Numerical simulation of concrete abrasion induced by unbreakable ice floes [Journal] // International Journal of Naval Architecture and Ocean Engineering. - [s.l.] : Elsevier B.V., 2019. - 1 : Vol. 11. - pp. 59-69.

38 **Korzhavin N. K.** Vozdeystviye l'da na inzhenernyye sooruzheniya [The effect of ice on engineering structures] [Книга]. - Novosibirsk : Publishing House of the Siberian Branch of the Academy of Sciences of the USSR, 1962. - стр. 204 p. (in Russian).

39 **Kovacs A.** Estimating the full-scale flexural and compressive strength of first-year sea ice [Journal] // Journal of geophysical research. - 1997. - C4 : Vol. 102. - pp. 8681-8689.

40 **Kovacs A** Sea Ice. Part I: Bulk Salinity Versus Ice Floe Thickness // CRREL Report 96-7. - USA : CREEL, 1996.

41 **Kovalev S. M., Lebedev G. A., Nedoshivin O. A., Sukhorukov K. K.** Mekhanicheskiye svoystvo morskogo l'da [Mechanical property of sea ice] [Book]. - St. Petersburg : Gidrometeoizdat,

2001. - p. 75 p. (in Russian).

42 **Langleben M. P., Pounder, E. R.** Elastic parameters of sea ice / ed. Kingery W. D.. - USA : MIT Press, 1963. - pp. 69-78.

43 **Li H. Bjerkås M., Høyland K. V., Nord T. S.** Panel loads and weather conditions at Norströmsgrund lighthouse 2000-2003 [Conference] // Proceedings of the 23rd IAHR International Symposium on Ice. - Ann Arbor : [s.n.], 2016.

44 **Li Liang** Ledovaya nagruzka na gidrotekhnicheskiye sooruzheniya s naklonnoy gran'yu: dis. … kand. tekh. nauk [Ice load on hydraulic structures with an inclined face: Cand. dis. (Eng.)]. - St. Petersburg : [s.n.], 2014. - 136 p. (in Russian).

45 **Liu J., Liu X., Chen Y.** Numerical Simulations of Ice Loads on Fixed and Floating Offshore Structures using the Discrete Element Method [Conference] // Proceedings of Arctic Technology Conference. - St. John's : Offshore Technology Conference, 2016.

46 **Lu W., Lubbad R., Løset S., Høyland K.** Cohesive Zone Method Based Simulations of Ice Wedge Bending: a Comparative Study of Element Erosion, CEM, DEM and XFEM [Conference] // Proceedings of 21st IAHR International Symposium on Ice. - Dalian : Dalian University of Technology Press, 2012. - pp. 920-938.

47 **Lu W., Heyn H.-M., Lubbad R., Løset S.** A large scale simulation of floe-ice fractures and validation against full-scale scenario [Journal] // International Journal of Naval Architecture and Ocean Engineering. - [s.l.] : Elsevier B.V., 2018. - 3 : Vol. 10. - pp. 393-402.

48 **Makarov O., Bekker A., Gogoladze D.** Analysis of constitutive plasticity models in relation to numerical modelling of ice impacts [Journal] // FEFU: School of Engineering Bulletin. - Vladivostok : FEFU, 2020. - 43 : Vol. 2. - pp. 141-154.

49 **Murat J. R., Lainey, L. M.** Some experimental observations on the Poisson's ratio of sea-ice [Journal] // Cold Regions Science and Technology. - 1982. - 2 : Vol. 6. - pp. 105-113.

50 **Nazintsev Yu. L., Dmitrash Zh. A., Moiseev V. I.** Teplofizicheskiye svoystva morskogo l'da [Thermophysical properties of sea ice] [Book]. - Leningrad : Publishing house of Leningrad State University, 1988. - 260 p. (in Russian).

51 **Nazintsev Yu. L., Panov V. V.** Fazovyy sostav i teplofizicheskiye kharakteristiki morskogo l'da [Phase composition and thermophysical characteristics of sea ice] [Book]. - St. Petersburg : Gidrometeoizdat, 2000. - 84 p. (in Russian).

52 ND 2-020201-015 Rules for the classification, construction and equipment of mobile offshore drilling units and fixed offshore platforms. - St. Petersburg : Russian Maritime Register of Shipping, 2018 г.. - 454 p. (in Russian).

53 **Nord T. S., Kvåle K. A., Petersen Øyvind W., Bjerkås M., Lourens E.-M.** Operational modal analysis on a lighthouse structure subjected to ice actions [Journal] // Procedia Engineering. -

2017. - Vol. 199. - pp. 1014-1019.

54 **Palmer A. Croasdale K. R.** Arctic Offshore Engineering [Book]. - Singapore : World Scientific Publishing Co. Pte. Ltd., 2012. - p. 372.

55 **Pernas-Sánchez J., Pedroche D. A., Varas D., López-Puente J.** Numerical modeling of ice behavior under high velocity impacts [Journal] // International Journal of Solids and Structures. - 2012. - 14 : Vol. 49. - pp. 1919–1927.

56 **Politko V. A.** Vozdeystviye ledovykh poley na odno- i mnogoopornyye gidrotekhnicheskiye sooruzheniya s vertikal'noy opornoy chast'yu: dis. … kand. tekh. nauk [Influence of ice fields on single and multi-bearing hydraulic structures with a vertical supporting part. Cand. dis. (Eng.)]. - Moscow : [s.n.], 2018. - 148 p. (in Russian).

57 **Richard M., McKenna R.** Factors influencing managed sea ice loads [Conference] // Proceedings of the 22nd International Conference on Port and Ocean Engineering under Arctic Conditions (POAC). - Espoo : [s.n.], 2013.

58 **Richter-Menge J. A., Jones K. F.** The tensile strength of first-year sea ice [Journal] // Journal of Glaciology. - [s.l.] : Cambridge University Press, 1993. - 133 : Vol. 39. - pp. 609-618.

59 **Rist M. A. Murrel S. A. F.** Ice triaxial deforntation and fracture [Journal] // Journal of Glaciology. - [s.l.] : Cambridge University Press, 1994. - 135 : Vol. 40. - pp. 305-318.

60 **Rüdiger von Bock und Polach, Sören Ehlers** Model scale ice — Part B: Numerical model [Journal] // Cold Regions Science and Technology. - [s.l.] : Elsevier, 2013. - 94. - pp. 53-60.

61 **Ryvlin A. Ya.** Metod prognozirovaniya predela prochnosti ledyanogo pokrova na izgib [Method for predicting the ultimate strength of ice cover in bending] [Journal] // Problemy Arktiki i Antarktiki - Problems of the Arctic and Antarctic. - 1974. - 45. - pp. 79-86. - (in Russian).

62 **Salganik E. A., Shkhinek K. N.** Ice induced vibrations of offshore structures [Journal] // Magazine of Civil Engineering. - St. Petersburg : Peter the Great St. Petersburg Polytechnic University. - 4 : Vol. 48. - pp. 72-78.

63 **Sand Bjørnar** Nonlinear finite element simulations of ice forces on offshore structures: doctoral thesis. – Luleå., 2008. - 264 p.

64 **Sanderson T. J. O.** Ice mechanics : risks to offshore structures [Book]. - London : Graham & Trotman, 1988. - 253 p.

65 **Schulson E. M.** Brittle Failure of Ice [Journal] // Engineering Fracture Mechanics. - 2001. - 17-18 : Vol. 68. - pp. 1839-1887.

66 **Schulson E. M., Duval P.** Creep and fracture of ice [Book]. - New York : Cambridge University Press, 2009. - p. 417.

67 **Schwarz J. Weeks W. F.** Engineering properties of sea ice [Journal] // Journal of Glaciology. - [s.l.] : Cambridge University Press, 1977. - 81 : Vol. 19. - pp. 499-531.

68 SP 38.13330.2018 Loads and impacts on hydraulic structures (from wave, ice and ships). - Moscow : Ministry of Construction of Russia, 2018. - 127 p. (in Russian).

69 STO Gazprom 2-3.7-29-2005 Metodika rascheta ledovykh nagruzok na ledostoykuyu statsionarnuyu platformu [Methodology for calculating ice loads on an ice-resistant stationary platform]. - [s.l.] : Gazprom LLC, 2005. - 16 p. (in Russian).

70 **Taylor R., Frederking R., Jordaan I.** The nature of high pressure zones in Compressive Ice Failure [Conference] // Proceedings of The 19th IAHR International Symposium on Ice. - Vancouver : St. Joseph Communications, 2008. - Vol. 2. - pp. 1001-1010. - ISBN: 978-0-9810446-0-6.

71 **The Abaqus documentation.** Abaqus. Elements. Special-Purpose Elements. Cohesive elements. Defining the constitutive response of cohesive elements using a traction-separation description.

72 **The Abaqus documentation.** Abaqus. Materials. Inelastic Mechanical Properties. Other plasticity models. Extended Drucker-Prager models.

73 **Thomas D. N. Dieckmann G. S.** Sea Ice. Second Edition [Book]. - Chichester : Blackwell Publishing Ltd, 2010. - p. 640.

74 **Timco G. W., Weeks W. F.** A review of the engineering properties of sea ice [Journal] // Cold Regions Science and Technology. - : Elsevier B.V, 2010. - 2 : Vol. 60. - pp. 107-129.

75 **Timko G. W., Frederking R. M. W.** Compressive Strength o f Sea Ice Sheets [Journal] // Cold Regions Science and Technology. - 1990. - 3 : Vol. 17. - pp. 227-240.

76 **Timko G. W., Frederking R. M. W.** Field Measurements of the Shear Strength of Columnar-Grained Sea Ice [Conference] // Proceedings of 8th IAHR International Symposium on Ice. - Iowa City : [s.n.], 1986. - Vol. 1. - pp. 279-292.

77 **Tyshko K. P., Cherepanov N. V., Fedotov V. I.** Kristallicheskoye stroyeniye morskogo ledyanogo pokrova [Crystal structure of sea ice cover] [Book]. - St. Petersburg : Gidrometeoizdat, 2000. - 66 p. (in Russian).

78 **Vaudrey K. D.** Ice engineering: Study of related properties of floating sea-ice sheets and // US Navy Civil Engineering Laboratory, Technical Report R 860. - 1977. - p. 81.

79 **Wang Y., Zou Z.-J., Wang F., Lu T.-C.** A Simulation Study on the Ice Fracture Behaviors in Ice-Lighthouse Interaction Considering Initial Defects and Change of Elastic Modulus [Conference] // Proceedings of the 29th International Ocean and Polar Engineering Conference. - Honolulu : International Society of Offshore and Polar Engineers (ISOPE), 2019. - Vol. 173. - pp. 433-449.

80 **Weeks W. F. Ackley S. F.** The growth, structure and properties of sea ice // CRREL Monograph 82-1. - Hanover : [s.n.], 1982. - p. 136.

81 **Weeks W. F., Assur A.** The mechanical properties of sea ice // U.S. Army CRREL Monograph. - Hanover : U.S. Army Materiel Command, 1967. - Vol. 2.

82 **Weiss J. Schulson E. M.** The failure of fresh-water granular ice under multiaxial compressive loading [Conference] // Proceedings of the 12th International Symposium on Ice of IAHR. - Trondheim : [s.n.], 1994. - Vol. 1. - pp. 495-504.

83 **Weiss J., Meyssonnier, J.** Micro Mechanics of Ice // LOLEIF-Report No. 7 EU-Contract No. MAS3-CT-97-0098. - 2001.